FURTHER STUDIES OF ELECTROFORMING EFFECTS IN MIM STRUCTURES

A THESIS PRESENTED

FOR THE DEGREE OF DOCTOR OF PHILOSOPHY

by

A. KOMPANY, B.Sc., M.Tech.

January 1980.

Brunel University,
Kingston Lane,
Uxbridge,
Middlesex,
England.

To my parents for their invaluable help, patience and encouragement.

ACKNOWLEDGEMENTS

I would like to take this opportunity to express my deep appreciation and gratitude to my Supervisor, Professor C.A. Hogarth for his supervision, guidance and encouragement throughout the course of this work.

I wish to thank Dr. A.E. Rakhshani for his helpful suggestions and discussions.

I would also like to thank my friends Dr. A. Nouruzi-Khorassani, Dr. H.S. Ebrahimi, Dr. H. Hekmat-Shoar, Mr. M.R. Varshuuchi and Mr. R. Hosseini-Abardah for their encouragement and stimulating discussions.

The technical assistance of Mr. D. Waterman, Mr. M. Schlachter, Mr. R. Stevens, Mr. H. Brown, Mr. L. Lightowler and Mr. T. Davis of the technical staff of the Physics Department has been of great value and is sincerely appreciated.

I also wish to express my appreciation to Mr. R. Bulpett of the Metallurgy Department for the experimental assistance in taking the scanning electron microscope photographs.

I am indebted to Mrs. A. Grant and Mrs. M. Houghton for typing this thesis.

Finally, I wish to express my deepest gratitude to my father, Mr. A.A. Kompany, without whose constant encouragement and support, this work would not have been possible.

ABSTRACT

Thin film sandwich structures of metal-SiO/B_2O_3-metal with the dielectric thickness in the range 400 to 4000 Å have been prepared by thermal evaporation in a vacuum of less than 10^{-5} torr. The metal electrodes used were Cu, Ag and Al.

After the electroforming process the devices showed a voltage-controlled negative resistance (VCNR) and emission of electrons into a vacuum. Devices with Cu electrodes were found to give the most suitable characteristics. The effect of air pressure and temperature on VCNR were studied. The vacuum-electroformed samples exhibited a pressure-voltage memory effect when operated in air at atmospheric pressure and the high-impedance state induced then could be erased by reducing the air pressure and by applying a bias voltage exceeding the threshold voltage, V_T. Thermal-voltage memory effects were investigated in devices carrying Cu electrodes and the time-dependent transitions of the high-impedance memory states to a normal low impedance state at low temperatures were measured. The results have been explained employing the filamentary model of Dearnaley, Morgan and Stoneham.

The localised defect regions on the surfaces of the samples, produced during the electro-forming process and electrical operation of the device, were investigated by means of a scanning electron microscope. The defects are believed to be mainly due to the formation of

conducting filaments across the insulator and to the consequential Joule heating and electrolytic processes occurring along the filaments.

A memory switching effect was observed in devices having Ag and Cu electrodes. The samples were formed initially in the atmosphere by the application of a direct voltage in series with a large resistance. The formed sample then could switch between a low-conductivity 'off' state and a high-conductivity 'on' state, which has an ohmic characteristic. The observed switching behaviour is explained in terms of a mono-filamentary model based on the formation of a metallic filament across the insulator during the forming process of the sample.

CONTENTS

Page No

Acknowledgements i

Abstract ii

CHAPTER ONE: Review of Electrical Conduction through thin Amorphous Dielectric Films (Prior to Electroforming)

1.1 Introduction 1

1.2 The Energy Band Structure 2

1.3 Metal-Insulator Contact 6

(a) Ohmic 6

(b) Neutral 8

(c) Blocking 8

1.4 DC Electrical Conduction Mechanisms ... 10

1.4.1 Schottky Emission 12

1.4.2 The Poole-Frenkel Effect 14

1.4.3 Tunnelling Effect 16

1.4.4 Impurity Conduction 18

1.4.5 Ionic Conduction 19

1.4.6 Space-Charge-Limited Current Mechanism (SCLC) 21

CHAPTER TWO: An Introduction to Electroforming and Related Phenomena in MIM Structures.

2.1 The Forming Process 25

2.2 Properties of the Formed Junctions 27

2.2.1 Voltage-Controlled Negative Resistance (VCNR) 27

2.2.2 Electron Emission 29

2.2.3 Electroluminescence 32

2.2.4 Memory Effects 32

(a) Voltage Memory 32

Page No

(b) Pressure-Voltage Memory 33

(c) Thermal-Voltage Memory 33

2.3. Models of the Forming Process and the Conduction Mechanism in Formed Devices... 34

2.3.1 Hickmott's Model 34

2.3.2 The Model of Verderber, Simmons and Eales 37

2.3.3 The Model of Greene, Bush and Rawlings 48

2.3.4 The Model of Barriac, Pinard and Davoine 50

2.3.5 The Model of Dearnaley, Morgan and Stoneham 54

2.3.6 The Model of Ralph and Woodcock ... 59

2.3.7 Discussion and Conclusion 66

2.4 Current-Controlled Negative Resistance (CCNR) and Switching 71

CHAPTER THREE: Experimental Techniques

3.1 Preparation of Devices 77

3.1.1 The Evaporation Unit 77

3.1.2 Preparation and Deposition Procedures 79

3.1.3 Thickness Measurements 81

3.2 The Vacuum Test System 83

3.3. Temperature Measurements 84

CHAPTER FOUR: Results.

4.1 Introduction 85

4.2 Film Structure 88

Page No

4.3 DC Stability, Operation and Characteristics of M-SiO/B_2O_3-M Structures. 88

4.3.1 Experimental Details 88

4.3.2 Electroforming and DC Device Characteristics 89

4.3.3 Effect of Air-Pressure on the VCNR 93

4.3.4 Thermal-Voltage Memory Effect in Cu-SiO/B_2O_3-Cu Structures 95

4.3.5 Summary and Conclusions 101

4.4 Investigation of M I M Device Surfaces by Means of the Scanning Electron Microscopy 103

4.4.1 Introduction 103

4.4.2 Principle of the Scanning Electron Microscope 106

4.4.3 Results and Discussion 108

4.4.4 Conclusion 111

4.5 Observation of Switching Phenomena ... 113

4.5.1 Introduction 113

4.5.2 Previous Work on Switching in Metal-Oxide-Metal Structures ... 113

4.5.3 Experimental Details 121

4.5.4 Results and Discussion 122

CHAPTER FIVE: Summary and Conclusions 127

REFERENCES: 132

FIGURES

CHAPTER ONE

REVIEW OF ELECTRICAL CONDUCTION THROUGH THIN AMORPHOUS DIELECTRIC FILMS

(prior to Electroforming)

1.1. INTRODUCTION

The unique properties of amorphous semiconductors and insulators and the advantages of producing them by means of a thin film process, which does not limit their size and makes them adaptable to integration with other solid-state technologies, have made these materials the base for a new area of science and technology. In the past two decades, thin film systems of sandwich type of metal-insulator-metal (MIM) have been used to a significant extent in practical situations as both passive and active elements[1].

Since the work by Kreynina et al[2] in 1960 and their report on the electro-forming and the so-called anomalous behaviour in MIM structures, extensive studies have been carried out in this field by many investigators. The emission of hot electrons from these structures has offered opportunities to use these devices as cold cathode emitters for display purposes. Further interests in this subject increased as a result of the discovery of switching in chalcogenide glasses by Ovshinsky[3] in 1968 and ever since many suggestions have been made to use thin films of amorphous materials for the preparation of switching and memory elements.

The more and more extensive application of thin solid films in technology in particular in micro-electronics necessitates continuous improvement in methods of preparing the thin films, and so accounts for the numerous studies on the conditions which will ensure the desired reproducible and controlled properties of the films. There are various methods for preparing thin films for research, development and production purposes such as thermal evaporation, cathodic sputtering, chemical deposition and some other techniques[1,4,5]. However, it is impossible to characterise the films so as to identify the best method of preparation which is applicable for all situations. Stability and reproducibility are the major characteristics required for studies of conduction processes in insulating films and in the case of applications of the films, these requirements are coupled to those of the economics of large scale production.

1.2 THE ENERGY BAND STRUCTURE

The theory of the electronic structure of solids has become common knowledge since the development of quantum mechanics in the 1920's and the advent of the band theory of metals, semiconductors and insulators. Ideally, a crystalline solid is a stoichiometric material characterized by the presence of a definite long-range order of the atomic constituents of the material. In a non-crystalline solid the situation is considerably different. Essentially, by definition, such a material does not present itself as a well-ordered array of the

atomic constituents and also practically there is no long-range order in the substance. Indeed, such an amorphous compound as a glass is in general not a stoichiometric compound.

However, it has been accepted that the theory of the energy band structure in fact owes relatively little to the periodicity of the lattice, but is due to the actual chemical bonds between the atoms, in other words the loss of periodicity of the lattice has relatively little influence on the band structure as long as the short-range order is preserved(6). Since in many amorphous materials the local binding forces in the short range are essentially the same as in the crystalline forms, the band theory which is strictly applicable to crystalline materials, may in modified form however, be applied to amorphous structures(7).

The sharp band edges of crystalline lattices become diffuse in amorphous materials and give rise to a gradual transition from conductivity states in which carriers are free to move to deep trapping levels in which carriers are strictly localised. Therefore, there is a sharp change in mobility between the non-localised and the localised states; the boundary where the mobility changes is termed the 'mobility edge' and the energy differences between the 'mobility edges' of conduction and valence bands is referred to as the 'mobility gap'. Hence, instead of a reasonably well-defined energy gap we have a mobility gap where the energy bands tail off into a range of localised states.

The concept of the mobility edge was first introduced by Cohen, Fritzsch and Ovshinsky (CFO model) in 1969 for covalent amorphous alloys[8]. This model assumes that the valence and conduction bands in amorphous semiconductors have 'tails' of localised states which can overlap near the centre of the mobility gap, Fig. 1.1 (a). Beyond E_c and E_V where the states are non-localised the carrier can move without thermal assistance, but the states between the mobility edges are localised and the conduction between these states can only occur by a thermally-activated process (hopping) similar to that occurring between centres in a heavily doped semiconductor and known as impurity conduction. The mobility associated with this process is small and is predicted to be a factor $\sim 10^2 - 10^3$ lower than that for conduction in the non-localised states. The mobility $\mu(E)$ for this thermally-activated hopping transport is normally written in the form[9]:

$$\mu(E) = \frac{eR^2(E)}{kT} \nu_{ph} \exp(-2\alpha R) \exp(-\frac{W}{kT}) \qquad 1.1$$

where R is the average hopping distance, which depends on density-of-states distribution and is thus a function of energy; the term $\exp(-2\alpha R)$ describes the overlap of the wavefunctions on neighbouring hopping sites, with the parameter α representing the spatial decay of localised wavefunction, and $\nu_{ph}\exp(-W/kT)$ represents the probability per second that the localised electron hops to a new site at an energy W above the original one.

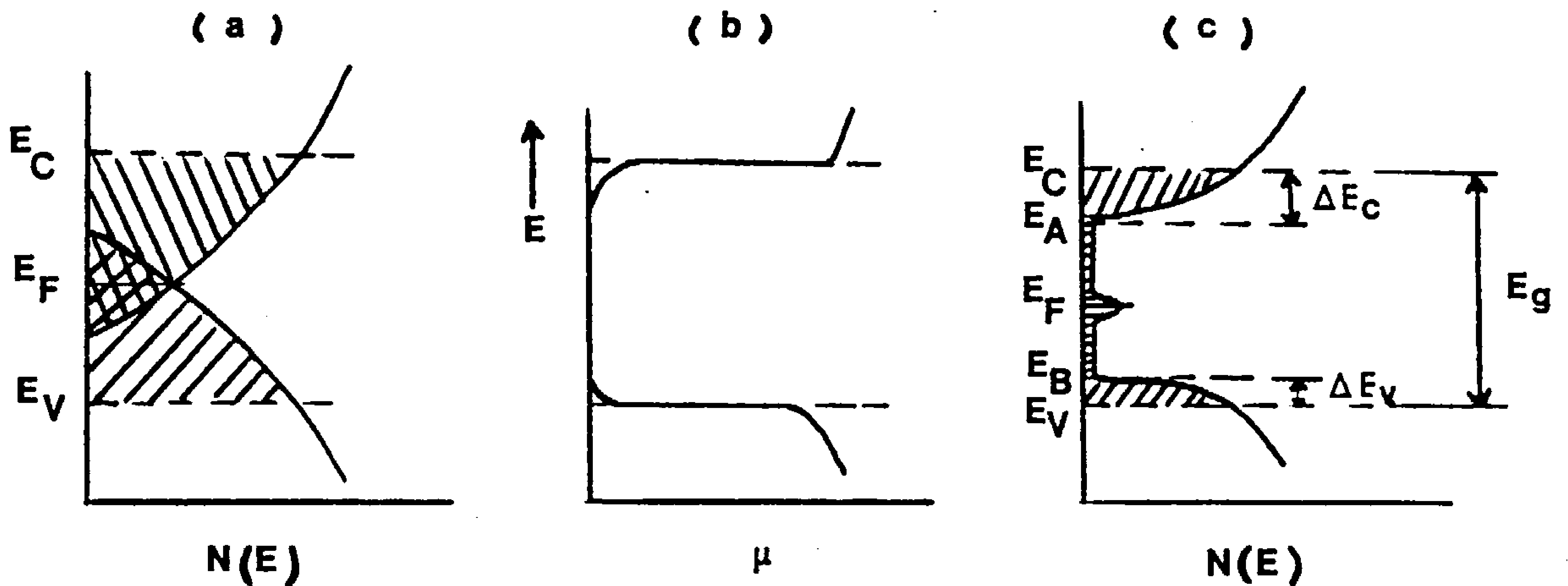

Fig. 1.1(a): Density of states, N(E) and
(b): mobility, μ, as functions of energy in a covalent amorphous semiconductor (CFO model)(8),
(c): Density of states suggested by Davis and Mott(10).

A modified model for the density of states in amorphous semiconductors proposed by Davis and Mott[10] is illustrated in Fig. 1.1(c). They believe that the localised states in the energy intervals ΔE_C and ΔE_V are due to the lack of long-range order and the localised extended tails between E_A and E_B are related to the presence of the defects such as impurities, vacancies, dangling bonds etc. in the lattice.

In the present work we are dealing with evaporated insulating films which tend to be deposited non-stoichiometrically because of the tendency for the lower vapour pressure of one of the components. For example, silicon oxide yields a film containing a mixture

of compounds varying from silicon monoxide to silicon dioxide as well as free silicon. However, these films are, in most cases, amorphous and best polycrystalline and which differ from the crystalline films by the absence of well-defined conduction band and valence band edges and the large density of localised states in the forbidden gap which act as traps. These features of the amorphous dielectric films make it possible to explain their electrical properties by means of models formulated for amorphous semiconductors.

1.3 METAL-INSULATOR CONTACTS

In order to understand how the carriers are made available in the insulator, resulting in the observed finite currents, it is necessary to understand the contact between the insulator and the metal electrode. The type of contact established will depend on the metal work function 'ψ_m' and the insulator work function 'ψ_i'. Contact phenomena have been reviewed by Campbell and Morley(11), and Simmons(12,13). Three different types of contact can exist at a metal-insulator interface; namely ohmic, neutral and blocking contacts(12).

(a) Ohmic Contact

In order to achieve an ohmic contact the electrode work function must be smaller than the insulator work function, i.e. $\psi_m < \psi_i$. In this case electrons are injected from the electrode into the insulator conduction band to satisfy the thermal-equilibrium conditions, that is the continuity of the Fermi and vacuum levels throughout the system. A negative space-charge accumulation

region is then created in the insulator with equal and positive charges on the metal electrode. The width of the accumulation region, λ_0, is given by Simmons[13] as:

$$\lambda_0 = \frac{\pi}{2}\left(\frac{2kT\varepsilon\varepsilon_0}{e2N_t}\right)^{\frac{1}{2}} \exp\left(\frac{\psi_i - \chi - E_t}{2kT}\right) \qquad 1.2$$

for a density of shallow electron traps N_t, positioned at an energy E_t, below the bottom of the conduction band where χ is the electron affinity of the dielectric. An ohmic contact acts as a reservoir of charge which is capable of supplying electrons to the insulator as required by the bias conditions. The conduction process is limited by the rate of electron flow through the bulk of the insulator and hence, the conduction process is bulk-limited. The simplest concept of the formation of an ohmic contact is provided by the energy diagram of Fig. 1.2. The interfacial barrier ϕ_0 is given by $\phi_0 = \psi_m - \chi$.

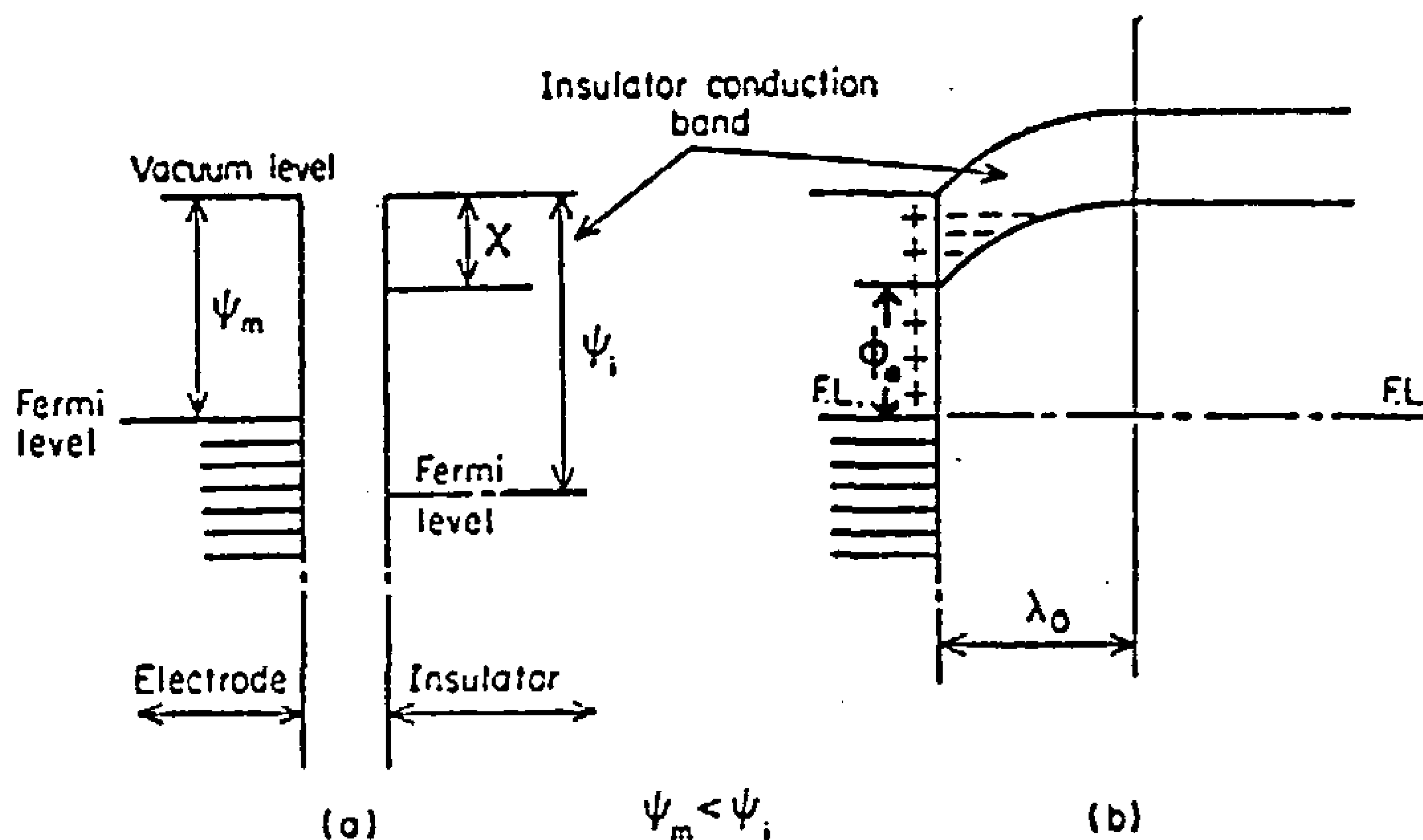

Fig. 1.2. The energy level diagram of a metal-insulator (a) before contact (b) after contact, when $\psi_m < \psi_i$.

(b) Neutral Contact

When $\psi_m = \psi_i$ the vacuum and Fermi levels of the insulator and electrode line up naturally without the necessity of charge transfer between the electrode and insulator. Since no space charge exists within the insulator, the conduction band is flat right up to the interface; that is no band bending is present, as shown in Fig. 1.3.

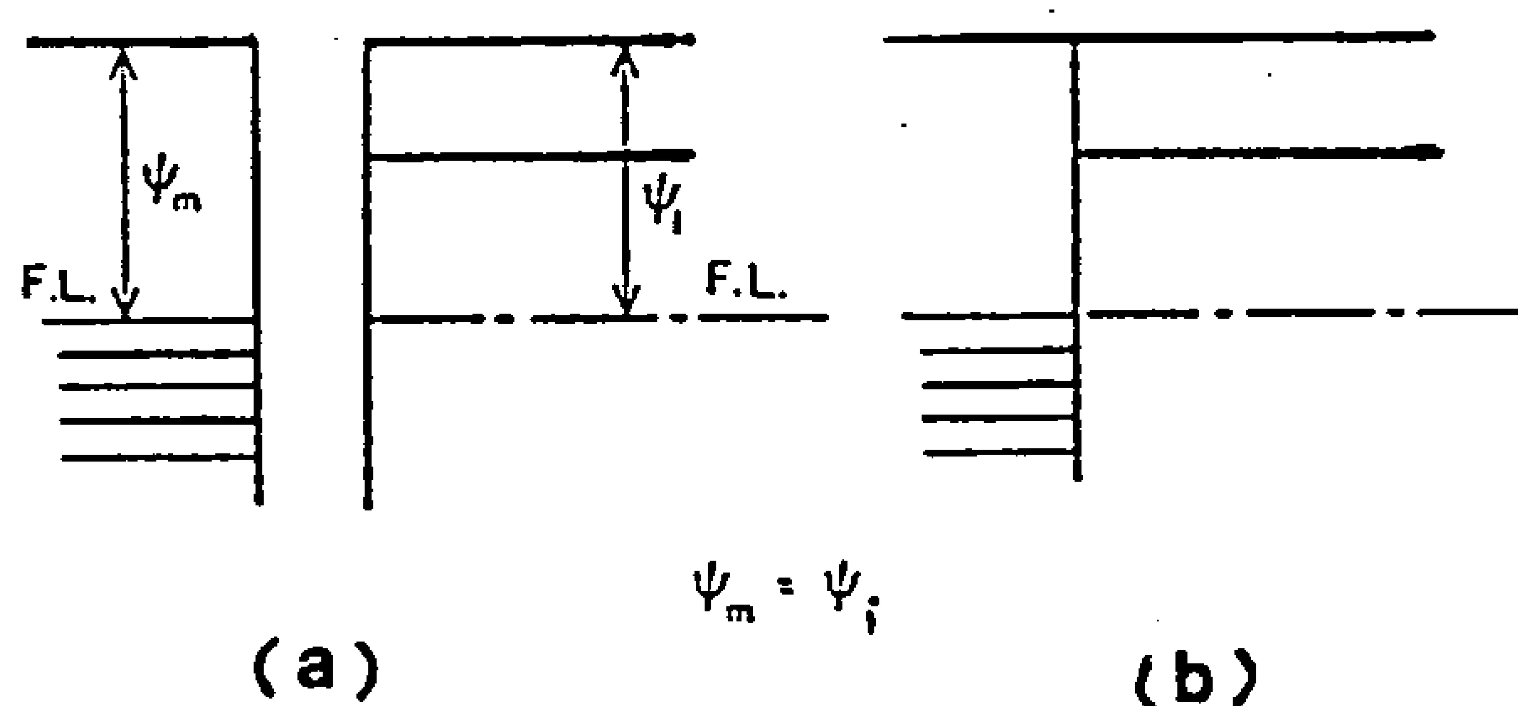

Fig. 1.3. Energy diagram of a metal-insulator in a case of neutral contact; (a) before contact, (b) after contact.

(c) Blocking Contact

A blocking contact occurs when $\psi_m > \psi_i$, and in this case electrons, which are emitted from the donor centres (positive when empty) in the insulator, flow from the insulator into the metal to establish thermal equilibrium conditions. A space-charge region of positive charge, the depletion region, is thus created in the insulator, and an equal negative charge resides on the metal electrode.

As a result of electrostatic interaction between the oppositely charged regions, a local field exists within the surface of the insulator. This causes the bottom of the insulator conduction band within the bulk of the insulator to bend downward. It is apparent from the energy diagram, Fig. 1.4.(b), that the free electron density at the interface is much lower than in the bulk of the insulator. Therefore, the rate of flow of electrons through the system will be limited by the rate at which they flow over the interfacial barrier, and hence, the conduction process is electrode-limited.

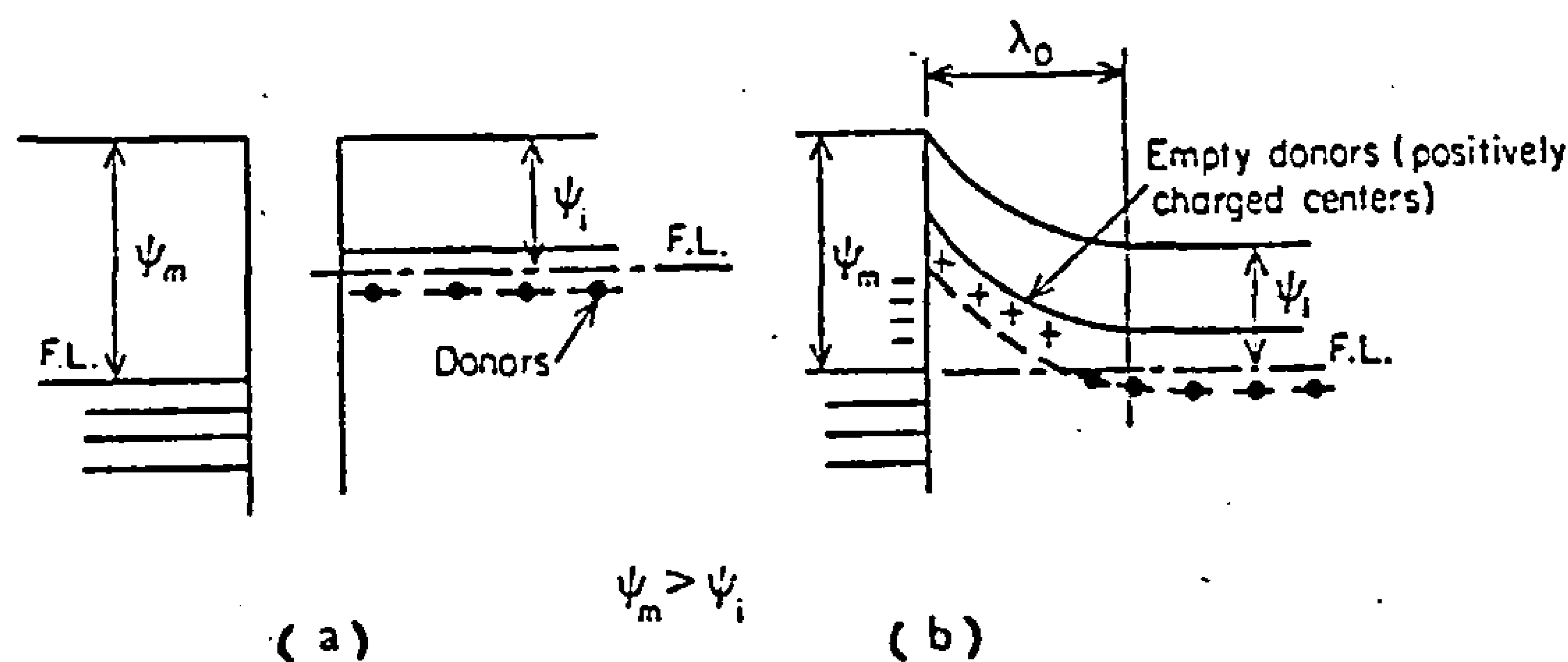

Fig. 1.4. The energy-band diagram of a metal-insulator contact when $\psi_m > \psi_i$, leading to a depletion region and a blocking contact; (a) before contact, (b) after contact.

For a blocking contact the width of the depletion region, λ_0 in Fig. 1.4 has been given by Simmons[13] as:

$$\lambda_0 = \left(\frac{2(\psi_m - \psi_i)\varepsilon\varepsilon_0}{e^2 N_d}\right)^{\frac{1}{2}} \qquad 1.3$$

where N_d is the donor density within the insulator and ε_0 is the permittivity of free space.

In the above discussion, it has been assumed that the barrier height of the metal-insulator interface is $\phi_0 = \psi_m - \chi$. If surface states exist on the insulator interface this is not necessarily true and analysis of the experimental results will be made more difficult. The presence of the surface states could be due to the displacement of the surface atoms from their ideal lattice position, the absorbed gas, water vapour etc.

1.4 DC ELECTRICAL CONDUCTION MECHANISMS

The various current transport mechanisms in dielectric thin films have been extensively studied by many authors[6,14,15,16,17]. The different mechanisms affecting current transfer through a thin insulator sandwiched between two metal electrodes (MIM structure) are illustrated schematically in the energy-band diagram shown in Fig. 1.5. in the presence of an applied field. This Fig. shows that the electrons can be injected into the conduction band of the insulator by means of thermal activation over the potential barrier at the metal-insulator interface (A); this process is referred to as "Schottky emission". The electrons may also be thermally excited into the conduction band from the trapping levels in the forbidden band of the insulator and this is termed the "Poole-Frenkel" effect (C). Electrons may tunnel into

the conduction band of the insulator directly; from the metal cathode (B), from the trapping levels within the insulator(D), or from the valence band of the insulator (F). It is also possible for the electrons to tunnel to the anode from the valence band of the insulator (G). When the insulator is thin enough (less than ~100Å) electrons will be able to tunnel directly between the electrodes.

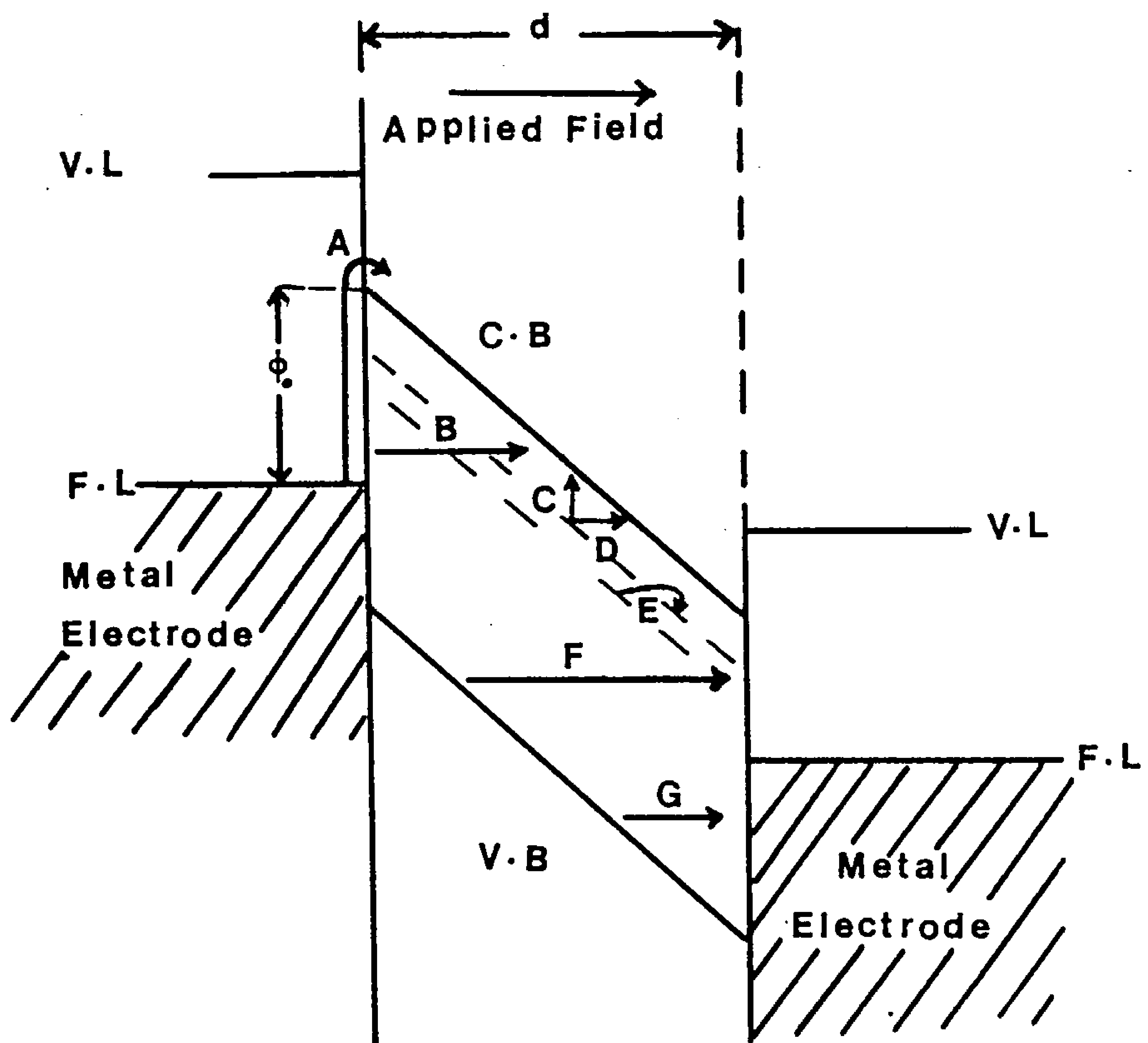

Fig. 1.5. The various possible conduction processes occurring in a metal-insulator-metal film structure.

Furthermore, the transport mechanism through the insulator may occur by means of defects in the insulator, which can be impurities in the dielectric, causing either impurity or ionic conduction. Impurity conduction involves electron transport from one stationary donor to an adjacent donor (E) in Fig. 1.5., whereas ionic conduction involves the actual movement of the impurity or defect contributing to the current. Charge injection into the conduction band, tunnelling or impurity conduction in some cases, results in a build up of space-charge within the bulk which modulates the transfer process. The effect is referred to as space-charge-limited conduction.

A number of the above mechanisms may operate simultaneously at one particular applied voltage, but generally one mechanism will dominate the observed current. Some of these processes will now be considered in a little more detail in the following sections.

1.4.1. Schottky Emission

The emission of electrons into the conduction band of dielectric from the metal-contact electrode, by thermal activation, over the interface barrier and under an applied electric field E, which reduces the height of the potential barrier, is called Schottky emission, Fig. 1.6. Reduction of the barrier height $\Delta\phi_s$, is due to the interaction of the electron image-force with the applied field and is equal to:

$$\Delta\phi_S = e(\frac{eE}{4\pi\varepsilon\varepsilon_0})^{\frac{1}{2}} = e\beta_S\ E^{\frac{1}{2}} \qquad 1.4$$

where $\beta_S = (\frac{e}{4\pi\varepsilon\varepsilon_0})^{\frac{1}{2}}$ is the Schottky field-lowering coefficient, ε is the dielectric constant, ε_0 the permittivity of free space and e is the electronic charge.

This type of electron emission from the metal at negative potential is completely analogous to thermionic emission. The current density for thermionic emission over a potential barrier ϕ, is given by Richardson's law:

$$J = AT^2 \exp\left(-\frac{\phi}{kT}\right) \qquad 1.5$$

where A is the effective Richardson constant, k is the Boltzmann constant and T is the absolute temperature.

Considering the potential barrier reduction for the case of Schottky emission the current density obeys the following equation rather than Richardson's law:

$$J = AT^2 \exp\left(-\frac{e(\phi-\beta_S\ E^{\frac{1}{2}})}{kT}\right) \qquad 1.6$$

which is the Richardson-Schottky equation.

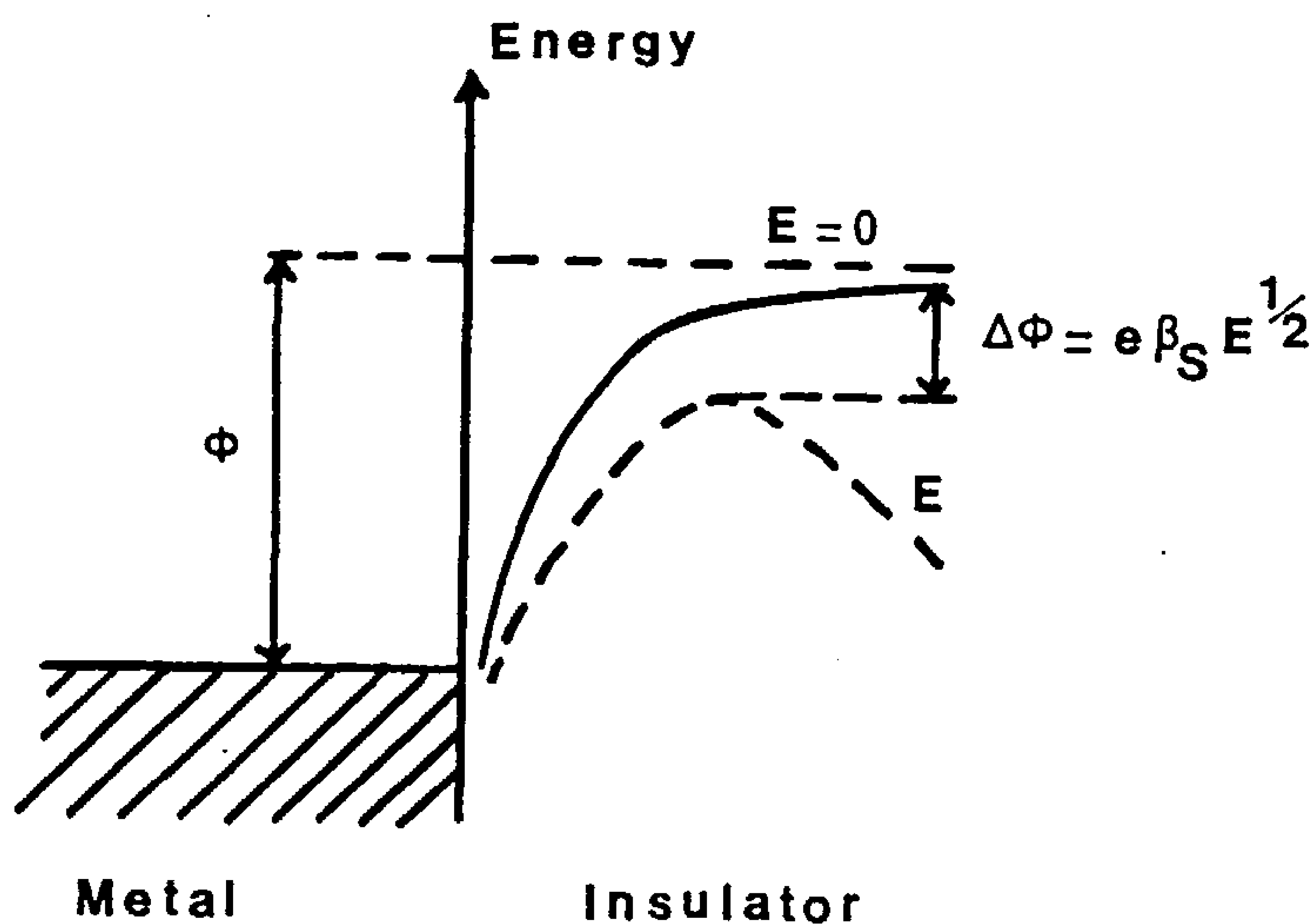

Fig. 1.6. The Schottky effect at the interface of a metal and an insulator.

1.4.2. The Poole-Frenkel Effect

The Poole-Frenkel effect (field-assisted thermal ionization) is the lowering of a coulombic potential barrier when it interacts with an electric field[18]. This is usually associated with the lowering of the effective ionization energy of a donor in the bulk of an insulator, Fig. 1.7, which increases the probability for the electron to be thermally excited from the trap into the conduction band of the insulator.

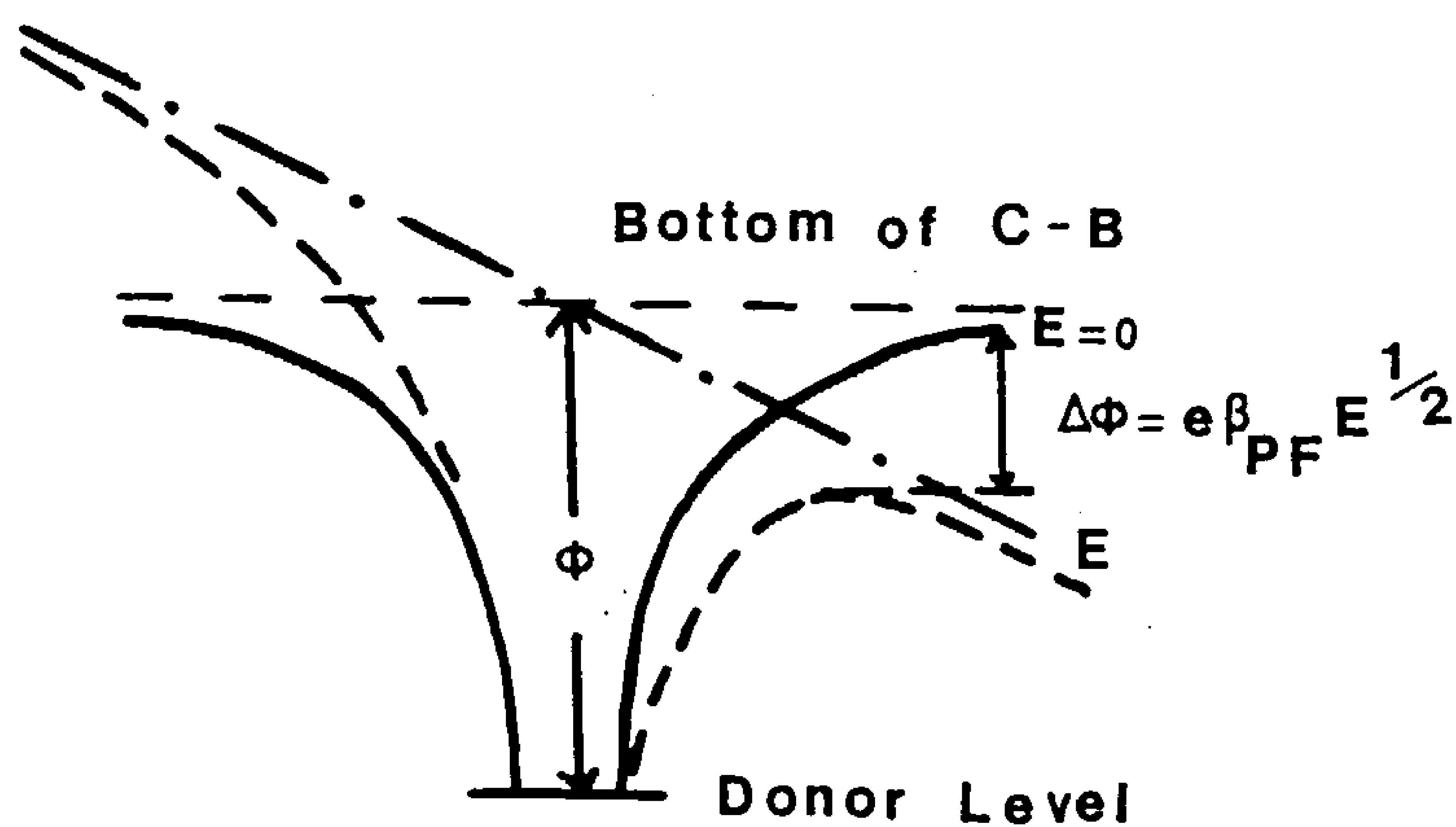

Fig. 1.7. Mechanism of the Poole-Frenkel effect. The solid line represents the coulombic barrier without a field. The dashed line shows the effect of an electric field on the barrier. The slope of dash-dot line is proportional to the applied field.

This process is the bulk analogue of the Schottky effect at an interfacial barrier, and the barrier lowering which is twice as large as that in the Schottky effect, is given by:

$$\Delta\phi_{PF} = e\left(\frac{eE}{\pi\varepsilon\varepsilon_0}\right)^{\frac{1}{2}} = e\beta_{PF}\ E^{\frac{1}{2}} \qquad 1.7$$

where $\beta_{PF} = \left(\frac{e}{\pi\varepsilon\varepsilon_0}\right)^{\frac{1}{2}} = 2\beta_s$ is the Poole-Frenkel coefficient. The equation for the current density then takes the form:

$$J = B\exp\left(-\frac{\phi}{kT}\right)\ \exp\left(\frac{e\beta_{PF}E^{\frac{1}{2}}}{kT}\right) \qquad 1.8$$

where B is a constant.

From the slope of the straight line given by a plot of LnJ versus $E^{\frac{1}{2}}$ at high field one can obtain the experimental value of the barrier lowering coefficient β; by comparing this value with the theoretical values of β_s or β_{PF} the type of conduction process in the sample can be determined, i.e. whether it is Schottky or Poole-Frenkel mechanism, provided that the high frequency dielectric constant is known. However, the experimental values for the barrier lowering coefficient (β_{exp}) may lie between the theoretically expected values of β_s and β_{PF} by using reasonable values for the dielectric constant, and in some cases, although the conduction is apparently bulk-limited, the value obtained for β is compatible with Schottky emission rather than the Poole-Frenkel effect[14,19]. These anomalous results have been explained by Simmons[20] who proposed a model on the basis of which the insulator contains levels of neutral shallow traps and deep donors and also the Fermi energy is assumed to lie midway

between the two level energies. The current density associated with this model is given by:

$$J = J_0 \exp\left(\frac{\beta_{PF}E^{\frac{1}{2}}}{2kT}\right) \qquad 1.9$$

where $J_0 = e\mu N_c E\left(\frac{N_d}{N_t}\right)^{\frac{1}{2}} \exp\left(-\frac{E_d + E_t}{2kT}\right)$ is the low field current density, μ is the mobility, N_c the effective density of states, $\left(\frac{N_d}{N_t}\right)$ is the ratio of the donor centres to the trap centres, and E_d and E_t are the energy levels of the donor and trap centres from the bottom of the conduction band. Therefore, in this case and from equation 1.6, the barrier lowering coefficient is $\frac{\beta_{PF}}{2}$ $(=\beta_s)$ although the conductivity is not electrode-limited.

1.4.3. Tunnelling Effect

In M I M structures with insulator thickness less than 100 Å there is a finite probability of the electron passing through the dielectric without surmounting the barrier existing at the metal-insulator interface. This process is known as quantum-mechanical tunnelling which is a consequence of the basic quantum mechanical nature of the electron. The formation of the current-voltage relationships is made difficult by the complex nature of the parameters involved. Basically, this involves the calculation of electron-tunnelling probabilities through a potential barrier. The other difficulties arise in formulating the barrier-shape which will depend on space-charge, image forces and the position and density of traps in the insulator.

However, a general equation for the net current

density of the electrons tunnelling through two conducting regions (1 and 2) separated by a thin dielectric film can be given by:

$$J = \frac{4\pi m^2}{h^3} \int_0^\infty \{f_1(\varepsilon) - f_2(\varepsilon)\} d\varepsilon \int_0^{\varepsilon_m} p(\varepsilon_x) d\varepsilon_x \qquad 1.10$$

where $f_1(\varepsilon)$ and $f_2(\varepsilon)$ are the Fermi-Dirac distribution functions in the regions 1 and 2 respectively, ε_m is the maximum energy of the electrons in the conducting regions, m is the electron mass, h is the Planck's constant, and $p(\varepsilon_x)$ is the probability that an electron can penetrate the barrier. Equation 1.10 can be applied to any tunnelling problem whether it be thin film sandwiches or p-n junctions. An approximate expression for the transition probability $p(\varepsilon_x)$, is given by:

$$p(\varepsilon_x) = \exp\left\{-2\int_{S_1}^{S_2} \left[\left(\frac{2m}{\hbar^2}\right)(\phi(x) - \varepsilon_x)\right]^{\frac{1}{2}} dx\right\} \qquad 1.11$$

where $\Delta s = S_2 - S_1$ is the barrier thickness, $\phi(x)$ is the barrier height above the metal Fermi level, and $\varepsilon(x)$ is the electron energy in X direction.

The following generalised formula which gives the tunnel current density in a M I M structure having a barrier of arbitrary shape has been given by Simmons(21).

$$J = J_0\{\bar{\phi}\exp(-A\bar{\phi}^{\frac{1}{2}}) - (\bar{\phi} + eV)\exp[-A(\bar{\phi} + eV)^{\frac{1}{2}}]\} \qquad 1.12$$

where

$$J_0 = \frac{e}{2\pi h(\beta\Delta s)^2} \qquad A = \frac{4\pi\beta\Delta s(2m)^{\frac{1}{2}}}{h}$$

$\bar{\phi}$ is the mean barrier height, Δs is the width of the barrier and β is a function of the barrier shape and is

usually approximately equal to unity. The above equation is derived for the electronic-energy distribution corresponding to absolute zero of temperature. Since the current density, J, is only very slightly temperature-dependent, this equation is also suitable for use at higher temperatures; nevertheless, the tunnel current at T°K is given by:

$$J(V,T) \simeq J(V,0)\left[1+ \frac{3\times10^{-9}(\Delta s T)^2}{\bar{\phi}}\right] \qquad 1.13$$

where J(V,0) is the current density at 0°K, ΔS is expressed in angstroms, $\bar{\phi}$ in electron volts, and T in degrees Kelvin.

Finally, for an ideal symmetric tunnel junction, and at high voltages equation 1.12 reduces to the Fowler-Nordheim form:

$$J = J_{FN}\,\frac{E^2}{\phi}\,\exp\left(-\beta_{FN}\frac{\phi^{3/2}}{E}\right) \qquad 1.14$$

where J_{FN} and β_{FN} are constants, ϕ is the height of the rectangular potential barrier, in that the effect of image force is neglected, and E is the field in the insulator.

1.4.4. Impurity Conduction

In an insulator having impurity levels within the forbidden gap, electrons may move from one occupied defect site to the next unoccupied one by either thermally activated hopping over a barrier height, by exchanging energy with phonons, and/or tunnelling through the potential barrier from one centre (full) to another (empty).

This type of current transport which occurs within the forbidden gap of the material is known as impurity conduction and was first observed by Hung and Gliessman[22] as a novel conduction mechanism predominant at low temperatures in doped germanium and silicon. Because of the low mobility of an electron in an impurity level at normal temperatures this process is more likely to be observed in a material having a low density of thermally-generated free carriers in the conduction band. It is also worth noting that in the case of doped semi-conductors, impurity conduction depends strongly on the concentration of donors or acceptors and conduction will only be possible if the material is 'compensated', i.e., both donors and acceptors are present[23].

For the hopping type of impurity conduction the current density has the form of:

$$J = J_h \, E \, \exp\left(\frac{-\Delta\varepsilon}{kT}\right) \qquad 1.15$$

where J_h is a function of the majority carrier concentration, E is the applied field, $\Delta\varepsilon$ the effective activation energy which is usually an order of magnitude less than that required to free an electron from a donor or a hole from an acceptor.

1.4.5. Ionic Conduction

In a dielectric the transference of the charged ions between the adjacent defect sites under the influence of an applied electric field is termed ionic conduction. The conduction mechanism is basically due to the jumps of ions (or vacancies) over a potential

barrier from one defect site to the next, separated by distance l. The applied electric field E lowers the potential barrier, ϕ, by an amount $Eel/2$ in the forward direction, and increases it by the same amount in the backward direction[24]. For a rather high electric field, $Eel \simeq kT$, the probability of ionic jumps in the backward direction can be ignored, and the current density is given by:

$$J = J_0 \exp(\frac{-\phi}{kT}) \exp(\frac{Eel}{2kT}) \qquad 1.16$$

Ionic conduction is usually recognised by having low mobilities and large activation energies in comparison with electronic conduction, with relatively higher mobilities and lower activation energies. This is indeed applicable in crystalline materials, but in the case of amorphous materials where the mobility may be very low and only the smallness of the activation energy remains, these distinctions may not be valid. However, the following properties of ionic currents should be noted:

(a) There will be polarisation effects in a direct field; i.e., the resistivity of the dielectric film at a constant direct voltage will increase with time.

(b) There will be transport of material from one electrode to the other, causing mechanical or chemical changes at the electrodes.

(c) The transit time for the ions will be large. This can be investigated by applying rectangular voltage pulses to the film and observing the delays in the current response.

1.4.6. Space-Charge-Limited Current Mechanism (SCLC)

When a suitable contact is applied to an insulator it should be possible to obtain injection of electrons from the metal-electrode into the conduction band of the insulator. This builds up a space-charge within the insulator and any further current flow through the insulator then will be limited.

At low applied voltages, if the injected carrier density, n_i, is lower than the thermally-generated free carrier density, n_0, Ohm's law is obeyed which gives the current density:

$$J = en_0\mu\frac{V}{d} \quad 1.17$$

where V is the applied voltage, μ the drift mobility of the charge carriers, and d is the thickness of the insulator. When the injected carrier density is greater than the free carrier density, the current becomes space-charge-limited.

However, two requirements need to be fulfilled in order to observe (SCLC) flow of significant magnitude(25).

(i) At least one of the two electrodes must make Ohmic contact to the insulator.

(ii) The insulator must be relatively free from trapping effects.

The mechanism of space-charge-limited currents in solids was first proposed by Mott and Gurney(24) who have given the following relationship for the simple case of one carrier trap-free SCLC in an insulator:

$$J = \frac{9}{8} \left(\frac{\mu \varepsilon \varepsilon_0}{d^3} \right) V^2 \qquad 1.18$$

where ε is the dielectric constant of the insulator, and ε_0 is the permittivity of free space.

When the insulator has localised trapping states in the forbidden gap, a large fraction of the injected space-charge condenses into the traps. Thus, only a fraction of the charge drawn into the insulator by the applied bias is available to conduct current. For a density N_t of shallow traps, all assumed to be at the same energy level E_t below the bottom of conduction band, the ratio of free charge to the trapped charge is given by:(25)

$$\theta = \left(\frac{N_c}{N_t}\right) \exp\left(\frac{-E_t}{kT}\right) \qquad 1.19$$

where N_c is the effective density of states in the conduction band, k is Boltzmann constant and T is the absolute temperature. Assuming $N_t = 10^{19}cm^{-3}$, $E_t = 0.25eV$ and taking $N_c = 10^{19}cm^{-3}$ at room temperature we have $\theta<10^{-5}$.

However, if only shallow traps are present, the current density given by equation 1.18 for SCLC flow must be multiplied by θ which reduces the current severely, thus:

$$J = \frac{9}{8} \theta \left(\frac{\mu \varepsilon \varepsilon_0}{d^3}\right) V^2 \qquad 1.20$$

Now, if sufficient charge is injected into the dielectric the traps can become filled and the current density in the diode will again be given by the Mott and

Gurney equation. The voltage at which this occurs is called the trap-filled-limited voltage, and is given by:

$$V_{TFL} = eN_t \frac{d^2}{2\varepsilon\varepsilon_0} \qquad 1.21$$

A typical J-V characteristic for an insulator having a shallow discrete trapping level is illustrated schematically in Fig. 1.8. As can be seen there are four discrete regions. These are (a) one in which the characteristic is ohmic, (b) a modified Mott and Gurney law due to the traps, (c) a trap-filled-limit region, and (d) a trap-free Mott and Gurney law.

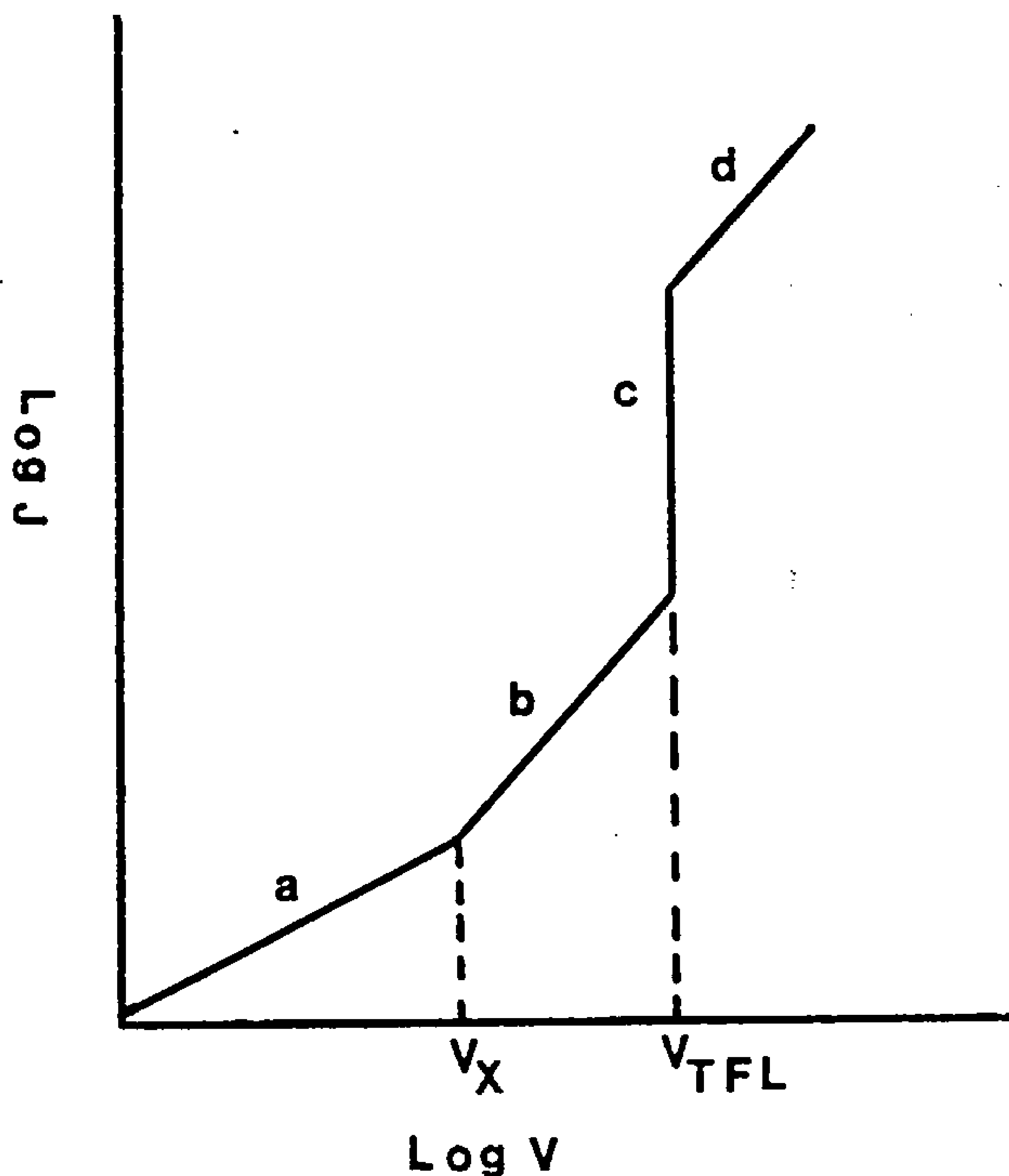

Fig. 1.8. One-carrier space-charge-limited J.V. characteristic for an insulator with shallow trapping centres.

In general, the traps will not be localised to 'shallow' levels as considered above and the form of the space-charge law will depend on the exact trap distribution. For a trap distribution whose density decreases exponentially as the energy from the band edge increases, the current density for the voltage V is given by:

$$J \simeq \frac{V^{n+1}}{d^{2n+1}} \qquad 1.22$$

where n is a parameter characteristic of the distribution of traps and d is the thickness of the specimen.

A general review about SCLC is given by Lampert and Mark[26].

CHAPTER TWO

AN INTRODUCTION TO ELECTROFORMING AND RELATED PHENOMENA IN MIM STRUCTURES

2.1 THE FORMING PROCESS

It is now well established that many thin insulating films sandwiched between two metal electrodes can, under certain conditions, undergo a forming process during which the electrical conductivity of the sample increases by some orders of magnitude (up to 10^8). Electroforming occurs when a voltage greater or equal to the forming voltage V_F, is applied across the device. Such samples subsequently display voltage-controlled negative resistance (VCNR), electroluminescence, electron emission into a vacuum and also switching and memory properties. The electroforming effect and negative resistance were first observed in Al-Al_2O_3-Ag system by Kreynina[2-27-28] and thereafter have been reported for many amorphous and polycrystalline insulating films with various combinations of metal electrodes and dielectrics such as oxides[29-30-31-32-85], halides[33], sulphides[34-90], polymers[35-36-37] and some organic compounds[38] fabricated by means of a variety of different techniques.

The forming process depends on several parameters which are given in the following:

(i) Atmospheric Environment. Forming is possible normally under ambient pressure of less than 10^{-2} torr, although

certain fluorides[39] and oxides[40-41] have been reported to be electroformed at atmospheric pressures. Hydrogen and inert gases appear to have less effect on the forming process than oxygen.

(ii) Temperature. The forming voltage V_F is rather insensitive to temperature, but the rate of forming (time taken for a sample to form) and the degree of forming (the maximum current that flows through the sample) depend on temperature. In other words, a sample formed at high temperature will form to completion at a faster rate and pass a higher current than if formed at a lower temperature. Verderber et al[42] reported that no Al-SiO-Au junction could be formed below 220°K and also that V_F decreased only 20% over a 300° increase in temperature.

(iii) Effect of Electrodes. Electroforming depends on the material of the positively biased electrode and the nature of the negatively biased electrode seems to be unimportant. Noble metals used as anodes readily allow forming to occur, but metals with a high chemical reactivity almost prevent it. Greene et al[33] found that the structure Al-SiO-M, where M chosen from Pd,Ir,Pt,Au,Ag, Cu,C,Si,Ni,Co,Fe,Sn, readily undergoes the forming transitions but forming is impossible for M based on Zn, Pb,Cr,In,Mn,Be,Al and Mg. However, electroforming has been observed in Al-SiO-Al sandwiches[43], although Verderber et al[42] had pointed out the impossibility of the forming process in this structure.

(iv) Insulator Thickness. Verderber et al[42] reported that the forming process is voltage controlled, i.e. V_F

does not depend on the thickness of the insulator, but Hickmott[44] describes this effect only for "dirty" oxides, whilst for "clean" oxides he claims that V_F is field dependent. "Dirty" oxide means that, in the technology used for the preparation, unknown impurities are involved. Electroforming tends to take longer for thicker samples, and it is not usually achieved for insulator thickness greater than 10,000 Å (d>10,000 Å). At the other extreme, with d<100Å, forming is also not possible. This is partly because a voltage V_F causes a field in the dielectric in excess of that for dielectric breakdown, and partly because electrode-electrode tunelling becomes significant[45]. However, the forming processes have been reported to occur in Al-Al_2O_3-Au samples with insulator thickness of only 24Å[46] and Hogarth and Taheri[47] observed forming effects in complex oxide devices with thicknesses up to 15,000 Å. The degree of forming decreases with increasing insulator thickness and obeys the approximate relation[45]

$$I_M \alpha d^{-3} \tag{2.1}$$

2.2. PROPERTIES OF THE FORMED JUNCTIONS

2.2.1. Voltage - Controlled Negative Resistance (VCNR)

Prior to forming and before applying a high electric field, the junctions are highly resistive and the conduction in the insulator is by one of the thermally activated mechanisms with I-V relation of the form $\mathrm{Ln} I \alpha V_b^{\frac{1}{2}}$, where V_b is the applied voltage. When V_b is

raised to some value of V_F a sudden increase in the current occurs, i.e. a decrease in sample resistivity. Reducing the voltage slowly to zero results in the permanent establishment of a VCNR characteristic. A typical d.c. I-V characteristic of a MIM structure exhibiting the VCNR at room-temperature in vacuum (curve OABCD) is shown in Fig. 2.1.

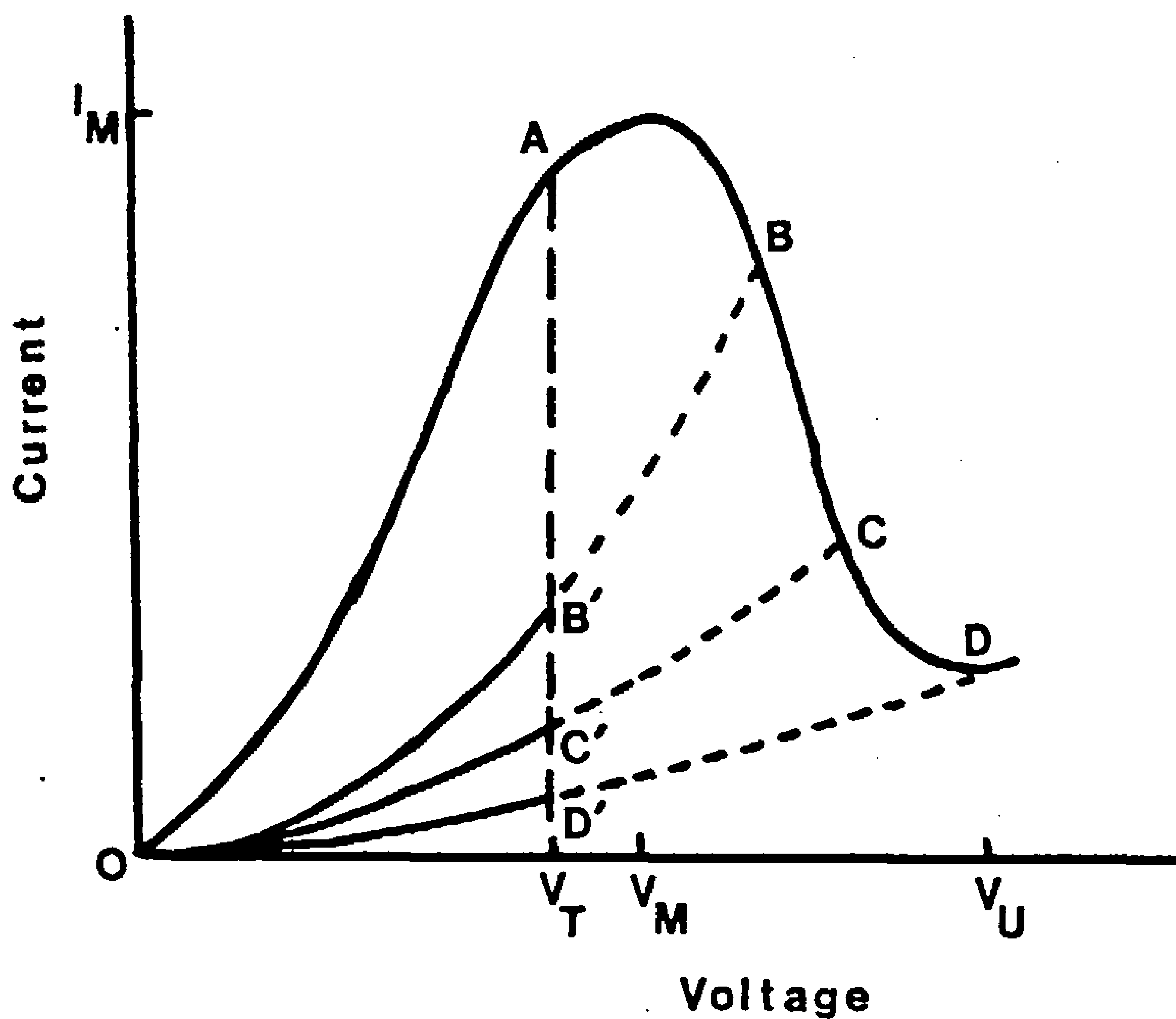

Fig.2.1. A typical I-V characteristic of an electroformed MIM structure.

The characteristic in the voltage range zero to approximately V_T is extremely stable and is described by the following relationship[30].

$$I = K \sinh kV \tag{2.2}$$

where K and k are constants. At higher voltages the current reaches a maximum value I_M at a voltage V_M. The

current then decreases with voltage approaching a valley position V_U. The a.c. characteristics do not show VCNR, but follow the curves OA,OB,OC or OD. The locus of the end points of these curves traces out the d.c. characteristic of the sample (Fig.2.1).

The common features of VCNR which have been established by many workers may be summarized as follows:

(i) V_M is approximately independent of the film thickness and temperature.

(ii) The maximum of the current I_M is higher for the increase than for the decrease of the voltage, V_b.

(iii) Current noise is usually observed above V_T and is appreciable in the negative resistance region and increases at higher temperature.

(iv) Once the device is electroformed, the I-V characteristics are more or less symmetrical with respect to voltage polarity at low pressures. At atmospheric pressure a polarity effect becomes noticeable.

(v) VCNR disappears in air, but inert gases as well as hydrogen have been found to have no significant effect on the I-V characteristics of the electroformed samples[48].

(vi) Negative resistance behaviour is destroyed at low temperatures, but can be re-established if the temperature is increased.

2.2.2. Electron Emission

Emission of electrons into a vacuum in MIM structures, can be detected after the development of VCNR. Hickmott[49] reported that electron emission in

$Al-Al_2O_3-Au$ developed simultaneously with conductivity for diode voltages of about 2V, which is less than voltages for the maximum current V_M, and appreciably less than the work function of the typical top electrode metals.

However, electron emission depends strongly on the bias voltage; at voltages below V_M there is very little emission but a sharp rise occurs at $V_b \simeq V_M$. Hogarth and Iqbal[89] (1979) found that, unlike the behaviour of many MIM structures, the rapid rise of emitted electron current in polypropylene thin films occurs not at a voltage corresponding to a current peak but a voltage corresponding closely to the initial forming voltage which is much higher than V_M. Hickmott examined electron emission for $Al-Al_2O_3-M$ diodes with five different top electrode metals (Au,Ag,Cu,Pb,In) and concluded that the dependence of the transfer ratio I_e/I_c (ratio of the emission current to the current circulating through the diode) is qualitatively the same. Thickening the top electrode,however, reduces the maximum energy of emitted electrons, as well as reducing their intensity for all diode voltages.

The emission is not uniform over the device area and appears to come from small localized regions. By means of an optical microscope, electron emission was observed to be uniform over the active area of the diode for voltages below 4.5V, but at higher voltages emission was localized [44-49]. Localized development of the electron emission of an $Al-Al_2O_3-Au$ sample during its lifetime has been demonstrated by Ahmed[50]. Taheri and

Hogarth[51] studied the electron emission of Ag-SiO/ B_2O_3-Ag(Cu) structures by means of the scanning electron microscope. They reported that emission of electrons occurred from the localized bright regions over the top electrode.

Simmons et al[52] and Gould and Collins[53] indicated that electrons which have undergone coherent scattering in the anode may only be emitted from pinhole edges. However, an important parameter associated with the emission is the attenuation length of electrons in the top-metal electrode. In other words, electrons entering the top electrode will be attenuated and the attenuation length, L, is given by the following relation:

$$\alpha = \frac{I_e}{I_c} = k \exp\left(-\frac{t}{L}\right) \qquad (2.3)$$

where α is the transfer ratio , t is the thickness of the top electrode and k is a constant. Hickmott[49] obtained $L \approx 200\text{Å}$ for $Al\text{-}Al_2O_3\text{-}Au$ and Gould, Hogarth and Collins[54] found values of L in the range 400 - 1000Å . The distribution of emitted electrons according to their total energy with respect to the film plane have been measured by Hrach et al[55] and Gould and Hogarth[56].

Electron emission is temperature-dependent and decreases with decreasing temperature[49]. At low temperatures, it can only be observed for voltages greater than V_M, but at very low temperatures no electron emission could be detected for all diode voltages.

2.2.3. Electroluminescence

Visible electroluminescence in MIM systems develops simultaneously with the development of VCNR and electron emission. The luminescence first appears at voltages just below V_M and increases rapidly with voltage, but unlike the electron emission, falls in the negative resistance region. The light intensity again increases slowly with applied voltage. Hickmott[49] showed, for $Al-Al_2O_3-Au$, that the light emitted appeared to be from the bright spots scattered at random on the diode. The majority of these spots were stable during repeated tracing of the I-V characteristic, although a few spots appeared or disappeared after a small number of traces. The spots were typically a few microns across and there was no conclusive evidence that they were the spots from which electron emission occurred. For $Al-Al_2O_3-Au$ diodes, the spectrum of electroluminescence covers the visible range with peaks at 1.8 eV, 2.3 eV and 4,0 eV, while in $Ta-Ta_2O_5$--Au samples, the light intensity is constant over most of the visible range, but has a maximum energy between 1.6 eV and 1.8 eV[44].

2.2.4. Memory Effects

(a) Voltage Memory.

If the voltage corresponding to any operating point on the negative resistance region (B,C,D in Fig.2.1) is turned off quickly (in less that 0.1 m sec) and then reapplied, the new characteristic will follow the path

OB', OC' or OD' and is essentially permanent, provided that the voltage does not exceed the threshold voltage V_T, which is rather less than V_M. The memory state is stable against mild heating and optical illumination and sometimes lasts for two years [45]. However, the original high-conductivity state, OA can be regenerated by applying a voltage slightly in excess of the threshold voltage. Simmons and Verderber[30] reported that for the Al-SiO-Au system, a voltage pulse longer than 10^{-7}sec was needed for switching from the high-impedance to low-impedance state, whereas a pulse of duration only $2x10^{-9}$sec was sufficient for the reverse process.

Before the sample can be returned to a high-conductivity state, a period of time, known as "dead-time", that may vary from microseconds to milliseconds must elapse. The dead-time is dependent upon temperature and the method of manufacture of the sample.

(b) Pressure-Voltage Memory

When an electroformed device is examined in an oxygen atmosphere, the current passing through the sample follows more or less the same I-V characteristic which is seen in vacuum, provided that the applied voltage does not exceed a certain threshold voltage, V_T. Increasing the voltage above V_T causes a decrease in the current and when the applied voltage is reduced to zero, a high-impedance memory state will be established[57-58-59]. After a considerable decrease in the pressure (say to 10^{-5} torr) the induced state of low conductivity can be erased on application of a voltage slightly higher than

V_T, after which the original I_c-V characteristic with VCNR is obtained.

(c) Thermal-Voltage Memory

Analogous to pressure-voltage memory, the electro-formed MIM structures can also exhibit a thermal-voltage memory. At low temperatures, VCNR can only be observed during the first voltage increasing across a formed device. On decreasing the voltage, the VCNR disappears and the current becomes a monotonic function of the voltage[30-58-60]. Any subsequent voltage cycling (fast or slow) of the sample, up to say V_u, at low temperature invariably generates the same high-impedance characteristic. Various high-impedance states can be induced at low temperatures simply by limiting the maximum applied voltage to lie between $V_b=V_T$ and $V_b=V_u$. These memory states are irreversible only if the sample is held at low-temperature; reheating the sample to room temperature and applying a voltage slightly greater than $V_b=V_T$ restores the original low-impedance characteristic.

2.3. MODELS OF THE FORMING PROCESS AND THE CONDUCTION MECHANISM IN FORMED DEVICES

We now survey the different mechanisms which have been proposed to explain the forming process and the associated phenomena in MIM structures.

2.3.1. Hickmott's Model

Hickmott made an extensive study of the forming and negative resistance phenomena on a number of different,

anodically prepared, MIM systems and was the first who suggested an explanation for the anomalous behaviour of these devices[61]. He assumed that, in the unformed state, a large number of immobile neutral impurity centres are distributed throughout the oxide layer with energy, E_I, approximately midway between the valence and conduction bands, Fig.2.2. The nature and number of these centres depend on the insulator and its method of preparation; they may be due to foreign atoms in the lattice or to structural faults.

When a voltage is applied across the device, Schottky emission over the contact barrier and Poole-Frenkel ionization of impurities will occur. As the applied voltage V_b reaches a critical value, V_F, the number of ionized impurity centres becomes large enough to form an impurity band in the insulator. Impurity ionization occurs nearly uniformly through the whole dielectric thickness and hopping conduction becomes significant through the impurity sites, indicated by (1) in Fig.2.2. In addition, modification of the metal-oxide interface (reduction of the barrier by means of the establishment of a positive dipole at the metal-oxide interface with the positive end of dipole in the oxide)[29] in such a way that electrons may pass readily into the insulator, without thermal activation, is a critical step in the forming which will depend on the metal electrodes. Therefore, the mobile charge carriers are electrons injected at the electrodes, but conductivity is controlled by positive impurity centres.

In order to explain the negative resistance, electroluminescence and electron emission an immobile acceptor level E_H has been postulated in the forbidden gap of the insulator between the impurity band and the valence band.

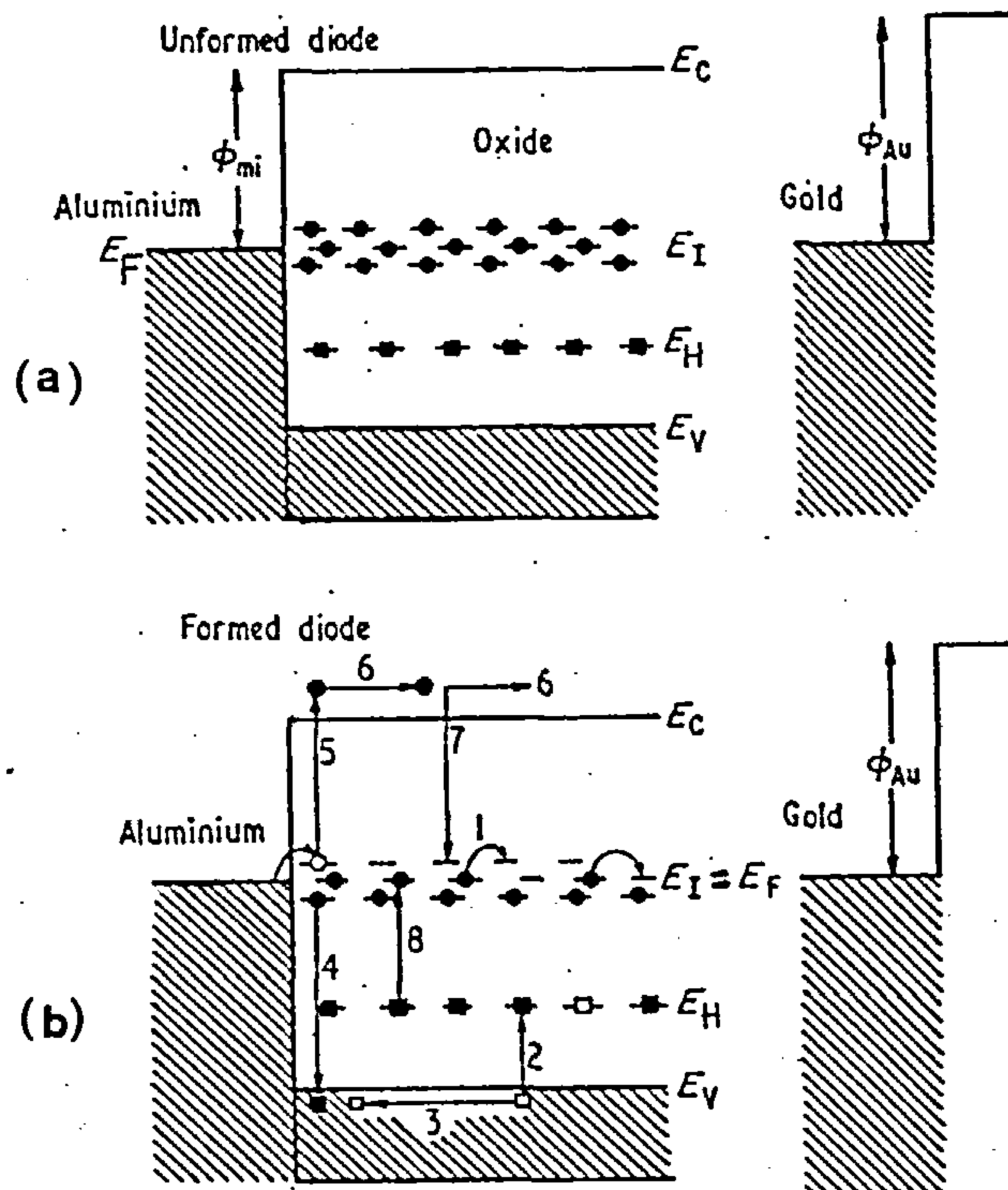

Fig.2.2. Schematic diagram of the energy band model of (a) the unformed state, and (b) the formed state of an Al-Oxide-Au diode (after Hickmott, ref. 61)

As the diode voltage is raised, in the high field region, free holes are created at the top of the valence band by electrons tunnelling to the acceptor level E_H,(2). A mobile hole moves towards the cathode under the influence of the high field (3). The hole then recombines with an

electron from the impurity band, (4), which in turn imparts its recombination energy to another electron trapped in an impurity state. This electron then can be excited into the conduction band of the insulator (5), where it is accelerated in the high field towards the anode (6). Electrons in the conduction band with sufficient energy to overcome the anode (Au) workfunction may be emitted into a vacuum while the other electrons can be captured by transition to the impurity band (7) giving light emission. Radiative transitions between the valence band, hole level E_H, and impurity band E_I can also contribute to the observed electroluminescence. The occurrence of the negative resistance at higher applied voltages is attributed to the neutralization of impurity sites by electrons tunnelling from the acceptor level to the impurity band (8). The processes of ionization and neutralization in the impurity band are equal at $V_b=V_M$, where a maximum in the I_c-V characteristic appears, followed by the VCNR region if the applied voltage is further increased.

2.3.2. The Model of Verderber, Simmons and Eales

Verderber et al[42] and Simmons and Verderber[30] have postulated that the forming process is caused by the homogenous injection of the positive metal ions from the anode into the insulator, where they introduce a broad band of localized levels within the forbidden gap. Fig. 2.3. shows the energy band diagram of an unformed MIM system at different bias voltages, V_b. At $V_b=0$, since

the metal workfunction ψ_m, is assumed to be larger than that of the insulator, ψ_i, the contacts between the metal electrodes and the insulator are blocking and electrons flow from the insulator to the metal electrodes. The establishment of the depletion regions of positive charge in the bulk of the insulator, in this way, is due to the ionizable centres in the unformed SiO which are provided by free silicon atoms. The charge accumulation, however, causes a local field to exist within the surface of the insulator which, in turn, results in bending the bottom of the conduction band downwards until it lies at energy ϕ_b, above the Fermi level, and is known as the bulk activation energy of the unformed insulator. Unlike metals, the workfunction of the insulators are not well defined, but may be given by

$$\psi_i = \chi_i + \phi_b \tag{2.4}$$

where χ_i is the electron affinity of the insulator. The barrier height, ϕ_o, at the metal-insulator interface is

$$\phi_o = \psi_m - \chi_i \tag{2.5}$$

and the field at the metal-insulator interface can be written as follows

$$E = \left(\frac{n_d e^{\frac{1}{2}}}{2\,\varepsilon\,\varepsilon_o}\right) (\phi_o - \phi_b - V_d)^{\frac{1}{2}} \tag{2.6}$$

where V_d is the voltage drop across the depletion layer, n_d is the density of ionizable centres, ε is the dielectric constant and ε_o is the permittivity of free space.

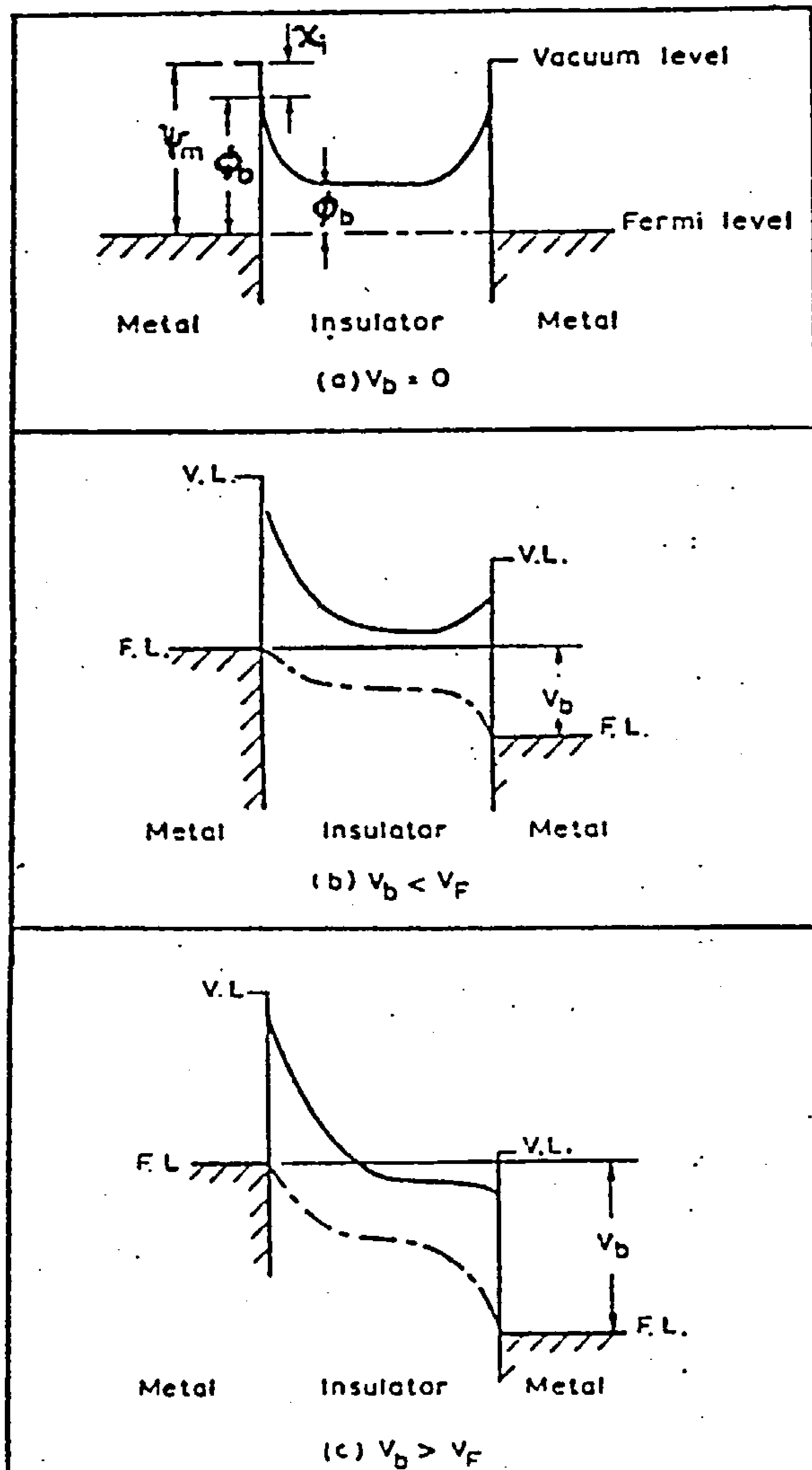

Fig. 2.3. An energy band diagram of the unformed device for various bias voltages; (a) V_b=0; (b) V_b<V_F, and (c) V_b>V_F (after Verderber et al, ref. 42)

The energy band diagram for the unformed system under voltage bias for V_b<V_F is shown in Fig.2.3.-b. The effect of the voltage bias is to increase the field and the width of the depletion region at the negatively biased electrode, and to decrease them at the positively

biased electrode. When the applied voltage across the diode reaches a critical value $V_b=V_F$ the retarding field at the anode-insulator interface, which prevents the ions from the anode entering the insulator, vanishes and consequently the ionic injection starts, Fig.2.3.-c. The injected positive metal ions from the anode are free to migrate throughout the insulator. According to equation 2.6, the field at the interface becomes zero when

$$V_d = \phi_o - \phi_b \qquad (2.7)$$

If we assume that a similar voltage is established across the depletion region at the cathode, therefore we have

$$V_F = 2\ V_d = 2(\phi_o - \phi_b) \qquad (2.8)$$

since ϕ_o and ϕ_b are constants independent of oxide thickness and donor density; thus V_F is unlikely to be affected by variations in the evaporating procedure, and the insulator thickness. However, the slight increase in the forming voltage with insulator thickness which has been observed is thought to be due to the small voltage drop across the bulk of the insulator which, of course, increases with the thickness. Furthermore, from equation 2.8 in the case of ϕ_o=3eV and ϕ_b=0.4eV we have V_F=5.2eV which is in a good agreement with the experimental observations. The degree of forming is postulated to be due to the solubility of the metal ion in the insulator which in turn depends on the defect nature of the insulator. The facts that the number of vacancies increases rapidly with temperature, and that the rate of ionic migration

falls off rapidly with decreasing temperature, explain qualitatively the temperature dependence of the rate and degree of forming.

In order to explain the electrical properties of the formed diode, it has been suggested that[30],(i) as previously pointed out, the injection of gold ions into the amorphous insulator provides a broad impurity band with a sharp defined top edge at the level ϕ_i (with respect to the Fermi level) in the forbidden gap of the insulator as is illustrated in Fig.2.4.a. This is in contrast with the case for an insulator having crystalline structure in which a discrete energy level, instead of a broad band, would be produced. (ii) The metal ions act as donor centres, neutral when filled and positive when empty. It is further assumed that the impurity density is so high (greater than $10^{19} cm^{-3}$) that electrons penetrating the barrier ϕ_o tunnel from one centre to another at levels which are very nearly equal in energy.

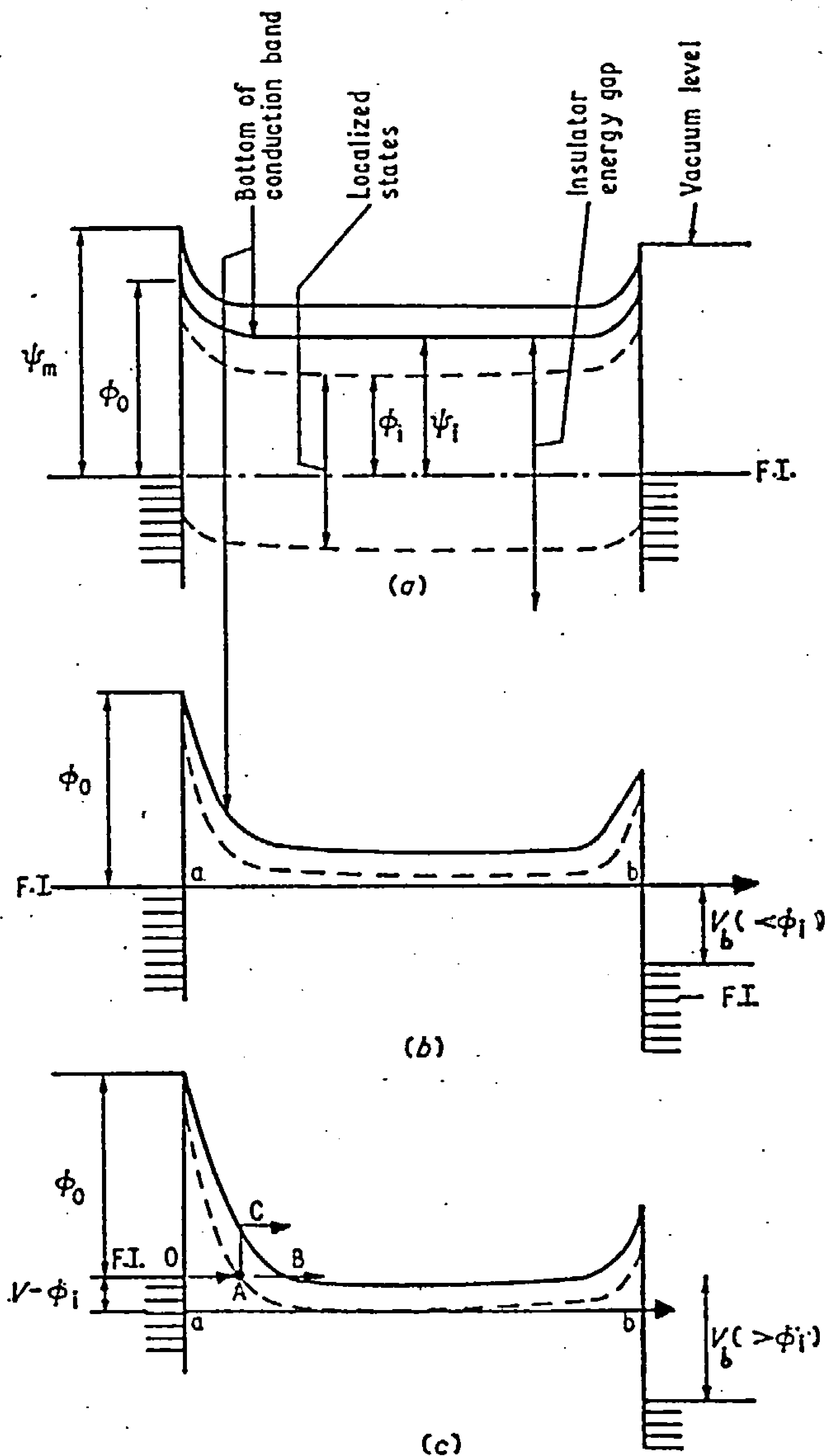

Fig.2.4. Energy diagram of a formed MIM structure for various bias voltages: (a) $V_b=0$; (b) $V_b<\phi_i$; (c) $V_b>\phi_i$ (after Simmons et al, ref.30)

For $V_b<\phi_i$, the electrons coming from the cathode pass through the insulator at the energy level equal to the Fermi level in the cathode. The line ab in Fig.2.4.b illustrates the passage of an electron through the

insulator which has been injected from the electrode. For applied voltages greater than ϕ_i, an electron injected from the Fermi level can penetrate the insulator only as far as the top of the localized band (A in Fig.2.4.c), and hence does not contribute to the conduction process. Only electrons on energy levels more than $V_b-\phi_i$ below the cathode Fermi level can still create the conduction current. Since the contribution to the current falls off rapidly with energy below the Fermi level, then the current through the device decreases with voltage. The maximum in the I-V characteristic appears for $V_b=\phi_i$, and is thus independent of the insulator thickness, which is in accordance with experimental results. However, at sufficiently high voltages, the electron arriving at the top of the localized level (Fig.2.4.c) can either tunnel (AB) or be thermally excited (AC) into the conduction band of the insulator. These two processes are thought to be responsible for the rising tail observed in the I-V characteristic for applied voltages greater than the valley voltage V_u in figure 2.1.

The electron emission for applied voltages less than that corresponding to the work function of the top-electrode is explained by electrons obtaining excess energy from the lattice of at least 1 eV[62]. Electrons at the top of the localized level can be excited into the conduction band by acquiring an energy $E_i=\psi_i-\phi_i$ from the lattice. These electrons are then accelerated in the conduction band, and those which do not lose any energy in the insulator will enter the anode having an energy

eV_b+E_i above the Fermi level. They can escape into the vacuum providing $eV_b+E_i>\psi_m$. The emission current is a fraction of the excited electrons into the conduction band of the insulator and is given by

$$I_e = e\, n_i \exp\,[-(E_i-\Delta E)/kT] \qquad (2.9)$$

where n_i is the number of electrons arriving at A (Fig. 2.4.c) per unit time and ΔE is the Schottky lowering of the barrier E_i. n_i and $\Delta E \alpha V_b^{\frac{1}{2}}$ are increasing functions of bias voltage and therefore it is clear why the emission current increases with voltage even in the negative resistance region.

The memory and switching phenomena have been described within this model by means of an electronic charge storage hypothesis. For the applied voltages greater than ϕ_i, across the device, electrons enter the insulator from energy levels extending from $E_1=E_F-(V_b-\phi_i)$ to $E_2=E_F$ (in eV). These electrons will then be trapped and stored in the localized levels near the top of the localized band, for example, as indicated by the points a b c d in Fig.2.5.a. When the voltage is reduced slowly to zero the stored charges will have sufficient time to leak out via the anode and hence the device remains in its original state. But if the voltage is reduced quickly to zero the stored electrons remain undisturbed in the same localized state they occupied under voltage bias for a period of time equal to $(\nu P)^{-1}$,where ν is the attempt-to-escape frequency and P is the tunnelling probability between adjacent sites. In general, P includes the factor $\exp\,(\frac{-\Delta\varepsilon}{kT})$, where $\Delta\varepsilon$ is the energy difference between the

two tunnelling sites. It will be noted that in Fig.2.5.b the electrons are stored in higher energy states than those into which they were injected. However, the electrons will eventually diffuse out of these storage levels, by a phonon-assisted tunnelling mechanism, and drift towards the centre of the insulator (that is, the direction of decreasing the potential barrier heights) where they become permanently stored, as shown by the points a' b' c' d' in Fig. 2.5.c. These stored electrons do not drop down below the Fermi level or to a lower energy site, because of the large $\Delta\varepsilon$ and consequently the very low probability for such a transition. The effect of the stored charge is to distort the band structure of the insulator and reduce the field at the metal-insulator interface by a factor of $\frac{en_s}{2\varepsilon}$ where ε is the dielectric permittivity and n_s the number of the stored electrons. The reduction of the field at the interface decreases the current passing through the system (i.e. increase in the impedance). The greater the applied voltage before being reduced quickly to zero, the higher the number of stored electrons n_s and the lower the field at the interface and hence the higher the impedance of the induced state. Therefore, an indefinite number of high impedance states can be induced, as has been observed experimentally.

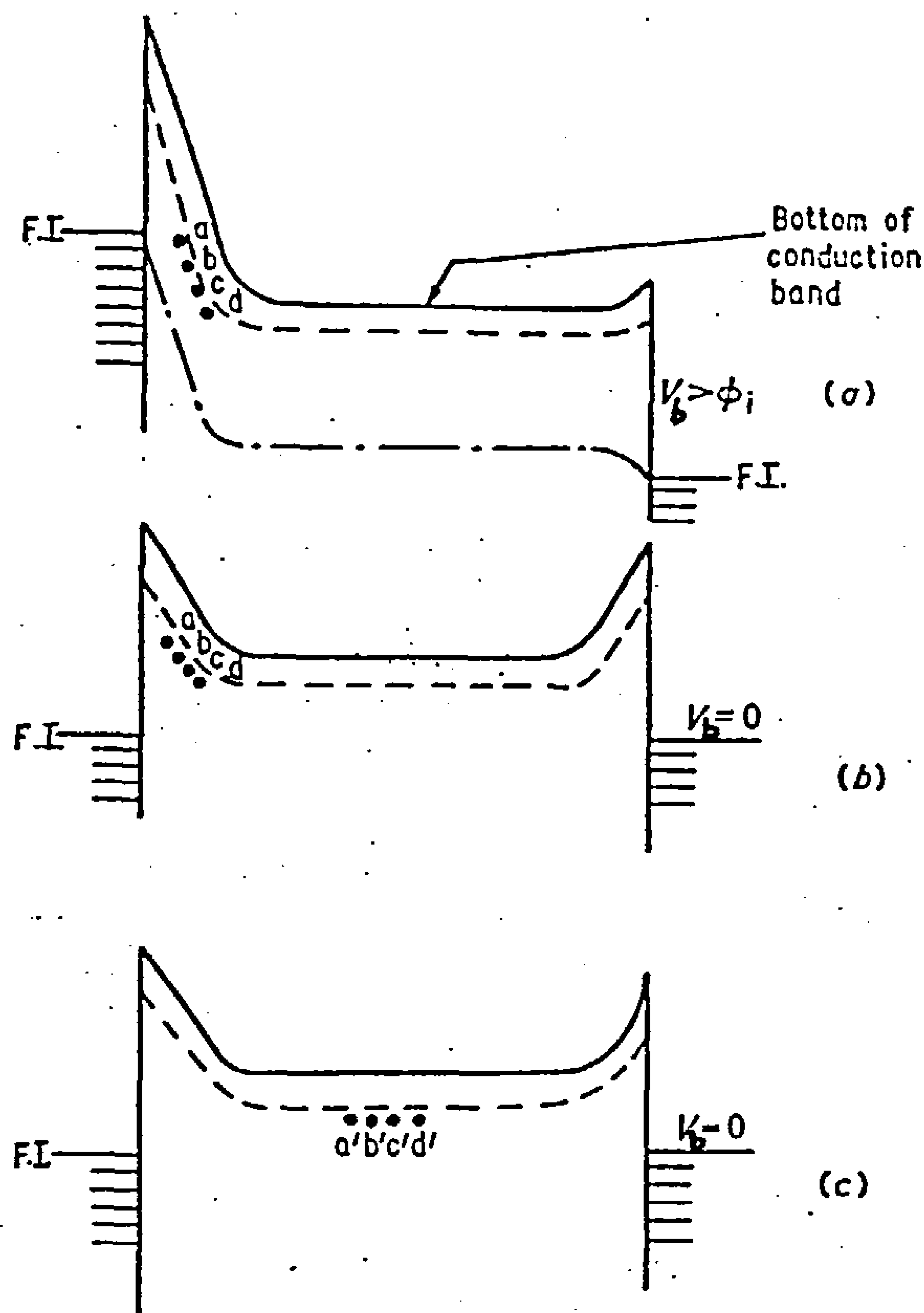

Fig.2.5. The energy diagram of a M-I-M structure showing the position of the stored charge relative to the Fermi levels (a) at a voltage bias $V>\phi_i$; (b) immediately after removal of the applied voltage in a time $t<(\nu P)^{-1}$; and (c) after elapsing a time $t>(\nu P)^{-1}$ (after Simmons et al, ref 30)

The erasure of the memory state may occur, at a threshold voltage $V_b \simeq V_T$, when the Fermi level of the cathode approximately lines up with the stored charge level. The concentration of the electrons near the cathode then exceeds the stored charge concentration, and the presence of this concentration gradient of electrons in

equivalent energy levels causes the stored electrons to be swept away towards the anode giving rise to the recovery of the low-impedance state in the diode.

As was mentioned earlier, the stored electrons in position a b c d, in Fig.2.5, need a period of time equal to $(\nu P)^{-1}$ to reach the position a' b' c' d'. However, if the applied voltage inducing a memory state is removed and reapplied in a time less than $(\nu P)^{-1}$, the stored electrons will not have sufficient time to reach the centre of the insulator. Therefore, $(\nu P)^{-1}$ is simply a measure of the dead-time associated with the switching effect. It is also worth noting that since P is the phonon-assisted tunnelling probability, thus it is temperature dependent.

Thermal voltage memory in this model has been described in terms of "dead time". At sufficiently low temperatues, since P becomes small, $(\nu P)^{-1}$ will be very large. Therefore, if the applied voltage, in the negative resistance region, is reduced to zero (either slowly or quickly) the stored electrons are unable to diffuse to the middle of the insulator and will remain in the states (even for $V_b > V_T$) into which they were injected under the voltage bias. However, the memory state can be erased by reheating the device to room temperature and applying a voltage slightly greater than V_T.

2.3.3. The Model of Greene, Bush and Rawlings

Greene et al[33] suggested that a high-field electrolytic process involving the insulator is responsible for the electroforming process. Anion vacancies are assumed to be injected into the insulator, giving rise to localized conduction paths through the layer provided that the insulator has a sufficient number of defects such as dislocations, grain boundaries and point defects.

For a hypothetical insulator MX consisting of M^+ and X^- ions, the electrolysis occurs normally under low-field conditions, with inert electrodes in an inert atmosphere. The reactions at the anode and cathode are

$$X^- \rightarrow \frac{1}{2} X^2 + e^- \qquad \text{(anode)} \qquad A$$

$$M^+ + e^- \rightarrow M \qquad \text{(cathode)} \qquad B$$

In reaction (A) the neutralized anions are given off which explains the evolution of oxygen from oxides and fluorine from fluorides. However, at high electric fields electrons are injected into the anion vacancies near the cathode.

$$\square_x + e^- \rightarrow \boxed{e^-}_x \qquad (C)$$

where $\square_x$ and $\boxed{e^-}_x$ represent the anion vacancy and the vacancy with a trapped electron, respectively. Further vacancies are produced by the discharge of x^- ions at the anode, and the diffusion of vacancies under the influence of the electric field establishes chains of defect centres (F-centre type) across the insulator

which results in the electro-forming of the device. Conduction in the formed device then occurs by the tunnelling of electrons through the chains of diffusing F-centres. However, forming does not occur uniformly over the whole area of the sample, but only in highly localized regions where the insulator is originally far from perfect. Since ionic motions are involved, the forming process is temperature-dependent.

The influence of oxygen on electroforming has been explained by the following reaction at the cathode

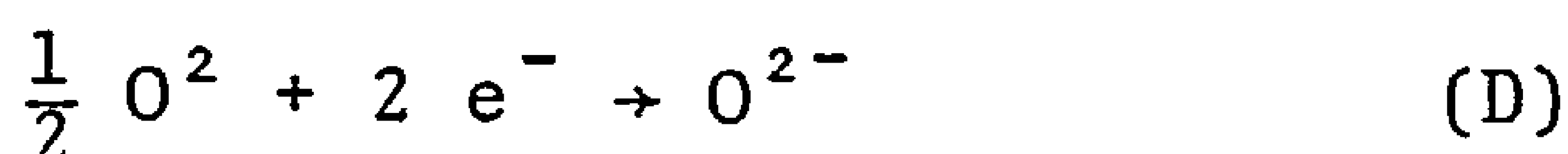

$$\frac{1}{2} O^2 + 2 e^- \rightarrow O^{2-} \qquad (D)$$

which competes with the reaction (C) and at sufficiently high pressure of ambient oxygen (C) will not take place, and hence forming cannot occur.

If the anode metal (Ma) is chemically reactive, an alternative to reaction (A) occurs at the anode which gives rise to ionization and injection of the metal atoms into the insulator

$$Ma \rightarrow Ma^{n+} + ne^- \qquad (E)$$

if the rate of entering of material into the insulator by reaction (D) and (E) exceeds the rate of material leaving the bulk according to the reactions (A) and (B), then the insulator thickness and the high-electric field which is necessary for the reaction (C) to occur falls and consequently the electroforming will be inhibited. Therefore, by reducing the ambient oxygen pressure and using less reactive materials for the anode, the optimum condition for the forming process could be obtained.

The memory and negative resistance phenomena may be explained in terms of a trapped space-charge produced when the applied voltage is sufficient to give some electrons enough energy to leave the conducting path and enter the surrounding unformed dielectric.

Electron emission is caused by electrons in the conduction band which are accelerated by the electric field to an energy sufficient to overcome the barrier at the anode.

2.3.4. The Model of Barriac, Pinard and Davoine

This model involves the injection of ions from the anode, giving ionic conduction and the space-charge needed for the mechanism of differential negative resistance[63]. When a voltage is first applied across the diode, at some values of the electric field, small sparks are assumed to be generated at the thinnest region of the film which causes the release of considerable heat. The perforation of the anode by local melting and evaporation then occurs, where positive ions enter the cracks which appear in the insulator. These positive ions migrate towards the cathode, under the influence of the applied field, where they create a layer of positive space-charge. The space-charge perturbs the field in such a way that almost all the applied potential is dropped across a narrow region, δ, which is much smaller than the whole insulator thickness, d. The effective field in the cathode region is thus $\frac{V}{\delta}$ and when δ reaches to a saturating value Δ, the effective field is replaced by $\frac{V}{\Delta}$, the level at which

tunnelling of electrons from the cathode begins. Since the tunnelling electrons have low energy, the majority of them cannot surmount the "ionic barrier" and contribute to the total current, but recombine with positive ions, i.e. neutralization of the space-charge. The bonding between the positive and negative carriers is of a chemical nature and is unstable in the absence of a sufficient maintaining field. As a result of the charge recombination, the total current through the device decreases and causes the VCNR to appear in the I-V characteristic.

The foregoing processes are applicable in four different voltage ranges and the I-V characteristic of the device can be divided into four zones as shown in Fig.2.6. At voltages $V<V_1$, the current is due to the migration of positive ions and is given by

$$I_1 = A \exp(\alpha V) \tag{2.10}$$

where $$\alpha = \left(\frac{\lambda s}{\delta}\right)\left(\frac{e}{kT}\right) \tag{2.11}$$

and $$A = 2\lambda_s \nu n \exp\left(-\frac{U_s}{kT}\right) \tag{2.12}$$

ν is the ionic vibration frequency, n the density of ionic carriers, U_s a surface activation energy and λ_s is the surface diffusion length of the ions.

At voltages $V_1<V<V_2$ the conduction is still ionic but the thickness δ of the space-charge layer saturates to a constant value Δ. The current is given by

$$I_2 = A \exp(a V) \tag{2.13}$$

where $$a = \left(\frac{\lambda s}{\Delta}\right)\left(\frac{e}{kT}\right) \tag{2.14}$$

At voltages $V_2<V<V_3$, the effective field near the cathode becomes sufficiently large so that tunnelling of electrons from the cathode into the space-charge layer becomes significant, but the saturated value of δ still persists. Assuming all the tunnelling electrons become trapped, the ionic current I_{ionic} then will be reduced by an amount equal to tunnelling current I_t. The net current is thus given by

$$I_3 = I_{ionic} - I_t \tag{2.15}$$

$$I_3 = A \exp(aV) - BV^2 \exp\left(-\frac{b}{V}\right) \tag{2.16}$$

where $$B = S\frac{e^3}{8\pi h\phi\Delta^2} \tag{2.17}$$

and $$b = \frac{8\pi\phi^{3/2}(2m)^{1/2}\Delta}{3eh} \tag{2.18}$$

S is the metal surface workfunction, ϕ the metal-insulator barrier height, e and m the electronic charge and mass and h is Planck's constant.

In the fourth zone ($V>V_3$), the ionic space-charge becomes increasingly neutralized and the thickness Δ begins to increase. This causes a decrease in the field at the interface and thus in the tunnelling current, so that the rate of decrease of the net current is diminished. The current in zone 4 is given by

$$I_4 = A \exp(\alpha V) - B' V^2 \exp\left(-\frac{\beta}{V}\right) \tag{2.19}$$

where $$B' = S\frac{e^3}{8\pi h\phi\delta^2} \tag{2.20}$$

and $$\beta = \frac{8\pi\phi^{3/2}(2m)^{1/2}\delta}{3\ eh} \tag{2.21}$$

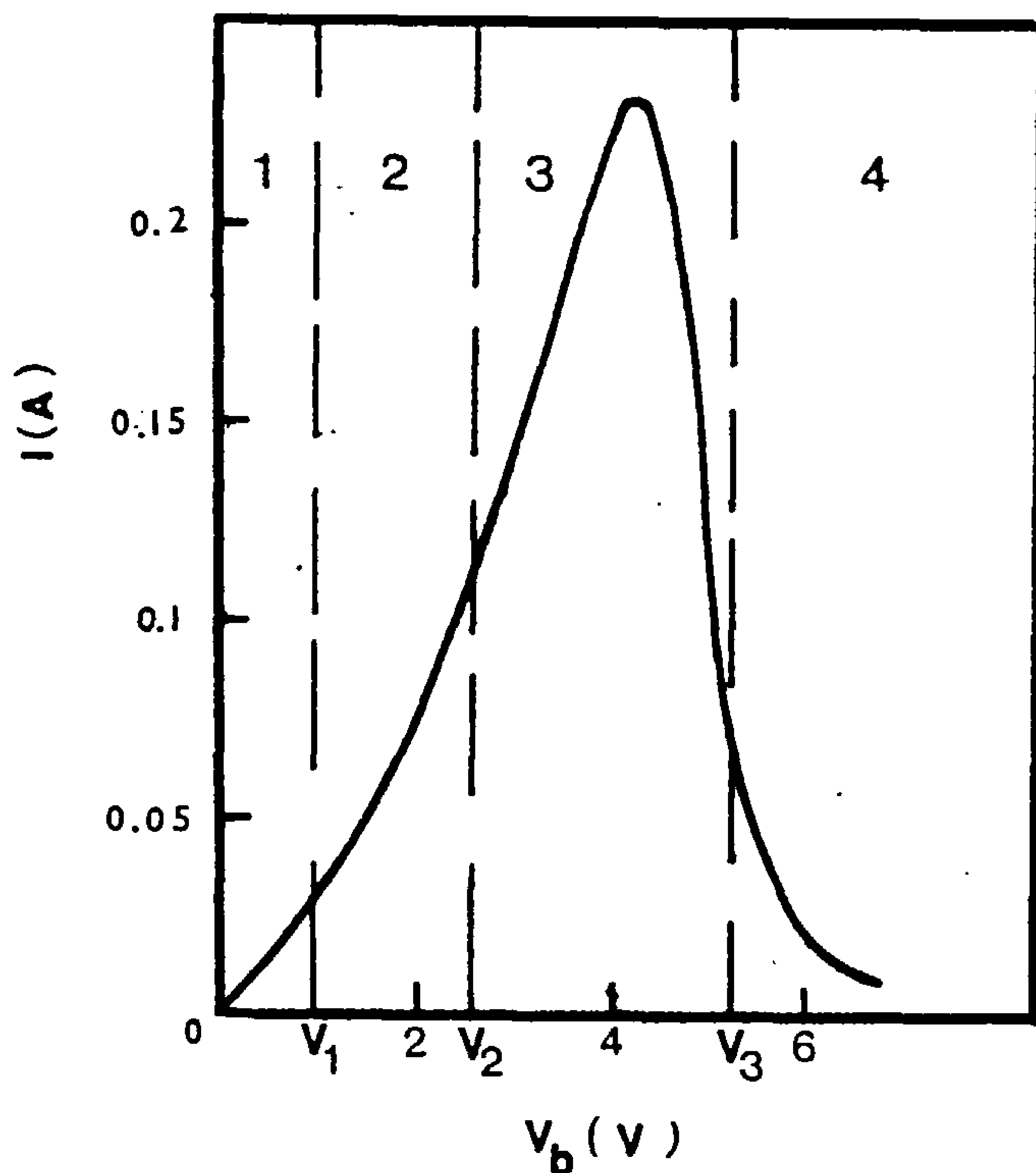

Fig. 2.6. Zones of schematic curve of I_c as a function of V_b (after Barriac et al, ref. 63)

This theory also predicts the value of the voltage for maximum current, V_M. Since the peak current occurs in zone 3, V_M can be found from the zero of dI_3/dV. This is dependent on all the constants, a, A, b and B and since a and A are temperature dependent, this model predicts a temperature dependent value of V_M.

The effect of oxygen is considered to arise from its penetration into pores and cracks where the following relation occurs,

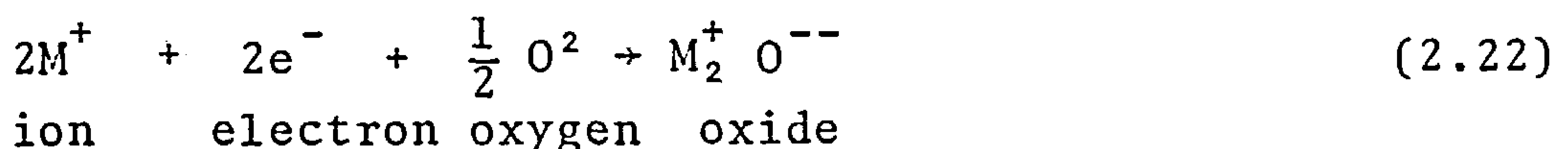

$$\underset{\text{ion}}{2M^+} + \underset{\text{electron}}{2e^-} + \underset{\text{oxygen}}{\tfrac{1}{2}O^2} \rightarrow \underset{\text{oxide}}{M_2^+ O^{--}} \qquad (2.22)$$

Thus forming a stable metallic oxide which inhibits the

forming process.

Electron emission takes place when the electrons have sufficient energy, after passing the "ionic barrier", to overcome the workfunction of the anode.

2.3.5. The Model of Dearnaley, Morgan and Stoneham

This is a novel model, based upon the development of many conducting filaments through the insulating layer during the electroforming process, which has been proposed to account for the observed behaviour of metal-oxide-metal structures[64-65]. Dearnaley et al have stated [45-65] that the boundary between the insulator and top electrode is not smooth, resulting in places with an enhanced electrical field which causes the structural changes in the insulator. At these places (nucleation sites) conducting filaments can grow across the insulator until the two electrodes are bridged. Although the precise structure of the filament is not well understood, the growth of chains of metal atoms alternating with anion vacancies is a possibility[64]. It has also been suggested that the filaments growth in SiO_x[64-66] materials can be due to the overlap in the π-orbitals in Si-O-Si chains. However, the filaments are not considered to be perfectly uniform, but having at least one weak spot which determines their resistance. They also exhibit ohmic conduction, with negligible thermal activation energy, because the sites involved are supposed to be close enough together so that hopping without activation may occur.

Once the device is electroformed (i.e. the development of the filaments) the current through each filament and its temperature, T, both increase with the voltage bias. Filaments begin to rupture at their weakest points when T exceeds some critical value T_{max}. The number of broken filaments increases rapidly for $V_b > V_M$ resulting in the appearance of VCNR in the I-V characteristic. The filaments can re-join but this depends upon their temperature, the ambient temperature, the electric field and possible space-charge effects. The temperature T, and the resistance ρ of each filament are supposed to be associated with the local regions of high resistance on a high conducting filament. Two terms contribute to changes in T, one due to the Joule heating and the other to heat loss to the insulator which is assumed simply to be proportional to the temperature difference between the filament and its environment. Therefore, the local temperature T can be given by

$$\frac{dT}{dt} = \alpha\frac{V^2(t)}{\rho} - \frac{1}{\tau_c}(T-T_o) \qquad (2.23)$$

where α measures the heating and τ_c characterizes the cooling. At a voltage V, and in the steady state situation $\frac{dT}{dt} = 0$, we have from equation 2.23

$$\rho = \frac{\alpha\tau_c V^2}{T-T_o} \qquad (2.24)$$

As the applied voltage V is increased the filaments having low resistances rupture and conduction takes place through the filaments with resistances greater than a minimum value ρ_{min} given by

$$\rho_{min} = \frac{\alpha\tau_c V^2}{T_{max}-T_o} \tag{2.25}$$

and thus the total current is

$$I = \int_{\rho_{min}}^{\infty} \frac{V}{\rho}\, p(\rho) d\rho \tag{2.26}$$

where $p(\rho)$ gives the probability distribution of the various resistances, and

$$\int_0^{\infty} p(\rho)\, d\rho = 1 \tag{2.27}$$

The detailed shape of the I-V characteristic is determined by $p(\rho)$. Since devices can be cycled below V_T without showing signs of filament breaking, therefore there can be very few filaments with resistances below ρ_T, given by

$$\rho_T = \frac{\alpha\ \tau_c\ V_T^2}{T_{max}-T_o} \tag{2.28}$$

similarly there are few filaments with resistances above ρ_U

$$\rho_U = \frac{\alpha\ \tau_c\ V_U^2}{T_{max}-T_o} \tag{2.29}$$

where V_U is the voltage at which the current has a minimum. Above V_U the current is close to that of the unformed device and the filamentary conduction cannot be appreciable.

Dearnaley et al have plotted the distribution function for filament resistances, $p(\rho)$, from

$$\frac{p(\rho)}{\rho} \sim \frac{d(I/V)}{d(V^2)} \tag{2.30}$$

which gives an approximately triangular distribution as is shown in Fig.2.7.

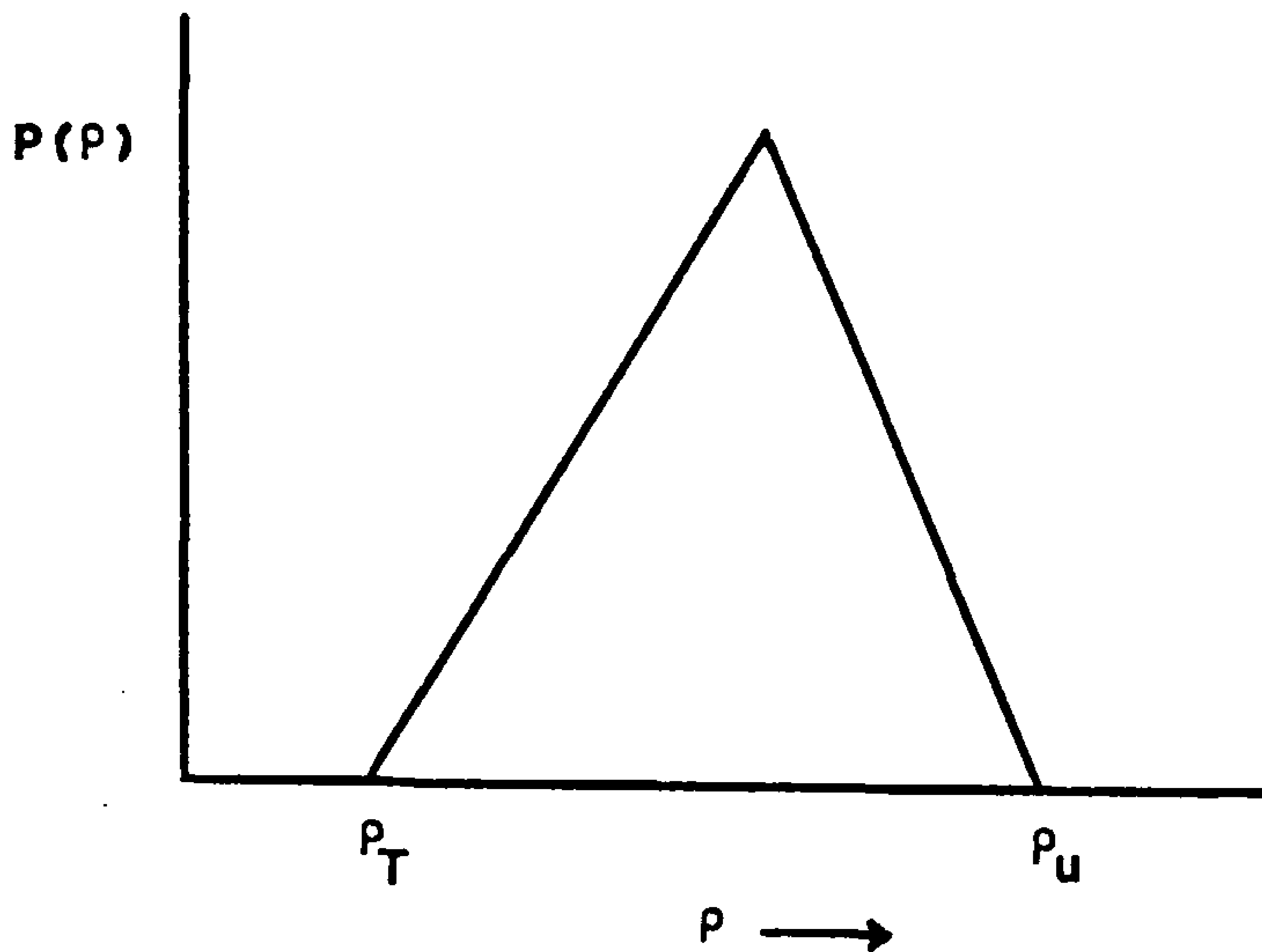

Fig.2.7. The simple triangular distribution of filament resistances.

The number of filaments per unit area, N, can be estimated by assuming that all filaments have the same resistance, ρ. The initial resistance of the device per unit area is ρ/N, and the filaments all burn out when $V \approx V_{max}$. Thus, from equation 2.24

$$\rho \sim \frac{\alpha\ \tau_c\ V_{max}^2}{T_{max} - T_o} \tag{2.31}$$

the cooling time, τ_c, is estimated by regarding each filament as a cylinder of radius r and temperature T cooling to a cylindrical sink of radius R and temperature T_o, it has been shown that

$$\alpha\ \tau_c = \frac{\mathrm{Ln}(R/r)}{4.18 \times 2\pi K L} \tag{2.32}$$

where K is the thermal conductivity of the insulator and L is the length of the filament. By combining equations 2.31 and 2.32 and introducing reasonable values for the

parameters, e.g. an initial resistance of $\rho/N = 5\Omega$, $L = 400\text{Å}$, $K = 0.002$ cal/cm^{2}sec.°K, $(T_{max}-T_o) = 1000$°K and $r \sim 10\text{Å}$, Dearnaley et al found ρ, the mean resistance per filament, to be $2.5\times10^7\Omega$ and $N = 5\times10^6$ filaments per cm^2.

Electron emission is believed to come from those filaments, in which almost all the voltage drop is in the weakest region situated near the anode. Energetic electrons generated in the weak spots are accelerated and enter the top electrode where they emerge into a vacuum.

Electroluminescence which occurs in scintillating pinpoint regions over the surface of the top electrode is thought to be due to the electrons released from filaments at their weak spots and scattered into the wide band-gap of the insulator, giving rise to radiative transitions.

"Dead time" which is assumed to be a measure of the time between the filament breaking and reaching a state from which it may re-form, has also been predicted in this model. During the rupture of the filament at a weak spot, electrons are scattered into the surrounding matrix where they will be trapped. The insulator then becomes highly "polarized" locally and will return to equilibrium after a period of time by a thermally-activated process, such as Poole-Frenkel emission from the traps. The filaments may then regrow by ionic migration in the electric field.

At low temperatures, depolarization of the insulator takes quite a long time and thus, if a device is cycled above the negative resistance region, reforming of the broken filaments will not occur and the device remains in

its high-impedance state. However, depolarization and consequently filament re-formation (under the influence of a sufficient field) takes place when the device is heated up to room temperature. The reason why switching from the low to the high-impedance state is rapid ($\sim 10^{-9}$sec), compared with switching from the high to low-impedance state which is relatively long ($\sim 10^{-7}$sec) is that, in the former case the controlling mechanism is the scattering of "hot" electrons leading to the polarization of the insulator, while in the latter ionic migration must take place and this is a much slower process.

Finally, the current fluctuation in the device which is large over the range of voltage, between V_T and V_U can be related to the continuously rupturing and re-forming of the filaments in this region.

2.3.6. The Model of Ralph and Woodcock

This model is a modification of the filamentary model and suggests that a complicated electronic process rather than a simple ohmic conduction can account for the conduction mechanism inside a filament.

According to Ralph and Woodcock[67] each filament contains an impurity band, similar to that of a heavily disordered semiconductor, which shows mobility edges at both the top and bottom of the band, giving rise to a mobility bandwidth which is less than the density-of-states bandwidth. All the states between the mobility edges and the density of states edges are localized and act as traps and recombination centres with a wide range

of lifetimes associated with different environmental conditions. The distribution of states into localized and non-localized regions appears to be determined by the ratio V_o/J, where $V_o{}^2 = \langle V^2 \rangle$ is the random excess potential at each impurity site and may arise from imperfections or the compensating charge centres, and J is the bandwidth which would occur in a perfect crystal due to overlap of the individual state wavefunctions. It is also proposed that due to non-uniformities in the initial layer before forming, the impurity band contains large variations in the density of centres. Due to this and to local fluctuations in V_o there will also be large variations in the mobility and density of states bandwidths. Regions of narrow mobility bandwidth are referred to as constrictions and each filament is considered to contain one dominant constriction of this type. This is illustrated in Fig. 2.8 as a symmetrical increase in density of states bandwidth E_I and a corresponding decrease in mobility bandwidth (E_M). The position of the impurity band and the Fermi level are assumed to be approximately in the centre of the energy gap of the insulator.

Above a critical value of V_o/J, however, the mobility bandwidth in the constriction region disappears and all the levels in the band become localized and non-conducting.

At low applied voltages the current flow in a filament is entirely by iso-energetic tunnelling through the non-localized states of the impurity band of Fig. 2.8. This type of conduction process has already been shown to have an I-V relationship of the form of

$$I \propto \sinh K V$$

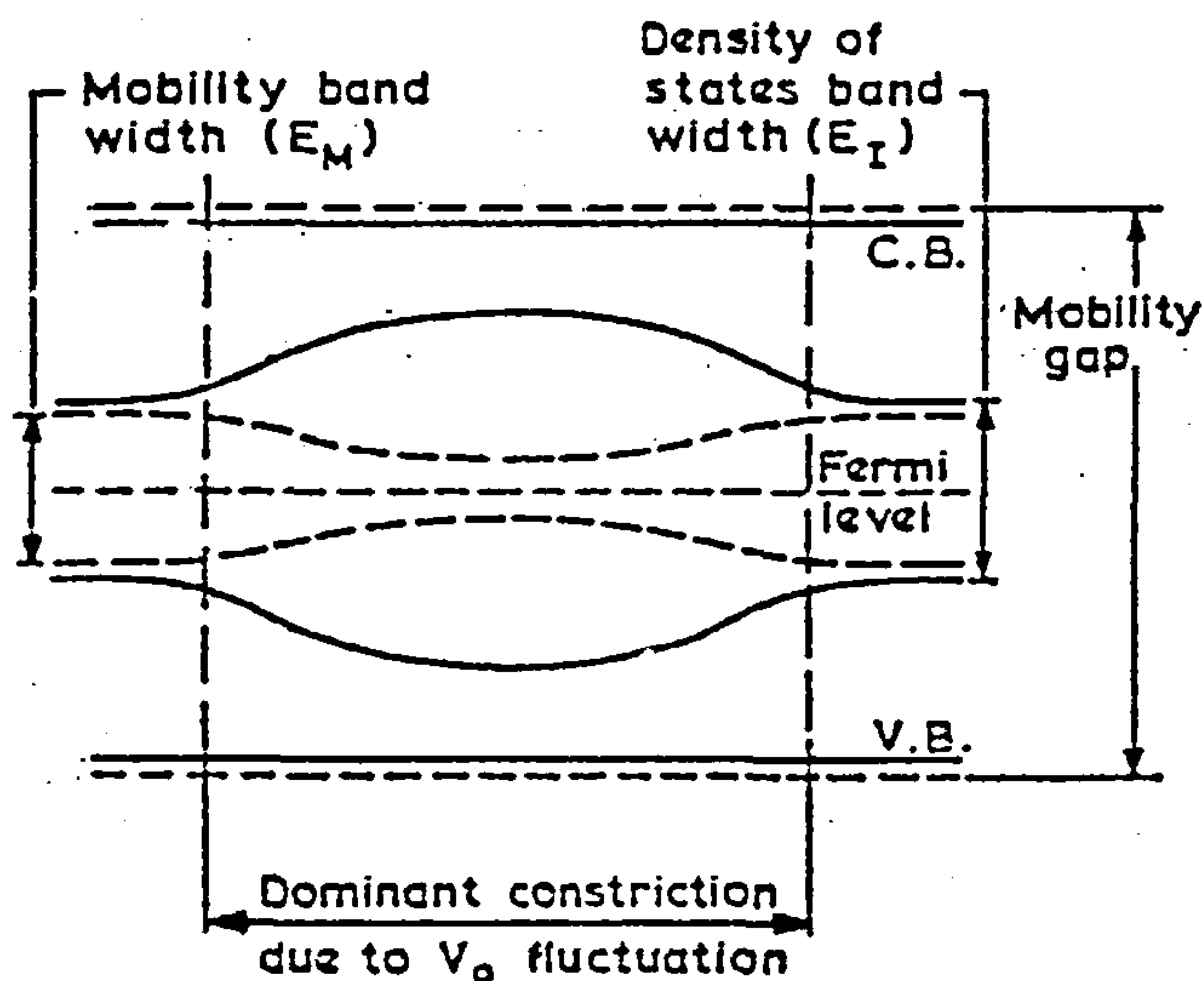

Fig. 2.8. The proposed energy band model for a conducting filament at a constriction region (after Ralph and Woodcock, ref.67)

As the voltage bias across the filament is increased, some electrons become sufficiently hot to enter the localized states around the constriction regions of rapidly decreasing mobility, as indicated by arrow (a) in Fig. 2.9. This is the onset of the process where the negative resistance appears in the I-V curve. Some electrons may also gain sufficient energy to enter traps in the surrounding materials. Over a limited range of voltages a given filament may contribute to conduction via the trapping centres either by recombination with a trapped hole (b in Fig.2.9) or by thermal degradation into states of lower energies (c) or by field emission into non-localized states (d)

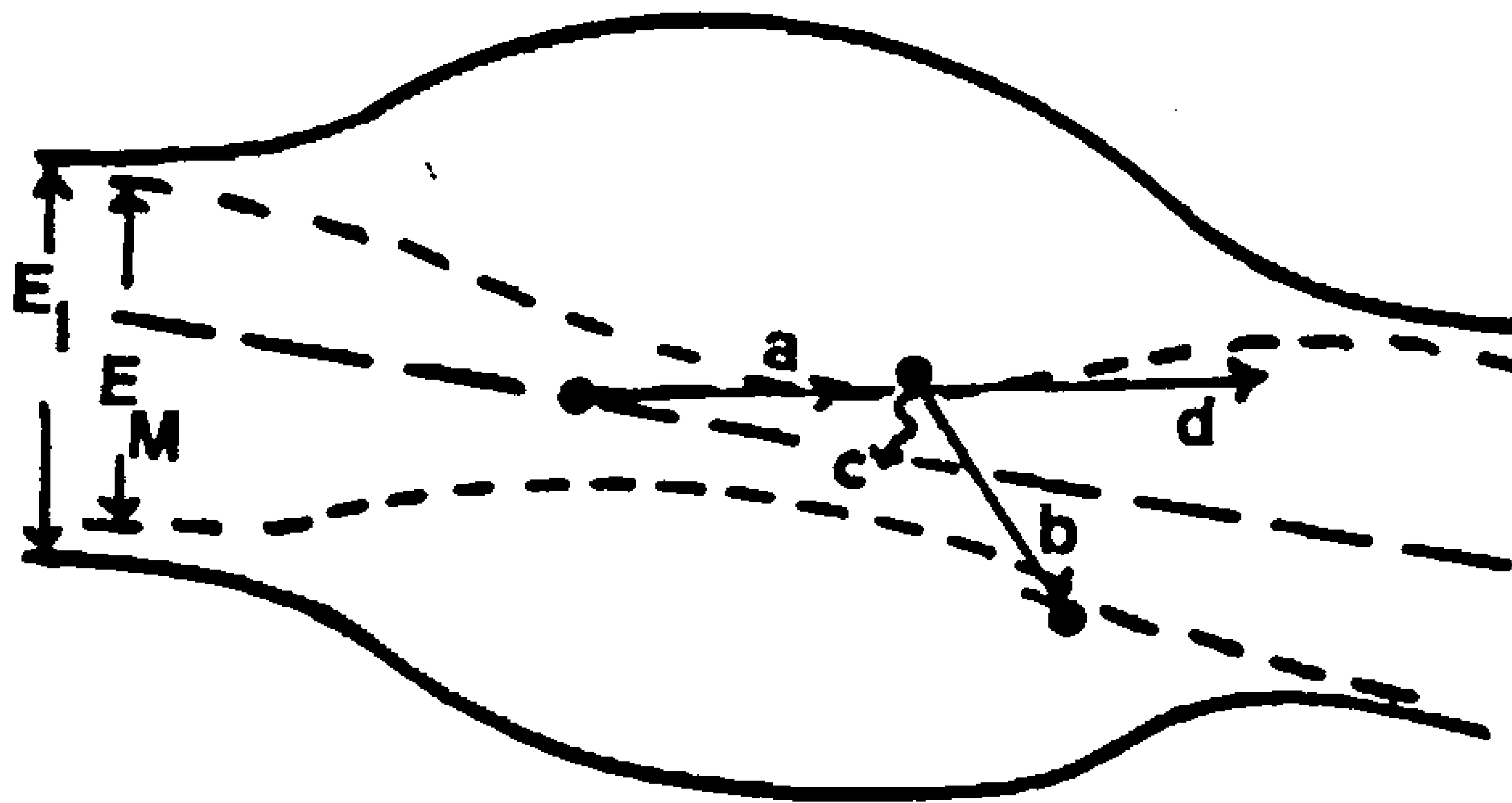

Fig. 2.9. Some processes which may occur in the constriction in a formed conducting filament; (a) iso-energetic tunnelling into the localized states region; (b) radiation recombination; (c) thermal degradation- (d) field emission (after Ralph and Woodcock, ref. 67)

Eventually, at sufficiently high voltages the trapping centres, both inside and outside the filament cause the filament to switch off, leading to cessation of conduction. There are two ways in which these traps might be expected to cause a filament to stop conducting. Firstly, a negative space-charge trapped in the material surrounding the filament would induce a positive charge in the conducting part of the filament. If this occurred in the constriction region, then the depletion of electrons could lower the Fermi-level into the region of localized

states at the bottom of the band, Fig.2.10. The constriction and hence the filament then stop conducting.

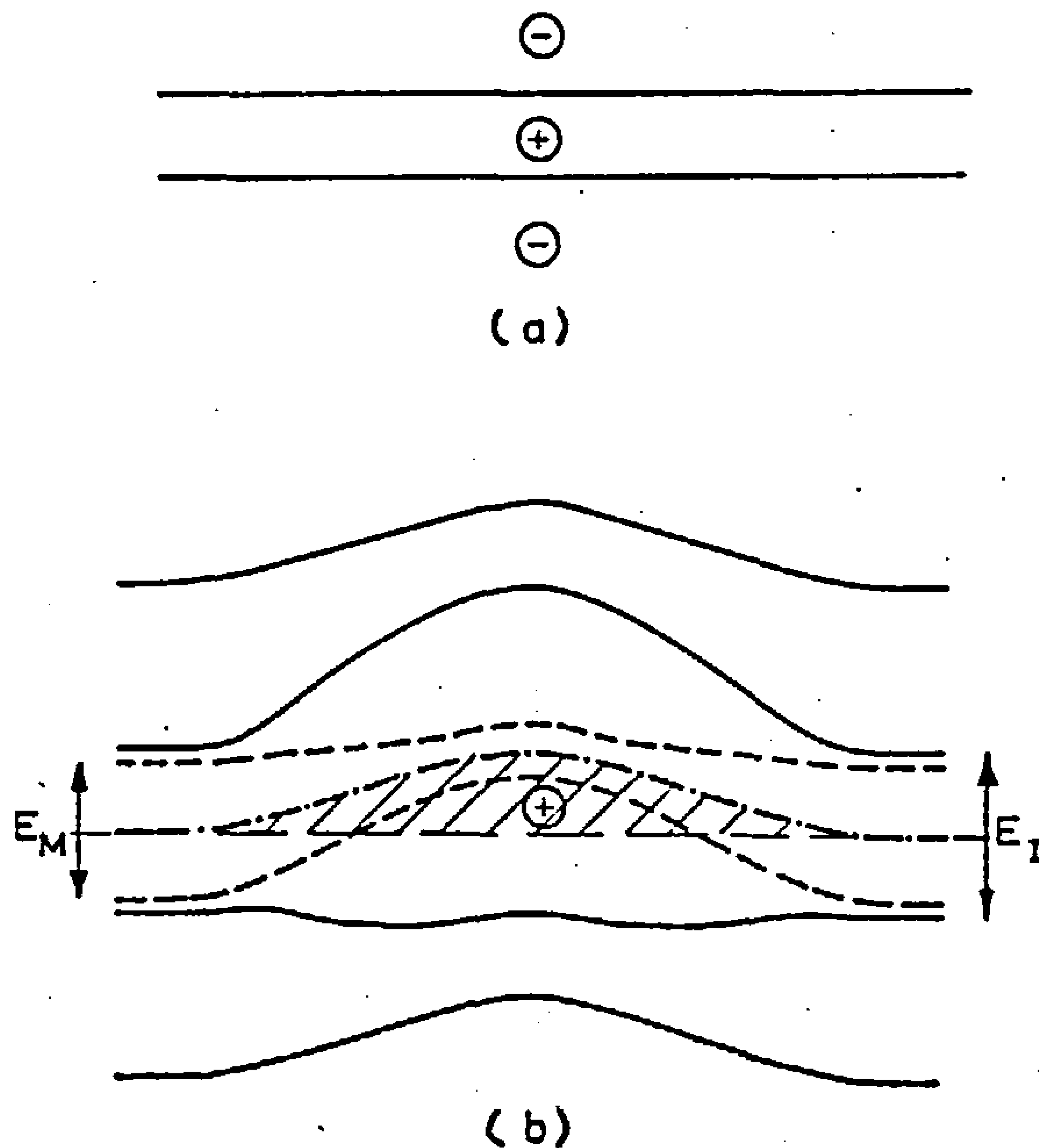

Fig.2.10. A possible non-conducting state of a filament as a result of the negative space-charge outside the filament (a) geometrical representation (b) the corresponding band diagram, (after Ralph and Woodcock, ref. 67)

Secondly, a small degree of trapping in the localized levels of a constriction could cause an increase in the random potential V_o experienced by the states in this region and thus increasing V_o/J. When this ratio exceeds a critical value the mobility gap disappears (Fig. 2.11) and all the states in the constriction region

become localized and non-conducting.

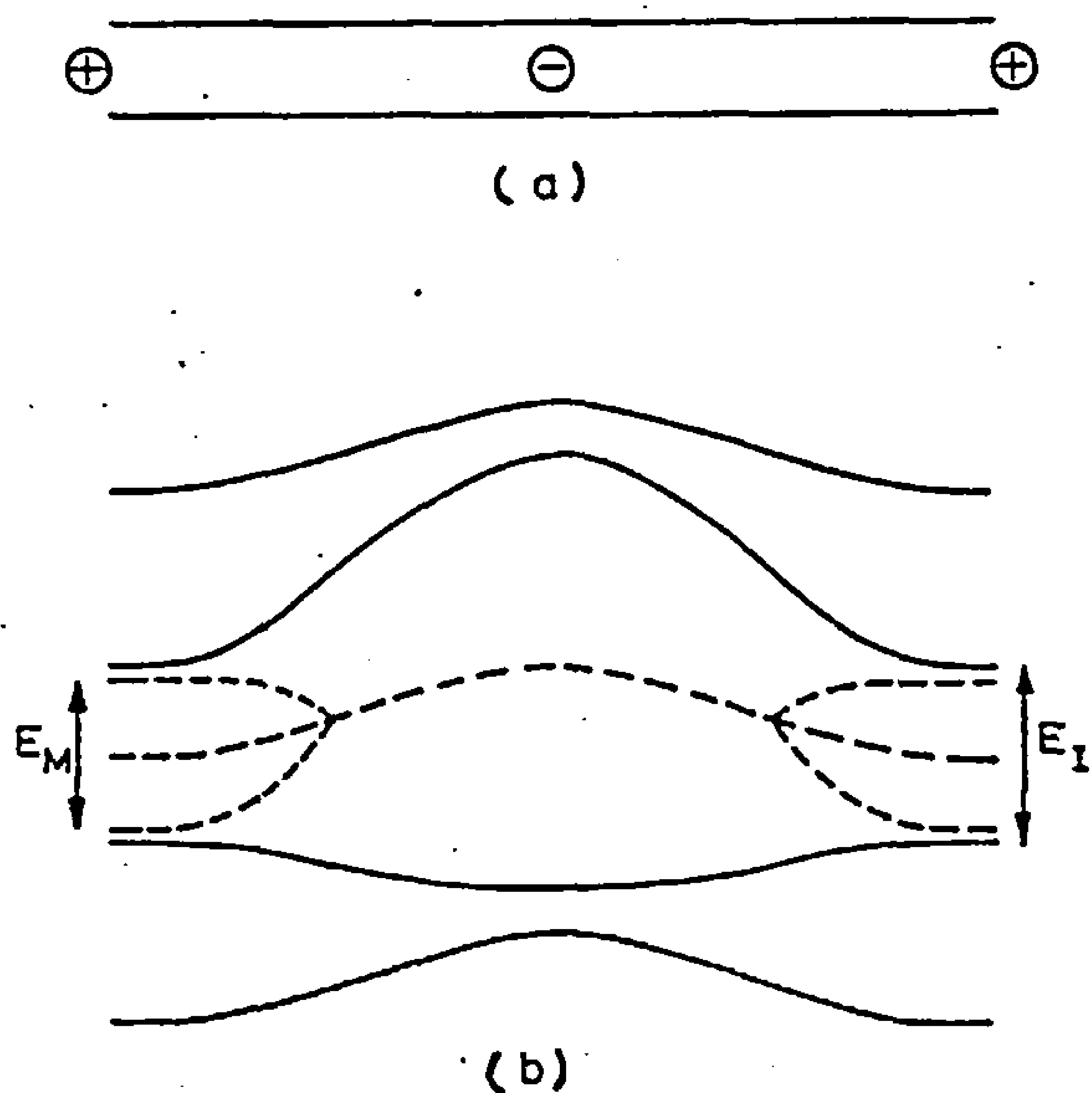

Fig. 2.11. The negative trapping charge in the localized levels of a constriction increases V_o until at a critical value of V_o/J the mobility gap vanishes, causing the filament to cease conducting. (a) Geometrical representation; (b) the corresponding band diagram for the filament (after Ralph and Woodcock, ref. 67)

The device is in a memory state if some of the filaments retain sufficient trapped charge to remain at high resistance when the applied voltage is removed. The memory state is erased when the trapped charge escapes and it is proposed that field emission is the de-trapping process.

The very long trapping times could be explained by

postulating that, either electrons in the traps outside the filament do not have an appreciable probability of recombination with spatially separated empty levels at lower energy in the non-localized region of the impurity band, or, the traps inside the filament retain their charge because all the available states below the traps are filled and non-conducting. However, inside a filament most of the applied voltage appears across the region of trapped charge in a constriction region causing a local high field. Consequently the traps within the filament can empty by field emission at a much lower applied voltage than those in the surrounding medium. It is then proposed that trapped charges outside the filament must relax into these empty states within the filament if the memory state is to be erased. The relaxation process has a temperature dependent time constant which describes the "dead time". The threshold voltage 'V_T' for memory erasure is the voltage across the filament constriction region which gives rise to field emission of electrons from the traps into the conduction band.

Electron emission which occurs from many small spots on the top electrode is expected to come from those constrictions which are close to the anode. Traps in this region become empty by the field emission and the released electrons are accelerated into the conduction band where they can reach the top electrode and emerge into a vacuum.

Electroluminescence arises from the insulator before switching off a filament, by recombination of hot electrons and holes in the impurity band, (process b, in Fig.2.9)

and after switching by recombination of carriers in the conduction and valence bands.

Current noise in the negative resistance region is believed to be the result of filaments switching individually and randomly.

2.3.7. Discussion and Conclusion

The various models given in the previous sections to account for the electroforming and anomalous behaviour observed in MIM structures can be classified in two main groups, namely, the band structure theory and the filamentary approach.

The first group consists of the models based on the existence of impurity or defect bands in the forbidden gap of the insulator. The formation of this band of states has been attributed to field-assisted diffusion of the anode contact material by Simmons and Verderber[30], to solid-state electrolysis of the insulator leading to oxygen vacancy centres by Greene et al[33] or to the injection of ions into the insulator by Barriac et al[63]. Hickmott[61] alternatively has proposed that an impurity band already exists in the insulator band gap and that forming consists of ionizing these centres by electrons tunnelling into the conduction band. The second group involves the formation of conducting filaments through the dielectric as postulated originally by Dearnaley[64] and then modified by Ralph and Woodcock[67].

However, none of these models can explain satisfactorily all the experimental results and some of them

have been criticised by the other workers. For instance, Hickmott's model is open to objections, as stated by Dearnaley et al[45], in that the memory state can last for several years without decay and it would appear unlikely that a non-equilibrium charge distribution could exist for so long in a device. Moreover, the very small values of the mobilities through localized states at the middle of the band gap would be incapable of explaining relatively large currents flowing through formed devices. Also, the influence of the surrounding atmosphere, and temperature switching phenomena have not been treated in detail in this model.

The model of Verderber, Simmons and Eales[42] which is based on the formation of a broad band of impurity states in the forbidden gap of the insulator can explain many of the observed phenomena in MIM structures. However, there has also been some criticism of this model[32]. Firstly, it is difficult to accept that a net negative space charge could persist for many years at room temperature within the insulator, or within part of the insulator at temperatures of 77°K. According to Mott, the d.c. conductivity of localized states tends to zero only at the absolute zero of temperature, and thus no mechanism is left to account for the containment of the negative charges. Secondly, the impurity or defect concentration between the top of the impurity band and the bottom of the conduction band is necessarily equal to zero in this theory. This is contrary to the model of the forms of impurity distribution determined by other

workers[68] which appear to fall exponentially from band edges with some pronounced humps superimposed on them for the case of heavily-doped amorphous structures. Furthermore, Dearnaley et al[65] measured the concentration of injected ions by Rutherford back-scattering and found that the Au concentration for Au-SiO-Si devices was at least a factor of 30 below that necessary for this theory. Finally, this model does not explain the influence of ambient atmosphere and the occurrence of electroluminescence.

Greene et al[33] suggested that the solid-state electrolysis involving the insulator is responsible for the electroforming process. Anion vacancies are injected into the insulator and thereby produce conduction paths. Chemical reactions occurring at the electrodes are proposed and the influence of oxygen successfully explained. This model is the only one which considered the evolution of gas during the forming process. The release of fluorine predicted during the forming of Al-CaF_2-Au structure was confirmed by experiment. An extension to this basic idea was proposed by Rakhshani, Hogarth and Abidi[41] who considered the effects of electrolysis along a filament and confirmed the expected results by scanning electron microscopy.

The model of Barriac et al[63], in which both electronic and ionic currents are involved, has been successful in explaining the effect of an oxygen environment. This is considered to arise from the penetration of oxygen into pores and cracks, where it reacts chemically with ions of the upper electrode. This model

accommodates the concept of a high field region, but assumes that conduction is uniform throughout the film. The localized nature of conduction has not been explained and the expression derived for the voltage peak V_M does not agree with experiment as temperature sensitive elements are involved.

The filamentary approach was first suggested by Dearnaley et al[65] to explain the phenomena observed in oxide films. Dearnaley's model envisages the growth of filaments through the insulating layer which conduct ohmically without thermal activation. It has been postulated that the filaments are constructed of the chains of metal atoms alternating with anion vacancies [64]. Conduction along ... Si-O-Si ... chains via a π-electron overlap for SiO was also suggested[64-66]. Filaments can rupture locally and then cease to conduct; they can re-join again under certain conditions. This model is applicable not only to insulators and semiconductors, but also to organic monomolecular layers[38] explaining most of the observed phenomena. However, in this model little is said concerning the exact nature of the filaments, their assumed model of growth, whether the mechanism of operation is electronic or ionic and how the contribution from impurities affects conduction.

Sutherland[34] (1971) has extended the concept of thermal rupture of conducting filaments to include the shift of the peak current V_M and predict the I-V characteristic to a better approximation than is possible with the model of Dearnaley. Instead of assuming that the

filaments conduct ohmically, Sutherland uses the experimetal equation for the characteristic determined by Simmons and Verderber which is-

$$I = K \sinh k V \tag{2.33}$$

where K and k are constants.

Under direct voltage bias the power dissipated in each filament is K V sinh k V.

Each filament is assumed to lose heat to the surrounding medium which is taken as a heat sink at constant temperature T_o. In the steady state,

$$K V \sinh k V = \frac{(T-T_o)}{R} \tag{2.34}$$

where R is a constant. If $T_{max}-T_o$ is the maximum temperature difference before a filament will rupture and if K is the same for all filaments then;

$$k_{max} = \frac{1}{V} \sinh^{-1} \left(\frac{T_{max}-T_o}{R K V}\right) \tag{2.35}$$

$$= \frac{1}{V} \sinh^{-1} \frac{Q}{V} \tag{2.36}$$

where $$Q = \frac{T_{max}-T_o}{R K} \tag{2.37}$$

so all filaments with $k>k_{max}$ are destroyed.

For Q>V

$$\frac{dk_{max}}{dV} = \frac{-1}{V^2} \left(\sinh^{-1}\frac{Q}{V} + 1\right) \tag{2.38}$$

The total current passed will be the sum of the currents through all the remaining filaments

$$I = \int_o^{k_{max}} K \sinh (k V)\, p(k)\, d k \tag{2.39}$$

where p(k) is proportional to the number of filaments with a particular k.

A further modification of the filamentary model is made by Ralph and Woodcock[67]. Using the concept of filamentary type of conduction, they assume that each filament contains an impurity band. The impurity band is consistent with the form determined for an amorphous semiconductor with localized states between the mobility edge and the density of states edges, which act as traps and recombination centres. The voltage-memory effect and the dependence on frequency of V_b is explained. Electron emission into a vacuum and electroluminescence are treated in this model in a similar way to that of Dearnaley et al.

To draw a conclusion, the filamentary approach appears to be capable of explaining most of the phenomena observed in MIM structures. The wider applicability of the filamentary theory, together with its success in explaining device properties, provides a good basis for formulating a more comprehensive theory.

2.4. CURRENT-CONTROLLED NEGATIVE RESISTANCE (CCNR) AND SWITCHING

Current-controlled negative resistance and/or switching effects have been observed in a wide variety of amorphous semiconducting materials, including niobium oxide[69-70-71], titanium oxide[72], nickel oxide[73], semiconducting chalcogenide glasses[3-74], transition metal oxides[75-76-77] and a variety of other thin insulating films[78-79-80]. Obviously there are enormous variations in the characteristics, parameters,

and quality of switching in all of these materials and thus many different fundamental mechanisms can be involved. However, as a general classification, devices showing current-controlled (s-shape) characteristics can be divided into four groups[81-87],

(a) negative resistance device

(b) negative resistance device with memory

(c) threshold switching

(d) memory switching.

In the first group, Fig. (2.11.a), the I-V characteristic of the device is traceable except for some hysteresis which is observed when the current is changed too rapidly for maintaining thermal equilibrium. With a proper choice of R_L (a protective load resistor placed in series with the switching unit) this negative resistance device can be kept at any point of the I-V curve. Fig. (2.11.b) shows the negative resistance device with memory which has two stable states. The first resembles that of (a) and the second is conductive. The conductive state is established at higher currents and remains without decay. The first state can be re-established by increasing the current above a certain value and switching it off rapidly.

The I-V characteristic of a typical threshold or monostable switch is illustrated in Fig.(2.11.c) which is very similar to that of the negative resistance device, except that no stable operating state exists along the negative resistance region. At low electric fields the current is ohmic and the device is in almost non-conductive

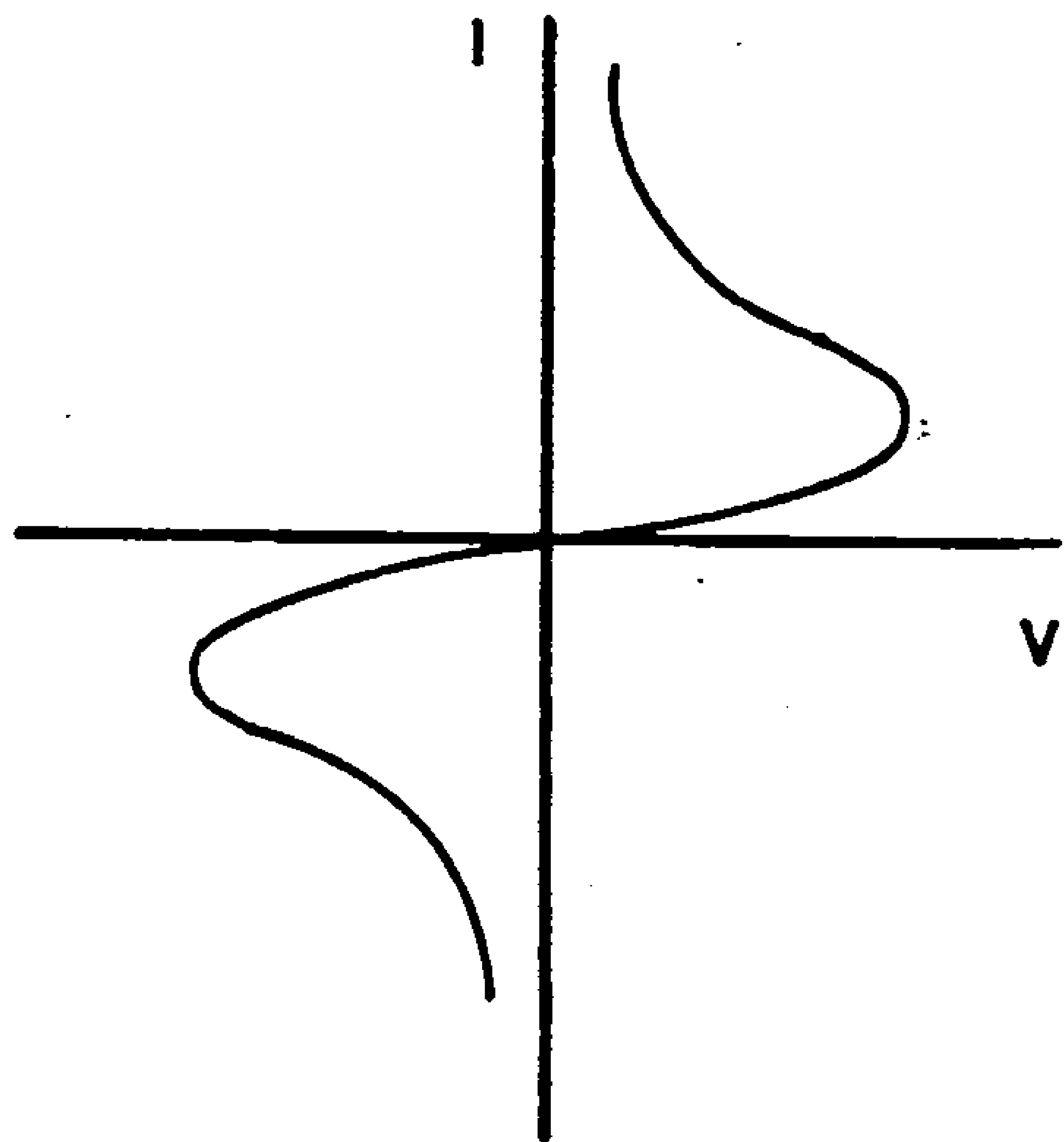

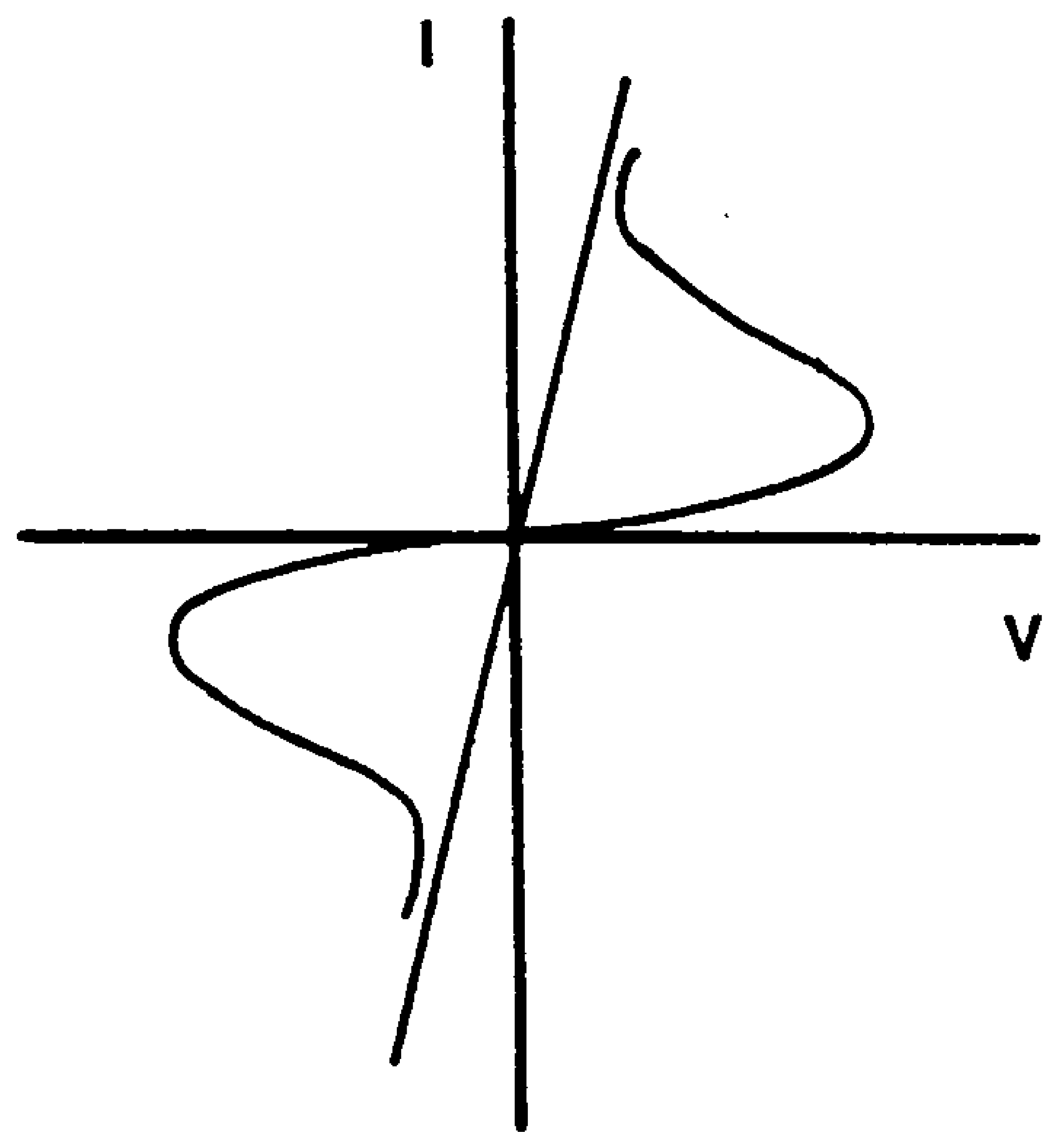

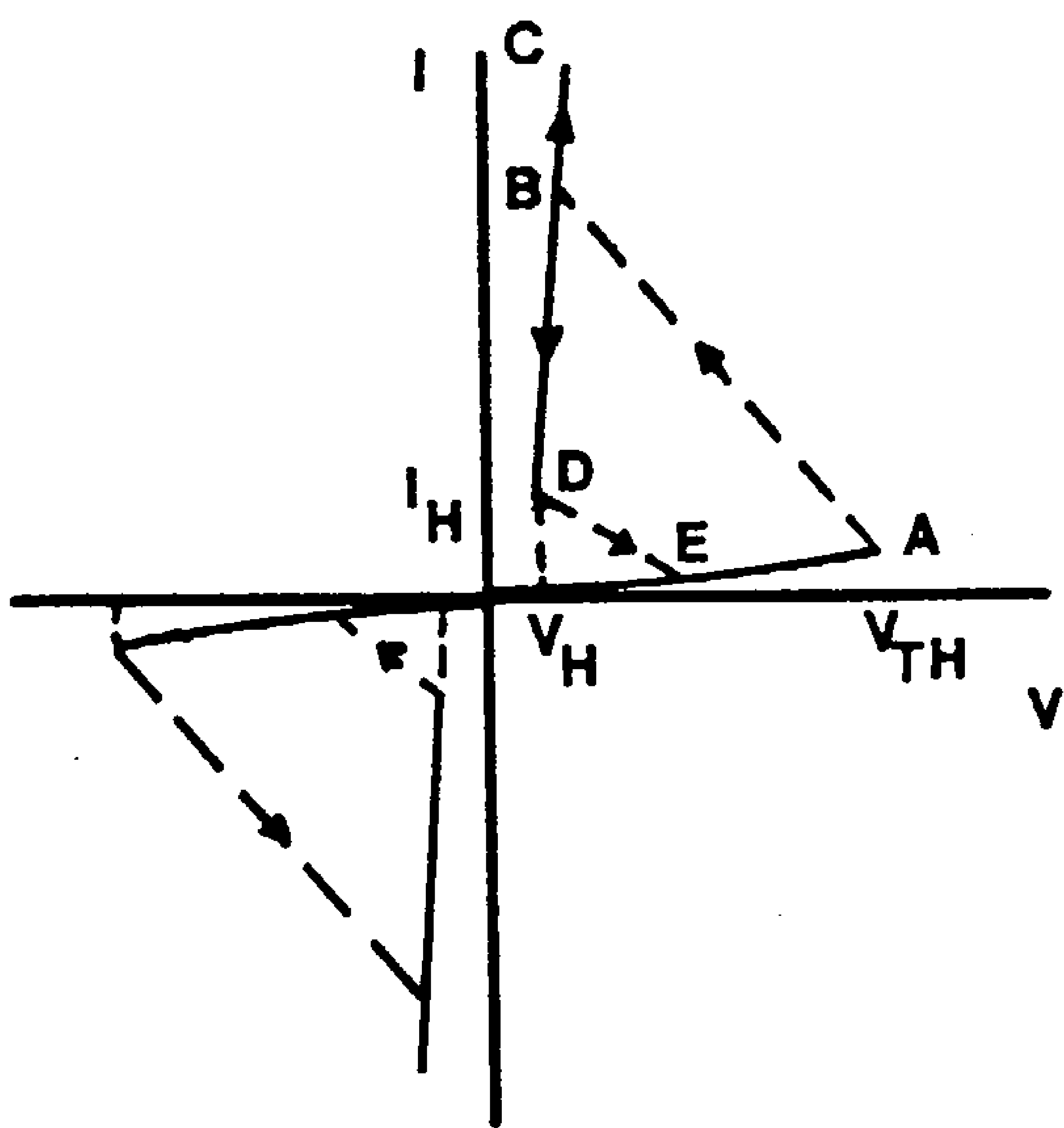

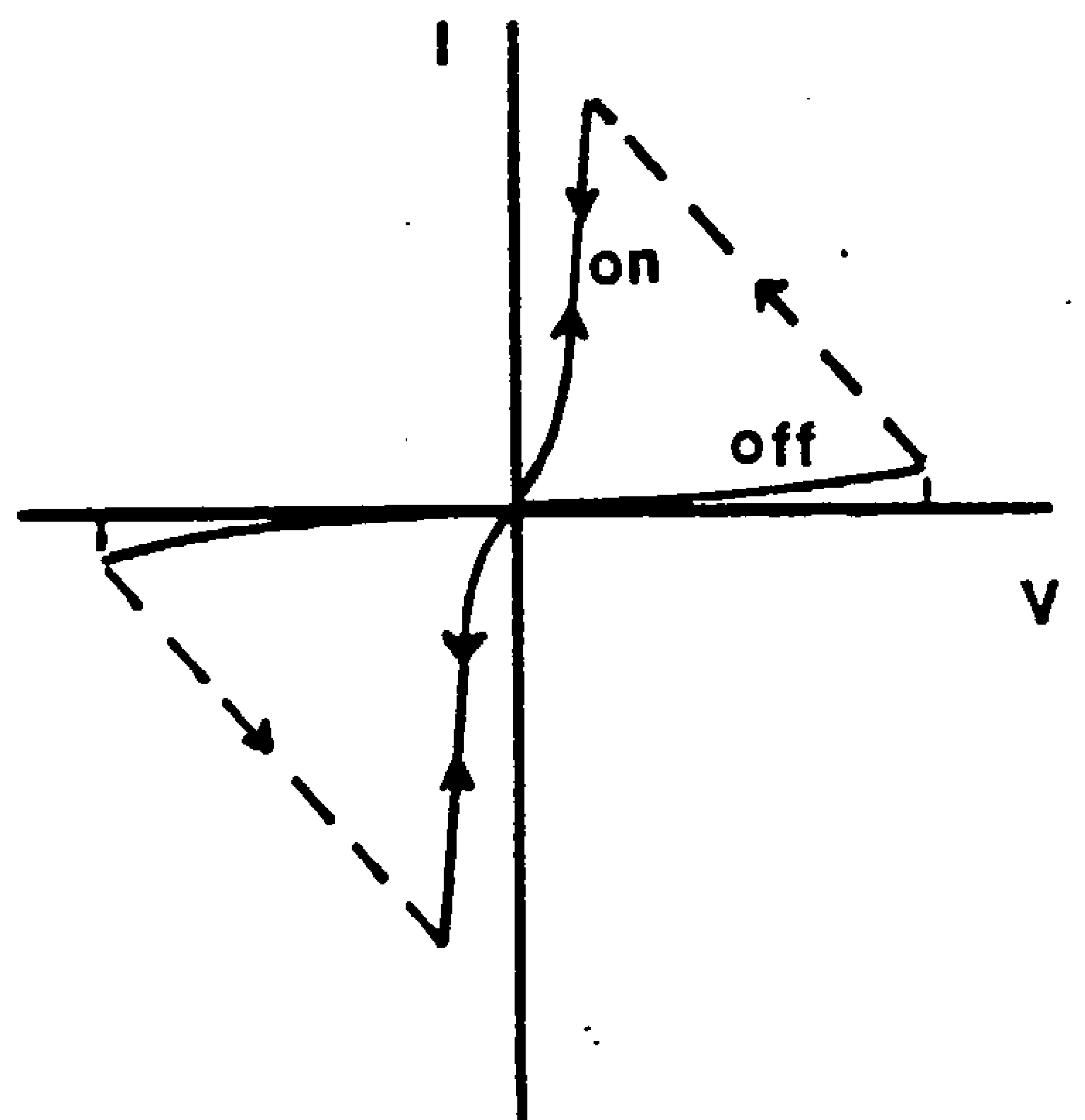

Fig. 2.11. Classification of current-controlled breakdown characteristics; (a) negative res istance device, (b) negative resistance device with memory, (c) threshold switching and (d) memory switching.

off-state , in which the resistance is typically in the range 10^5-$10^7\Omega$ at room temperature. Above a certain threshold voltage V_{TH}, the resistance drops drastically and the device switches into a high-conductive on-state , along the load line AB, which is maintained at much lower voltages. The on-state (curve BC) observed after switching is sustained as long as the current exceeds a certain minimum value I_H known as the holding current. If it falls below this value (as it does at some stage when the applied voltage is withdrawn), the operating point D returns to the low-conductive state. A memory switch behaves initially just like a threshold switch and has a very low conductivity until a given voltage is reached. At this voltage and after a delay time, there is a rapid switching to a highly-conductive on-state. In contrast with threshold switches, memory devices remain in the on-state even after the applied electric field is reduced to zero and they are thus bistable devices. However, the device can be brought back again into the low-conductive state by applying a sufficiently strong current pulse in the on-state.

Two distinct models, namely "purely electronic" and "purely thermal" have been proposed to explain the switching phenomenon. But in a real case it may be extremely difficult to separate these two mechanisms and a hybrid of them (electrothermal theory) could be the best to describe the instability. The electronic model is connected with the change in space-charges, in carrier lifetimes, in rates of impact ionization and in

other properties of the material. The most common class of electronic model (the double injection theory) postulates that, in the on-state carriers are injected from both electrodes giving a high density of non-equilibrium carriers in the valence and conduction bands. Henish, Fagen and Ovshinsky[82] (1970) assume that in the off-state, the injected carriers are trapped, and during the delay time, two space-charge regions advance gradually into the centre of the layer- the transition to the on-state occurs when all traps are filled and the carriers move freely. The return to the off-state occurs when the current falls to a value such that recombination processes dominate the injection.

The thermal explanation is based on the formation of a hot conducting filament as a result of power dissipation in the device. The observed filaments are structurally altered regions due to the high temperatures, phase separation in the specimen, and/or diffusion of electrode material. It has been shown theoretically that in cases of CCNR, a filament of high current density would be expected[83]; also a direct visual observation of the growth of such a conducting filament on the surface of bulk samples of As-Te-Ge glasses has been reported by Uttecht et al[84]. However, it is now generally accepted that the high-conductivity memory on-state in glassy materials is due to a localized transformation from an amorphous to a crystalline filament between the electrodes [77-86]. The low-conductivity off-state can be obtained when such filaments are destroyed or undergo a phase change

due to the rapid heating and quenching which occur by applying a high current pulse to the sample.

In the threshold switch, on the other hand, the duration of the switching process is only about 10^{-10}sec (memory switches show much slower switching times of the order of 10^{-3}sec) and for this reason the mechanism of switching process is considered to be electronic in nature. In chalcogenide glasses, however, it seems to be certain that threshold switching is an electronic effect which to a certain degree is thermally initiated and which does not involve changes of the material structure [87].

CHAPTER THREE

EXPERIMENTAL TECHNIQUES

3.1 PREPARATION OF DEVICES

3.1.1. The Evaporation Unit

MIM devices used in the present investigation were prepared by thermal evaporation at high vacuum in a Balzers 510 19-inch coating unit equipped with a DIFF 1500 9-inch 220V, 800W, diffusion pump and a DU 25 500 r.p.m. rotary pump. The system was capable of producing pressures in the chamber down to 10^{-7}torr using the liquid nitrogen trap facilities. The bell-jar assembly of the unit was of double-walled construction which facilitated the cooling of the system by admitting cold water into spiral tubes inside the wall of the chamber. A radiant heating element was mounted at the top end, inside the chamber, for the purpose of substrate heating and also baking out the whole system to achieve lower ultimate pressures. The substrate holder was a circular disc made of stainless steel capable of holding three 3"x1" glass substrates from which the middle one was used for the purpose of thickness measurements which will be described later. A rotary disc with four positions, provided for the masking systems, was placed as closely as possible below the substrate holder. By rotating this disc the desired mask could be brought under the substrates, and hence a maximum of four different layers could be

osited. A shutter capable of being rotated from tside was used to isolate the mask and substrates from ne evaporants when desired. An additional shutter operating from outside, through a window, enabled part of the masks to be completely shut off during evaporation allowing samples of different electrode or insulator thicknesses to be deposited on a single substrate. Two different masking systems, made of stainless steel, were used to give two different device configurations as shown schematically in Fig.3.1. A maximum of 6 and 16 devices with the active areas of 0.125 cm^2 and 0.063 cm^2 could be made on each substrate for configurations 1 and 2, respectively.

Three evaporation sources used were made in the form of boats from tantalum and molybdenum, and spiral wire from tungsten. They were bolted to thick copper rods positioned 30 cm below the substrates. Silicon monoxide and boric oxide were evaporated from tantalum and molybdenum boats respectively, silver and copper from either tantalum or molybdenum, and aluminium from a tungsten spiral. The design and material used for the source fabrication depended on its working temperature (1,000 - 2,000°C), reactivity with the evaporant, and whether or not the evaporant sublimed. The designs used for the various evaporation sources are shown schematically in Fig.3.? Aluminium shields were placed between the sources in order to prevent the contamination of one source by another. Evaporation of the two oxides (SiO and B_2(simultaneously was possible by passing large curr

through the corresponding boats as has been described by Hogarth and Wright[88]. Two a.c. power supplies were employed to provide the high currents.

Quartz crystal monitors were used to measure the evaporation rate and the total thickness of oxide or metal film, and were mounted above the evaporating sources near the substrates. For their operation, the monitors depend on the change in frequency of vibration of a thin quartz crystal when its mass changes due to the deposition of a thin film on its surface. A heat radiation shield and a water-cooled jacket around each crystal holder were employed to minimize the temperature-induced frequency shift in the crystal. The radiation shield also provided the deposition of each crystal only by its corresponding material. The source-substrate configuration and the positions of the crystal monitors are shown in Fig.3.3.

3.1.2. Preparation and Deposition Procedures

Devices used in this study were prepared by successive evaporation of the various layers in unbroken vacuum. The evaporation materials were deposited onto 3"x1" Corning 7059 borosilicate glass slides. Before deposition, the cleaning process for every substrate was as follow:

(a) Boiling in a solution of Teepol in distilled water for approximately 15 minutes.

(b) Rinsing in hot distilled water.

(c) Placing in the steam of boiling isopropyl alcohol, for about 10 minutes, in order to remove the final traces of grease and Teepol.

(d) Airdrying and removing the remaining dust particles by means of compressed air.

(e) Final cleaning by ionic bombardment, which was facilitated inside the vacuum chamber, for about 10 minutes during the pump-down sequence, at a pressure of 0.1 torr. The inside of the evaporation chamber was also cleaned and covered by aluminium foil to reduce the contamination of the evaporated films. Since boric oxide contains large quantities of water after evacuation of the system to pressures of about 10^{-4} torr the boat containing the B_2O_3 material was heated up to some temperatures below its evaporation temperature for about 30 minutes. This expelled the water from the oxide.

After baking out the whole system and achieving the high vacuum, the heater was switched off and the cooling water was switched on. The temperature of the substrates was measured using a copper-constantan thermocouple connected to a Comark type 1623 electronic thermometer. Deposition of the layers was carried out in a pressure of about 10^{-6} torr at a substrate temperature of 100-150°C. The base electrodes were first deposited onto the substrates by passing a large current through the middle source and evaporating the corresponding metal. Then a mixed layer of SiO and B_2O_3 was deposited by means of the co-eveporation technique with deposition rate in the range 8-12 Å /sec. The weight percentage of

the two oxide materials was controlled by the individual rates of the frequency shift of the corresponding crystal monitors. In the construction of devices with configuration 1 in Fig.3.1., before the deposition of the top electrodes, the insulating layer at the edges of the base electrodes was thickened by depositing additional strips of SiO (≈3000Å thick) at these regions. This was for avoiding the destructive dielectric breakdown which could originate from the field-enhanced regions near the edges. All evaporation times and rates and the net frequency shifts on the crystal monitors as well as the temperatures and pressures during evaporations were recorded.

After the completion of the deposition procedures, the whole system was allowed to cool down gradually to room temperature before the removal of the specimens out of the chamber and storing in an evacuated desiccator. Rapid cooling would result in an instantaneous uneven heat distribution within the specimen and substrate causing internal mechanical stresses with the possible occurrence of micro-cracks.

3.1.3. Thickness Measurements

The thicknesses of the deposited layers were measured by means of an interferometric technique using Fizeau fringes of equal thickness. This was in addition to the quartz crystal monitoring method, used during the evaporation processes, which yielded the approximate value of the film thickness.

As was mentioned earlier, from the three substrates

used in each evaporation the middle one was for the purpose of the thickness measurements. This substrate was masked by a thin wire in close contact to its surface. After the deposition procedure, the wire was removed and the whole surface (coated and uncoated) of the substrate was covered with a thin layer (≈1000Å) of silver. The thickness of the film t which is given by the depth of the step in the silver layer at the masked area was measured using a M-100 Angstrometer multibeam interferometer. The apparatus consisted of two slightly inclined optical flats, one of them supporting the film, which form a step on the substrate. When the second optical flat was brought in contact with the film surface and the interferometer was illuminated with a parallel monochromatic beam (from a sodium vapour light source with $\lambda \approx 5890$Å) at normal incidence and viewed with a low-power microscope, dark fringes could be observed. The fringes show a displacement d as they pass over the film step. By adjusting the relative positions of the flats to form a wedge-shaped air gap, the fringes can be made to run in straight lines perpendicular to the steps on the opaque film. The thickness of the film t then could be deduced from the following relation:

$$t = \frac{\text{fringe displacement (d)}}{\text{fringe-to-fringe spacing (D)}} \cdot \frac{\lambda}{2}$$

3.2. THE VACUUM TEST SYSTEM

Some of the electrical measurements in this work were carried out in vacuum. The vacuum test unit used consisted of a 4" water-cooled Edwards E04 diffusion pump backed by an Edwards ES 150 rotary pump. Pressures were measured by Sadla-Vac Pirani and Penning gauges. An Edwards needle valve could be used to control the chamber pressure in the range 10^6-1 torr. A 12" diameter bell jar was placed on a 1" thick aluminium base-plate. The jar could be covered by either a 1" thick glass top-plate or an assembly of a ½" thick stainless steel top-plate soldered to a cold stage metal box for the purpose of low-temperature measurements as will be described later. The vacuum sealing was completed by using rubber seals between the chamber and the plates. A photograph of the vacuum test system together with the equipment used for measurements is shown in Fig.3.4. The substrates were mounted on a perspex assembly positioned in the centre of the chamber. Electrical connections to the sample electrodes were made by using spring copper contacts joined with silver paint. A 2.5 cm x 7.5 cm x 0.25 cm silver plate was placed 2 cm above the substrate to collect the electrons emitted from the sample.

3.3. TEMPERATURE MEASUREMENTS

Electrical measurements at low temperatures were performed with the specimens in a cryostat. This consisted of a 11.5 cm x 5.8 cm x 6.7 cm brass box soldered to two 1.7 cm stainless steel tubes which were soldered to a ½" thick stainless steel top plate. Liquid nitrogen was introduced into the box from outside the vacuum system through the stainless steel tubes. The substrates could be attached to the flat surface of the box by the pressure contacts which also provided the electrical contacts. To reduce the thermal resistance it was useful to fill the gap between the substrate and the box with a layer of silicon vacuum grease. However, low temperatures as low as -163°C could be achieved.

Heating of the specimens was made possible by inserting a small electric heater between the box and substrate. A Coutant LB 500.2 power supply unit was used to feed the heater; temperatures up to +130°C as well as intermediate values could be obtained by varying the voltage across the electric heater. The electrically-isolated heater was so designed that it would not have an undesirable magnetic influence on the electrical properties of the samples. A Copper-constantan or chromel-alumel thermocouple, which were attached to the surface of the substrate by applying a small drop of silver paste, monitored the temperature.

CHAPTER FOUR

RESULTS

4.1. INTRODUCTION

Amorphous mixed layers of silicon oxide/boric oxide (borosilicate) were first prepared in this department by Hogarth and Wright [88] (1968), using a co-evaporation technique. They were found to have a good mixing quality and uniformity of the non-crystalline structure with a much higher resistivity than simple silicon oxide films. However, the borosilicate films containing more than 50% B_2O_3 are highly affected by atmosphere following the absorption of water vapour; a composition of 30% B_2O_3 and 70% SiO was found practically suitable to give a good dielectric stability in these films.

Timson and Hogarth [93] made co-evaporated films of silicon oxide and boric oxide with thicknesses in the range 10,000 to 20,000 Å . They reported that the direct current-voltage characteristics of the films with aluminium electrodes were in general of the form $I_c \alpha V^n$, where n varied between 4 and 6. The a.c. conductance σ_{ac} at frequency f was of the form $\sigma_{ac} \alpha\ f^n$ with n≃0.9 to 1.0. The electron spin resonance (e.s.r.) measurements obtained for SiO and SiO/B_2O_3 prepared under similar conditions revealed that the spin density is reduced by a factor of about 5 for SiO/B_2O_3; this is consistent with a reduction in the number of dangling

bonds and of conduction electrons. In other words, the normally unpaired electrons on dangling bonds in silicon oxide are partly satisfied by the added boric oxide.

Hogarth and Taheri[94] and Taheri, Hogarth and Gould [95] extended these measurements to thinner films having SiO (70%)/B_2O_3 (30%) layers of thicknesses 3000 - 6000 Å. They showed that Al-SiO/B_2O_3-Al structures could undergo an electroforming process, after which the samples exhibited voltage controlled negative resistance (VCNR) and electron emission into a vacuum. The maximum peak current circulating through the devices occurred at about V_M = 30V which seems to be rather high in comparison with the corresponding value in other thin film sandwiches reported in the literature. The maximum emission current density and the maximum value of transmission ratio α were found to be 10^{-5} A/cm^2 and 10^{-3}, respectively. Some of the samples showed remarkable stability at high applied voltages of the order of 500 - 600V without the occurrence of destructive breakdown.

Following the work of Taheri et al, Bidadi [96] studied the electroforming phenomena in these structures employing noble electrode metals such as gold, silver and copper. Both circulating current I_c and emission current I_e were considerably higher in these systems [97] compared with devices having aluminium electrodes as previously reported by Taheri et al[95].

In the present work, the electroforming process and properties exhibited by the electroformed M-SiO/B_2O_3-M devices with the composition of 70% SiO and 30% B_2O_3

(unless stated) have been examined. The dielectric thicknesses were in the range 400-4000 Å and different metal electrodes of Cu, Ag and Al of a few hundred Å thickness have been used. The defects produced on the surface of electrodes during the device operation, switching phenomena and the behaviour of the vacuum-electroformed Cu electrodes devices at low temperatures such as thermal-voltage memory effect and relaxation of the induced memory states have been studied in particular. Our main concern was (a) to investigate the mechanisms involved and find out the best given theory which can match the observed behaviour of these structures and (b) to determine the feasibility of any possible application.

4.2 FILM STRUCTURE

Layers of SiO/B_2O_3 sufficiently thin for transmission electron microscopy ($\sim$400 Å) were deposited onto clean cellulose acetate paper using the co-evaporation technique as previously described. A small part of the deposited film was floated off in a solution of pure acetone, picked up on copper grid (200 mesh, T ABB LAB), and then examined in a J.E.M.-7 electron microscope. Fig. 4.1 shows a typical transmission electron diffraction pattern of a SiO (70%)/B_2O_3(30%) (by weight) thin layer indicating that the structure of the film is 'amorphous'.

4.3 DC STABILITY, OPERATION AND CHARACTERISTICS OF M-SiO/B_2O_3-M STRUCTURES

4.3.1. Experimental Details

Most of the electrical measurements were carried out in vacuum at a pressure of less than 10^{-5} torr. However, some devices were examined in air at atmospheric pressure and also at intermediate pressures. The current-voltage characteristics of the specimens were measured by traditional methods. The electrical circuit for measuring the circulating current I_c, emission current I_e and for recording the time dependence variations of the circulating current is shown in Fig. 4.2. The input voltage was supplied by a Solartron AS1414.2 60V, 1A and/or a Coutant LA 1002 power supply unit. The voltage across the sample was measured by a Heathkit high input impedance valve voltmeter so that the current through it was negligible compared with the current passing through the device. In

order to collect the emitted electrons from the samples the collector plate was positively biased with respect to the device top electrode by biasing the top electrode at -100V, using a Keithley 241 regulated H-T power supply. A Keithley 610 electrometer was used for measuring the low conductivity current and emission current. The high circulating current in electroformed samples was measured by a Cambridge L-269830 milliammeter. A Venture RE511.20 chart recorder was employed for recording the time-dependence of the relaxation of the induced memory-states, using the voltage drop across the milliammeter.

4.3.2. Electroforming and DC Device Characteristics

Electroforming of the samples was performed by increasing the direct voltage across the electrodes (with the top electrode positive) in 0.5V steps with an approximately 15 seconds delay between steps, until the forming voltage, V_F, was reached. At this voltage a rapid increase in the circulating current through the sample was observed and the device conductivity then became time-dependent. Fig. 4.3. shows the increase with time of current at a voltage of 4V in a Cu-SiO/B_2O_3-Cu device having a dielectric thickness of 600Å. The time required to develop the conductivity at V_F was normally from some tens of seconds to a few minutes for devices with copper and silver electrodes, but it took much longer time for the samples carrying aluminium electrodes. Some devices with Cu and Ag electrodes were first short-circuited. This effect disappeared at bias voltages of 2-3V. This has been attributed to the rupture of metallic paths

which are formed by a diffusion process during the evaporation procedure.(96) Devices made with Cu and Ag electrodes formed readily and the forming voltage varied between 3 and 12V depending on the thickness of dielectric and the age of the sample. As an example, the required voltages to form four devices with different insulator thicknesses of 600, 1000, 2000 and 2600 Å, prepared on the same substrate, with copper electrodes, under similar conditions were 3.5, 4, 7 and 9V respectively. Higher voltages of 15-22V were needed for initiating the electroforming process when aluminium electrodes were used. Some aluminium devices with thicker dielectrics however, did not form, although voltages up to 50V were applied. A curve of LnI versus $V^{\frac{1}{2}}$ for such a device with SiO (80%)/B_2O_3(20%) dielectric having a thickness of 3500Å is shown in Fig. 4.4. The good straight line at high fields can be attributed to either Schottky emission or Poole-Frenkel effect as described in Chapter 1. The simple means for distinguishing these two mechanisms is to compare the experimental value of the barrier lowering coefficient β_{exp} with the theoretical values of Schottky and Poole-Frenkel coefficients which are given by the following equations, respectively:

$$\beta_S = \left(\frac{e}{4\pi\varepsilon\varepsilon_0}\right)^{\frac{1}{2}} \qquad 4.1$$

$$\beta_{PF} = \left(\frac{e}{\pi\varepsilon\varepsilon_0}\right)^{\frac{1}{2}} \qquad 4.2$$

Having the dielectric constant $\varepsilon \simeq 4.1$ for the complex of SiO(80%)/B_2O_3(20%)(88), the value of β_S and β_{PF}

calculated from equations 4.1 and 4.2 are 1.87×10^{-4} and 3.74×10^{-4} $eVCm^{\frac{1}{2}}V^{-\frac{1}{2}}$, respectively. The experimental value of β can be calculated from

$$\beta_{exp} = S.kT.d^{\frac{1}{2}} \qquad 4.3$$

where S is the slope of $LnI-V^{\frac{1}{2}}$ plot in Fig. 4.4, k is the Boltzmann constant and d is the thickness of the insulator. The value of β_{exp} obtained from equation 4.3 is 1.99×10^{-4} $eVCm^{\frac{1}{2}}V^{-\frac{1}{2}}$ which is comparable with the value of β_s. Therefore the conduction mechanism involved in this structure seems to be in favour of Schottky emission rather than the Poole-Frenkel effect.

After the electroforming process, most devices exhibited voltage controlled negative resistance (VCNR) characteristics and electron emission into a vacuum (in suitable conditions) which was in general agreement with the observations reported earlier in the literature. Figs. 4.5, 4.6 and 4.7 show the variation of the circulating current, I_c, and emission current, I_e, plotted against the applied voltage, V_b, for borosilicate films with copper, silver and aluminium electrodes, respectively. All the three samples had the same dielectric thickness of d ≈ 1700Å and were electroformed in vacuum. The measurements were carried out at the pressures less than 10^{-5} torr at room-temperature and repeated for several voltage cycles. The original I-V relationships were found to be reproducible each time with a fair degree of accuracy. The level of circulating current in devices with copper electrodes was considerably higher than in the samples with silver and aluminium

electrodes. The maximum peak current I_M in Fig. 4.5 is about 10 times higher than I_M in Fig. 4.6 and 100 times higher than in Fig. 4.7. In addition, the circulating current through devices with Ag and Al electrodes showed erratic fluctuations particularly in the negative resistance region in contrast to the samples with Cu electrodes which had fairly stable currents with more reproducible characteristics. The peak voltage V_M varied usually between 3 and 5V for different devices but was constant for a given device.

The onset of the emission current in the three structures coincides approximately with the voltage corresponding to the peak current as shown in Figs. 4.5, 4.6 and 4.7. The emission current rises sharply first and reaches a peak, after which it decreases with further voltage increase. The maximum emission current density is of order 10^{-4}A/cm^2 for devices with Cu electrodes and of the order of 10^{-5}A/cm^2 for devices with Ag and Al electrodes. Because the circulating current through the sandwiches with Al electrodes is lower than in devices with Cu and Ag electrodes, therefore the transmission efficiency is higher in Al devices.

Electroforming was possible with negative polarity (top electrode negatively biased) in devices having Cu and Ag electrodes. Negatively electroformed samples showed VCNR with erratic current fluctuations in their I_c-V characteristics; the degree of forming was considerably less than the samples electroformed with positive polarity. However, after the complete electro-

forming process with top electrode positively biased, the change of polarity had no significant effect on the I_c-V characteristics. Fig. 4.8 shows the I_c-V characteristic of a Cu-SiO/B_2O_3-Cu device with a dielectric thickness of 1250 Å; (a) after being electroformed with negative polarity (at a bias voltage of 5V for one hour) and (b) after complete electroforming with positive polarity.

Devices carrying Cu and Ag electrodes could also be electroformed in air at atmospheric pressure. Most of air-electroformed samples exhibited VCNR for the first few voltage cycles, but the negative resistance region disappeared completely in further runs. Fig. 4.9 shows the I_c-V characteristics of a 1250Å thick device with Cu electrodes which had been electroformed in air at a voltage of 6V for 90 minutes. However, some of the air-electroformed samples showed very little differential negative resistance with small current peak-to-valley ratio. Such an I_c-V curve for a 1720Å thick Ag-Sio/B_2O_3-Ag device is shown in Fig. 4.10.

The forming voltage increased with decreasing temperature and electroforming was not possible for temperatures less than a certain value; this was found to be -50°C for devices with copper electrodes which is in agreement with the results of Bidadi and Hogarth[60].

4.3.3. Effect of Air Pressure on the VCNR

Vacuum-electroformed devices with Ag and Cu electrodes were examined at the various pressures of air. The effect of different air pressures on the I_c-V characteristics

of an electroformed Ag-SiO/B_2O_3-Ag structure having a dielectric thickness of 3170Å is illustrated in Fig. 4.11. It can be seen that the current density of the sample depends strongly on the pressure of ambient air. The measurements were obtained by varying the ambient air from low to high pressures; at each pressure the VCNR could be repeated by voltage tracing of the sample. The peak current and the negative resistance region disappeared at pressures approximately just above 1 torr.

The vacuum-electroformed samples also showed a pressure voltage memory effect when operated in air at atmospheric pressure. Fig. 4.12 shows the I_c-V characteristics of a 1500Å thick Cu-SiO/B_2O_3-Cu device obtained at a low pressure of 10^{-5} torr and in air at atmospheric pressure. For the first voltage increase in air the I_c-V characteristic of the sample showed VCNR with a maximum current of 7mA (at $V_M \approx 2V$) which is less than one-tenth of the maximum current passing through the sample at 10^{-5} torr. On decreasing the bias voltage the VCNR disappeared and the current became very low. The high-impedance state established in this way remained unchanged, during further voltage cycles, so long as the sample was kept at the high pressure. The erasure of the induced high-impedance memory state was accomplished by reducing the air-pressure again to 10^{-5} torr and applying a voltage of $V_b = V_T$ across the sample. The I_c-V characteristic of the sample during its recovery is shown in Fig. 4.13. Transition from the high-impedance to a low-impedance state occurred at $V_T \approx 3.5V$ and the current

flowing through the device showed considerable noise fluctuations for the first voltage increase. The current became stable after decreasing the bias voltage and applying the second voltage tracing when the normal VCNR characteristic was observed, Fig. 4.13.

4.3.4. Thermal-Voltage Memory Effect in Cu-SiO/B_2O_3-Cu Structures.

As mentioned in the previous sections, the I-V characteristics of Cu-SiO/B_2O_3-Cu structures had been found to have relatively higher stability with greater degree of reproducibility than devices made with silver and aluminium electrodes. Therefore, devices carrying copper electrodes were expected to be more suitable to be used in low temperature measurements, in order to obtain further reliable information.

On decreasing the temperature the level of the circulating current decreased in a similar manner to its decrease with increasing air pressure. The general shape of the I_c-V characteristics remained nearly unchanged and the negative resistance region persisted until the temperature was lowered below a certain critical value. This varied somewhat between samples, but was usually in the range -43 to -35°C. At temperatures below the critical value the I_c-V characteristic of the sample for the first voltage increase is very similar to that of the room-temperature as is shown in Fig. 4.14 for a device of thickness 600Å at -65°C. Decreasing the voltage, however, resulted in inducing a high-impedance memory state. Further

voltage tracing of the sample more or less generated the same high-impedance (low-current) I_c-V characteristics. Different high-impedance memory states such as OA, OB and OC, shown in Fig. 4.15, could be easily induced by limiting the maximum applied voltage to V_A, V_B and V_C, respectively.

Electron emission into a vacuum was also temperature-dependent. The level of emission current was found to be lower at lower temperatures as can be seen in Fig. 4.16.

The observed thermal-voltage memory has been explained by Simmons and Verderber in terms of a 'dead-time' effect. According to these authors the memory state is erased when stored electrons, which are assumed to be injected under the original voltage bias and which subsequently tunnel towards the centre of the insulator at zero bias, are swept away to the anode at a threshold voltage V_T (see 2.3.2.). The length of time the electrons take to tunnel to the centre of the insulator is given by the dead-time. This is inversely proportional to the phonon-assisted tunnelling probability; at low temperatures this will be very low and hence increasing the dead-time to very large values. Thus there is insufficient time for the stored electrons to diffuse to the centre of the insulator, and the memory state cannot be erased, unless the dead-time is decreased by the raising temperature.

Another explanation, also involving the release of trapped charge, has been given by the filamentary model of Dearnaley et al (see 2.3.5.) in which the dead-time

is assumed to be a measure of the time between the filament rupturing and reaching a state from which it may re-form. According to this model the total current flowing through the device at voltage V is:

$$I = \int_{\rho_{min}}^{\infty} \frac{V}{\rho} P(\rho)\, d\rho \qquad 4.4$$

where $P(\rho)$ is the resistance distribution of the filaments and ρ_{min} is the minimum resistivity of the conducting filaments at voltage V. Filaments with resistance less than:

$$\rho_{min} = \frac{\alpha\tau_c V^2}{T_{max}-T_o} \qquad 4.5$$

are assumed ruptured due to the Joule heating. In equation 4.5 α measures the heating and τ_c characterises the cooling effect in a filament. T_{max} is the maximum temperature which a filament can bear before rupturing and T_o is the surrounding temperature. At a voltage of V_A in the negative resistance region, all the filaments satisfying the condition

$$\rho < \frac{\alpha\tau_c V_A^2}{T_{max}-T_o} \qquad 4.6$$

are broken and conduction is through the filaments having higher resistivity.

Under suitable conditions, by lowering the applied voltage from V_A to V_B new filaments with resistance ρ will regrow where

$$\frac{\alpha\tau_c V_B^2}{T_{max}-T_o} < \rho < \frac{\alpha\tau_c V_A^2}{T_{max}-T_o} \qquad 4.7$$

Therefore the current through the sample increases and VCNR is exhibited.

In the presenceof unfavourable circumstances such as operating the device atalow temperature not only are new filaments not re-formed, but the current decreases through the unbroken filaments with

$$\rho > \frac{\alpha\tau_c V_A^2}{T_{max}-T_o} \tag{4.8}$$

as a result of the voltage decrease. Thus the conduction type through the individual filaments characterises the current-voltage characteristic of a memory state which is given by:

$$I = \int_{\rho_A}^{\infty} \frac{V}{\rho} P(\rho)\, d\rho \tag{4.9}$$

for a V_A memory state. ρ_A is the minimum resistivity of the conducting filaments at voltage V_A.

However, once a thermal-voltage memory is induced, it remains until all the broken filaments are re-joined. The mechanism of rejoining the filaments, and hence recovery of the low-impedance state, can be explained successfully using the filamentary theory of Dearnaley et.al.(65). The rupture of a filament at a weak spot is accompanied by scattering of the electrons into the surrounding matrix of the insulator where they become trapped. The insulator then will be highly polarised locally near the broken parts of the filament. Only after the depolarisation of the insulator will the filament be capable of re-joining and thus restoring the low-impedence

characteristic. Relaxation of the polarised insulator is assumed to be due to a thermally activated Poole-Frenkel emission of the trapped electrons, and a long dead-time is expected at low-temperatures.

The normal low-impedance characteristic in our devices could be achieved, i.e. the erasure of the memory state, in two ways. First, by heating the sample up to room temperature, while it is kept under zero bias voltage, and then reducing the temperature again back to low temperatures and applying a voltage higher than a threshold value V_T across the sample. The I_c-V characteristics of a 600Å thick device before the transition (in its memory state) and after the transition to the low-impedance state are shown in Fig. 4.17. As it can be seen a fast transition from the high to low-impedance state occurs at $V_T \simeq 3.3V$. V_T was found to be relatively temperature-independent and varied between 2.5 and 3.5V in the temperature range of +23 to -160°C. Temperature cycling of the sample is believed to cause the release of the trapped electrons at higher temperatures. This leads to depolarisation of the dielectric, but the filaments still remain broken until V_T is applied. Under such conditions the electric field will tend to re-join the filaments by some kind of ionic migration possibly similar to what has been proposed in the model of Greene et al. (see 2.3.3.).

The second method of achieving the normal low-impedance state at low temperatures (when the device is in one of its memory states) is by loading the sample with

a bias voltage for a relatively long time. Fig. 4.18. shows the time dependence of relaxation of a V_A = 10V high-impedence state at three different temperatures; the applied voltage was reduced quickly from V_A=10V to a loading voltage of V_1 = 5V in all the three cases. As is observed the transition time is longer at lower temperatures which is in agreement with the proposed mechanism of the dielectric depolarisation. An observed increase of the transition time with decreasing loading voltages also predicted by the depolarisation proposal, is illustrated in Fig. 4.19 for the same device as for Fig. 4.18. The high-impedance memory state had been induced at V_A = 10V and the transition time was measured for different loading voltages of 5, 6, 7, 8 and 9V. After each transition to the low-impedance state and before measuring the next one at a different value of V_l, the temperature of the sample was raised to room-temperature and more or less the same high conductivity I_c-V characteristic could be re-traced. The time-dependence of the relaxation of a set of memory states at the same loading voltage of V_1 = 5V is shown in Fig. 20. It can be seen that the transition time increases with increasing impedance of the memory state, i.e. with increase of V_A. In other words, as the maximum resistance of the broken filaments increases, it takes longer for the filaments to re-join. This is consistent with the field-assisted emission of trapped electrons at lower effective electric fields around the broken parts of the high-resistance filaments.

Reduction of the conductivity just after the

completion of the transition shown in Figs. 4.19 and 4.20 could be due to the relatively high power dissipation in the sample which causes partial evaporation of the top electrode in the vicinity of some filament terminations[41].

4.3.5. Summary and Conclusions

M-SiO/B_2O_3-M Structures with different electrodes of copper, silver and aluminium could be electroformed in vacuum at pressures of less than 10^{-5} torr. Copper and silver electrode devices were readily electroformed, but higher voltages and longer time were needed for the forming process in devices with aluminium electrodes. The forming voltage was also found to increase with the insulator thickness. Vacuum-electroformed samples exhibited VCNR and electron emission into a vacuum in general agreement with the results previously reported. Copper and silver electrode devices also had higher levels of circulating current I_c and emission current I_e than those made with aluminium electrodes. However, devices with copper electrodes exhibited relatively stable current-voltage characteristics with a higher degree of reproducibility than the other two which showed current fluctuations in their I-V curves.

Electroforming was achieved in air at atmospheric pressure in devices with Cu and Ag electrodes showing VCNR characteristics, although in some samples the peak-to-valley ratio was very small. However, the negative resistance region in air-electroformed devices vanished after a few voltage cyclings.

Devices with Cu and Ag electrodes could also be electroformed with negative polarity, although the level of circulating current was low compared with positively-biased electroformed samples. In addition, they showed random erratic current fluctuations in their I_c-V characteristics. Electroforming was not possible for temperatures less than a certain value; this was found to be -50°C for copper electrode devices.

The behaviour of the vacuum-electroformed samples, depended strongly on the pressure of the ambient air. The height of the peak current decreased with the increase of air pressure and differential negative resistance disappeared at pressures greater than about 1 torr. A pressure-voltage memory effect has been observed in air at atmospheric pressure and the erasure of the induced high-impedance memory state, i.e. transition to the low-impedance state, was achieved by reducing the pressure to 10^{-5} torr and applying a threshold voltage of about 3.5V. The sensitivity of our devices to atmosphere and also the establishment of the high-impedance state in air may be explained by considering the physical structure of the assumed conducting channels in the filamentary model of Dearnaley et al[65]. The ambient atmosphere probably reacts with the filaments; and prevents conduction by oxidation or neutralisation of the traps by oxygen.

At low temperatures VCNR was observed only during the first increasing voltage run. Decreasing the bias voltage from any point in the negative resistance region

resulted in a monotonically decreasing current. Any subsequent voltage tracing of the sample at a low temperature generated more or less the same high-impedance I_c-V characteristic. The erasure of the induced memory state was possible either by the temperature cycling of the device and then applying a threshold voltage of $V_T \approx 2.5 - 3.5V$, or by loading the device by a voltage at a low temperature for relatively a long time. Transition time using the second method was found to depend on the temperature of the device, the maximum voltage by which the memory state is induced V_A and the loading voltage V_1. The observed thermal voltage memory and the relaxation of the high-impedance memory states can be explained by the filamentary model of Dearnaley et al[65], using the polarisation and depolarisation mechanisms of local regions of the dielectric.

4.4. INVESTIGATION OF M.I.M DEVICE SURFACES BY MEANS OF THE SCANNING ELECTRON MICROSCOPY

4.4.1. Introduction

It has been shown by many workers that the observation of the surfaces of electrically-operated M.I.M. structures can give valuable information about the regions which take part in the conduction. Park and Basavaiah[98] examined the physical changes that had occurred on the surface of a Zr-ZrO_2-Au junction, after the operation of device, using a scanning electron microscope. During the forming and switching from the high

to the low-resistance state a number of spots ranging between 5-7 μm in size were formed. In the low-resistance state the current was found to be concentrated mostly around a single spot. Electron microprobe analysis of the spots showed a compositional change of oxygen deficiency in the oxide layer around the rim of the spot.

Emmer[58] observed two different kinds of defects on the surface of the top electrode (Au) in Al-Al_2O_3-Au structures. The first kind which has been described as single-hole non-shorting breakdown of the dielectric layer were found in samples which had been operated at higher voltages during the electrical measurements. Defects of the second type were observed in all devices which showed VCNR. The formation of these defects, with a remarkably circular shape, is believed to be accompanied by strong local heating which is also responsible for the partial evaporation of the top electrode in the region of the defects. Moreover, Emmer has also suggested that the emission of electrons from the top electrode is attributed only to the second type of defects.

Taheri and Hogarth[51] reported that electron emission in Ag-SiO/B_2O_3-Ag was related to the local bright spots that appeared, near the edges of the defects, over the surface of upper electrodes.

Rakhshani, Hogarth and Abidi[41] studied the different kinds of damage produced during the forming process of VCNR in Ag-SiO/BaO-Ag structures. They concluded that the defects were associated with the formation of the filamentary channels bridging the two

electrodes across the insulator. The structure of the filaments was found to be different at the two ends and would take the geometrical form of truncated cones rather than cylinders[99]. It was also proposed that the presence of a high field region somewhere along the filaments could be responsible for the initiation of an electrolytic process giving rise to the evolution of oxygen from the positive electrode and the congestion of metal ions at or near the negative electrode. Evolution of oxygen has also been reported by Budenstein and Hayes[100], to occur during the breakdown of thin-film Al-SiO-Al structures. They proposed that the breakdown was due to the following electrochemical solid reaction; $Si\text{-}O\text{-}Si + \text{(breakdown electric field)} \rightarrow Si\text{-}Si^{+} + O + e$. The breakdown field is assumed to be local and not the average field through the dielectric. The right-hand side of the equation shows the results of the reaction which are; two atoms of silicon bonded as in crystalline silicon (one ionised), a free atom of oxygen, and an electron that is injected into the surrounding dielectric medium.

By using an electron-microprobe analyser Rakhshani and Hogarth[99] investigated the composition of the materials corresponding to the different parts of the damaged region in their Ag-Sio/BaO-Ag devices. The centre of a defect at the anode was found to be a region of silicon deficiency, whereas the composition of silicon was rather high in the vicinity of the defect where the silver electrode had been largely removed. The edge of the defect was rich in silver as a result of a thermally

assisted diffusion of silver from the centre of the defect towards the edge. At the cathode the silver and silicon line scans showed no particular compositional variation across the defects.

4.4.2. Principle of the Scanning Electron Microscope

The Scanning Electron Microscope (SEM) is an electron-optical instrument, which was developed in the same decade as the Transmission Electron Microscope (TEM), but did not become commercially available until some 25 years later than the TEM, in 1965.

Fig. 4.4.1. illustrates the principle of the SEM. A finely-focussed electron beam strikes a point in the specimen surface. The interaction between the electrons and the solid generates a variety of signals. Each of these can be collected and amplified. The resulting signal is utilised to control the brightness on a cathode ray tube (c.r.t).

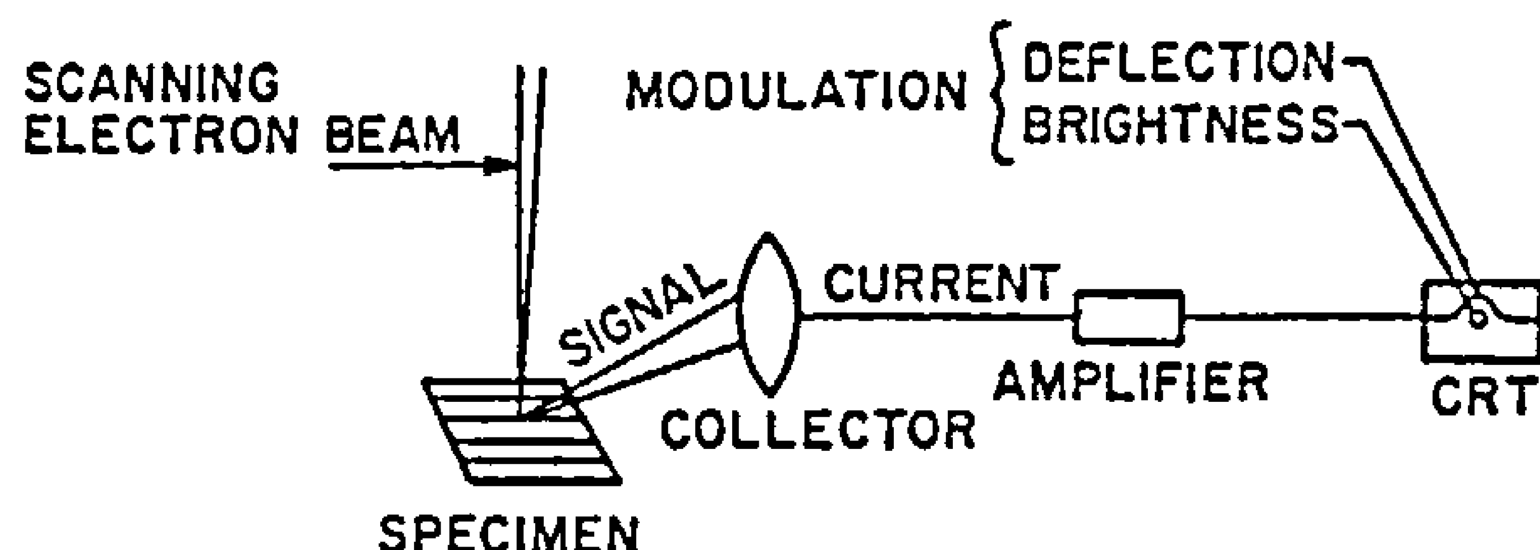

Fig. 4.4.1. The principle of the SEM

To obtain signals from a particular area, the electron beam is scanned in a TV-raster fashion over the specimen surface by two pairs of electro-magnetic coils. Because the c.r.t. scan is synchronised with the beam scan, the signals are transferred point to point and a signal map of the scanned area is displayed. Changes in brightness represent changes of a particular property within the scanned area of the specimen. Operating parameters, such as accelerating voltage, beam diameter and current, angle of incidence, and line and frame speeds are selected so as to optimize the quality of the resulting image and to ensure complete coverage of the c.r.t.[101].

Fig. 4.4.2. shows the various mechanisms of signal generation[102]. These signals are generated when electrons of energies up to 50kV penetrate the specimen surface and interact with atoms of the solid. In the coulomb field of the nucleus the primary electrons are elastically scattered, i.e. their path is changed without energy loss. The majority of the scattering events are inelastic collisions with electrons of the host atoms. The inelastic collision is an energy transfer from the incident electron to the bound electron. The path of the primary electron is changed and its energy reduced. The bound electron is excited, or it becomes a free carrier electron, or it leaves the ionized atom.

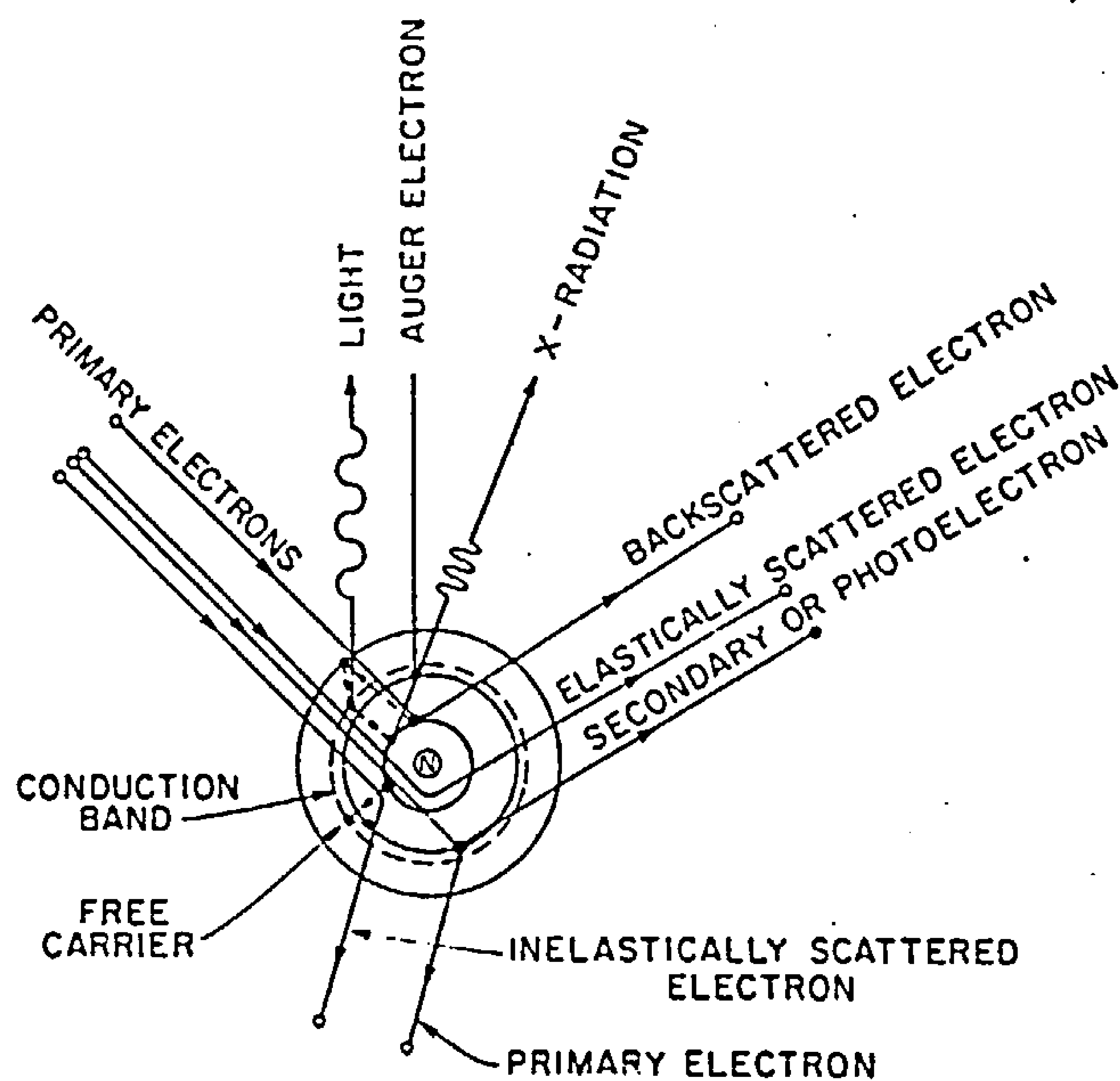

Fig. 4.4.2. The interaction between the primary electrons (o) and the host atom and its electron(●) lead to the generation of a variety of signals.

The generated signals shown in Fig. 4.4.2. such as secondary, back scattered, and Auger electrons emitted from the specimen surface carry a mixture of topographical and chemical information. Radiation energy in the form of X-rays, infrared emission, and cathodoluminescence carry other compositional information.

4.4.3. Results and Discussion

Devices studied in the SEM were prepared by the thermal co-evaporation technique in the manner fully described in Chapter 3. Thin films were deposited on 1"x3" well-cleaned Corning glass substrates. The

thicknesses of the dielectric layers (SiO/B_2O_3) were 1700Å for all the samples and the electrode materials were silver and copper with thicknesses in the range 600-1100Å. Samples were electrically operated and electroformed both in a vacuum (10^{-5} torr) and at atmospheric pressure of air, and then examined in a scanning electron microscope (Cambridge stereoscan S4) operating in the secondary mode.

Fig. 4.21. shows a scanning electron micrograph taken from the top electrode surface of an Ag-SiO (65%)/ B_2O_3 (35%)-Ag device after it had been electrically operated in vacuum. The thicknesses of the dielectric and top electrode were 1700 and 600Å respectively. Maximum voltage applied across the sample (with counter-electrode positive) was V_b = 4.8V, i.e. the forming voltage. Fig. 4.21. shows that a hole with a diameter of about 10 μm, has been formed by local evaporation of the electrode material and the electrode layer is partially lifted around the hole. The brightness of the hole may be due to the charging effect of the dielectric. The physical changes in the structure of the surface, however, can be the result of the formation of filaments and evolution of gas (probably oxygen, due to the dissociation of the dielectric) during the development of conductivity. It seems from the figure that the pressure of accumulated oxygen under the electrode layer has not been high enough to tear off the blister, and has been able to penetrate out of it possibly through the damaged region on the right hand side of the blister. A defect on the top electrode

of another sample, but on the same substrate as the sample in Fig. 4.21. is represented in Fig. 4.22. This device had been electroformed, with its top electrode positively biased, showing VCNR and electron emission into a vacuum. Such a pattern appears to be the result of a blister rupturing due to the pressure of oxygen accumulated under the electrode and also from localised heating leading to the local melting and evaporation of the electrode material. Figs. 4.23 and 4.24 show electron micrographs from the counter electrode of a Cu-SiO (65%)/ B_2O_3(35%)-Cu device electroformed in vacuum. The counter electrode had a thickness of ~1000Å and was biased positively. Defects at the top electrode have more or less circular shapes with a typical size of about 5μm and in some exceptional cases up to 10μm. Such a defect with larger size probably is a coalescence of two or more punctures forming a multiple defect. Electron emission into a vacuum is believed to take place from separate sources which correspond to the punctures at the top electrode[51,103].

Defects observed at the negative electrode were quite different from those on the positive electrode. An electron micrograph from the surface of a sample, electroformed in vacuum with negative top electrode is shown in Fig. 4.25. These defects, as has already been suggested[41], seem to be the area where the cations are congested as a result of the electrolytic process.

As was pointed out earlier in 4.3.2., our devices carrying Cu and Ag electrodes could be electroformed at atmospheric pressure of air and most of them showed the

negative resistance region in their I-V curves. Fig. 4.26 shows an electron micrograph from the surface of an Ag-SiO/B_2O_3-Ag device electroformed in air with positively biased top electrode of 600Å thickness. A SEM picture from one of the observed defects (with higher magnification) is shown in Fig. 4.27. This type of defect seems to be porous in structure which never peels off, probably because of the pressure of air which neutralises the pressure of oxygen under the electrode layer. In addition, these defects are expected to be different from the compositional point of view, from those observed at the anode of vacuum-electroformed samples. This can be related to the compositional changes occurring at gas-metal boundaries at high temperatures produced at the filaments termination (local oxidation).

4.4.4. Conclusion

We observed many tiny local defects over the surface of our samples after being electrically operated and electroformed both in vacuum and atmospheric pressure of air. These defects are believed to be the result of the formation of conducting filaments across the insulator in some parts of the device. Accumulation of gas (probably oxygen) under the positive electrode layer supports the idea of an electrolytic process occurring along the filaments. Operating a device at higher voltages and after several voltage cyclings causes the pressure of accumulated oxygen to increase and this eventually ruptures the blister (Fig. 4.22). In addition, a considerable

heating due to the current carried by the filaments gives rise to the local evaporation and melting of the counter electrode.

Although, it is always difficult to be sure that conduction is necessarily occurring through the visible defects, the level of circulating current I_c and emission current I_e seem to depend on the density of damaged regions formed on the surface of the samples. Our observation of the surface of electroformed samples showed that the number of defects formed on the top electrode in devices with copper electrodes were remarkably higher than for the samples carrying silver electrodes. This is in favour of the electrical measurements which showed that the maximum current passing through devices with copper electrodes were higher than those having silver electrodes.

Defects observed at the cathode could be explained as the result of the local congestion of materials on the negative ends of the filaments, as suggested by Rakhshani, Hogarth and Abidi[41]. There are some similarities from the shape point of view between defects produced in vacuum and those formed in air on the positive electrode. The latter however, do not peel off may be due to the pressure of air acting on the surface and neutralising the pressure of oxygen under the electrode layer.

4.5 OBSERVATION OF SWITCHING PHENOMENA

4.5.1. Introduction

Electrical switching effects have been observed in a number of thin oxide and complex oxide films sandwiched between two metal electrodes. Various proposals have been put forward to account for the switching behaviour in these devices, but no general agreement has yet been reached on the details of the mechanism involved. This disagreement arises because many of the switching properties are consistent with more than one model of the event and because the nature of the event is complex and often determined by more than one process. However, switching phenomena are frequently initiated and developed by electronic or thermal processes. The role of the thermal processes is extensive, as these are not restricted to thermally-initiated switching but may determine also the continuation of an event initiated by an electronic process. In the following section we briefly review some of the switching phenemena previously observed in thin oxide films.

4.5.2. Previous Work on Switching in Metal-Oxide-Metal Structures

Current-controlled negative resistance and bistable switching events have been observed in a variety of amorphous thin oxide films including Nb_2O_5[69,70,71,104,105,106], TiO[72], Al_2O_3[107], NiO[73], ZrO[98], GeO_2[108] SiO[107,109] and the complex oxide SiO/BaO[80]. By increasing the reverse current through a thin (50-500Å)

niobium oxide sandwich structure up to about 100mA/cm^2 it was observed[70] that the characteristic of the device was transformed irreversibly from a rectifying characteristic to a symmetrical one; exhibiting CCNR for both directions of the current flow. The short relaxation time ($<10^{-6}$ sec) determined from the self-sustained oscillations of more than 60 MHz and also the very weak dependence of the CCNR region on temperature down to 77°K, led Chopra to suggest that an avalanche multiplication of electrons in the insulator was the mechanism responsible for CCNR in the I-V characteristic. Beam and Armstrong[104] reported that conduction and CCNR in Nb_2O_5 occurred at filamentary singularities and the current passing in the 'on' state was found to be independent of the active area of the device. Different metal contacts were used, but no significant change was observed in the I-V characteristic. The authors however, suggested that the mechanism involved in the observed CCNR is largely electronic.

Bistable switching between two conductance states, in Nb-Nb_2O_5-Bi structures, has been reported by Hickmott and Hiatt[105], and Basavaiah and Park[106]. Freshly prepared samples were found to be rectifying and the direction of easy current flow was with Bi positive[105]. The forming procedure which has been reported to be necessary for the development of switching could be accomplished either by application of a direct voltage across the device in the direction of easy current flow or by voltage pulses of appropriate amplitude. However, at the forming voltage sudden breakdown occurs to a

high-conductivity state. Bistable switching then could occur between this state and two other states with higher conductivities, which exhibit CCNR in their I-V characteristics, Fig. 4.5.1.

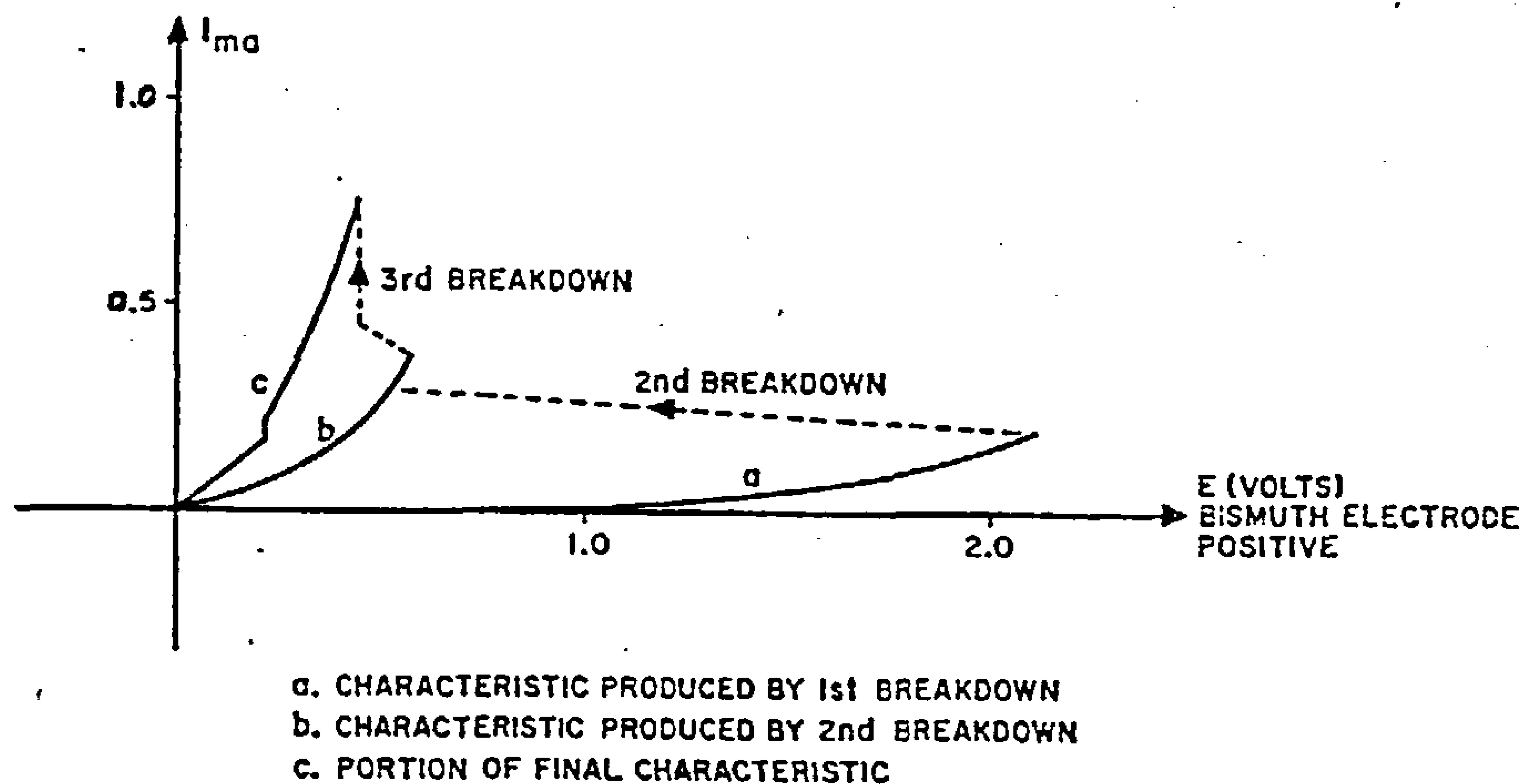

Fig. 4.5.1. Stages in breakdown of $Nb-Nb_2O_5-Bi$ diode to a high conductivity-state (after Hickmott and Hiatt Ref. 105)

The speed of switching, the low voltage and the amount of power required for the switching processes led Hickmott and Hiatt to postulate that an electronic mechanism rather than melting or a phase change, was the cause for the observed phenomena.

Further works on switching in the $Nb-Nb_2O_5-Bi$ system have also been carried out by Basavaiah and Park[106]. They found that a number of these devices were stable for more than a million pulse switching

operations without noticeable degradation and a few of them could withstand switching operations in excess of 10^9 for sinusoidal voltages. In order to initiate the switching process a forming voltage of about 30V (for a 1300Å thick oxide layer) was applied across the device via a current limiting resistor of 50kΩ with the Bi positively biased. The breakdown of the initial high-resistance state was usually associated with the appearance of a single spot of a few square microns ($\sim 2\mu m^2$) observable on top of the bismuth film. Conduction mechanisms in the unformed samples were shown to be due to electron injection and space-charge-limited current at high temperatures and low voltages, a bulk-controlled Poole-Frenkel process at intermediate voltages and low temperatures, and field-assisted tunnelling at very high fields and very low temperatures. After the forming process of the sample, it could be switched between a high-resistance state (typically greater than 60kΩ) and a low resistance state (less than 5kΩ) by applying voltages of proper magnitude and polarity. The bismuth electrode had to be biased positively for switching from the high-resistance to the low-resistance state and negatively for the inverse transition. The conduction mechanisms in the two states were different; the high-resistance state had a characteristic activation energy, whereas the low-resistance state was characterised by its very low temperature dependence, near-ohmic behaviour at low voltages, a current-controlled negative resistance kink between 0.2 and 0.3V, and a power law

behaviour of current at higher voltages.

Recently Fuschillo et al[110] investigated the switching effects in Nb-Nb_2O_5-Nb structures where the Nb counter-electrodes were either evaporated or RF sputtered onto the amorphous films of Nb_2O_5. These authors reported that the need for the forming procedures used by others[105,106] to initiate the switching process was eliminated by an implantation-diffusion process in the amorphous Nb_2O_5 films, resulting from the sputtering of Nb electrodes. The advantage of an implantation-diffusion process by Nb atoms in Nb_2O_5 amorphous layers, which allows switching from the initial state, is that it represents a well-controlled process resulting in a reproducible fabrication of the device with similar characteristics. Of practical interest is also the change in the threshold voltage and initial resistivity of samples with the sputtering voltage.

The titanium-anodized titanium oxide-metal structures are reported to switch between three distinct conductivity states[72]. Counter-electrodes of Al, Cu, Ti and Bi were made by evaporation of appropriate metals. Switching from one state to another state could take place either in vacuum, in the atmosphere or in liquified nitrogen at any temperature in the range 77°- 500°K. Switching could be brought about either by voltage cycling or by applying pulses as described by Hiatt and Hickmott[71]. The three observed conductivity states were found to be symmetric with respect to voltage and exhibited memory at room temperature. The characteristic of the first state at

higher fields showed a steep power law whose exponent was approximately six. The second state had an V-I characteristic showing a three halves power law for lower fields and becoming steeper at higher fields. The third state showed a purely ohmic characteristic independent of temperature. After several switching cycles some samples failed, either remaining in the initial 'off' state or in the final 'on' state.

Switching between a high-resistance state (25MΩ) and a low-resistance state (100Ω) has been observed in Ni-NiO-metal (Al-Ag-Au) systems by Gibbons and Beadle[73]. These workers have suggested that switching from the 'off' to 'on' state occurs in these devices because of the formation of a metallic filament across the insulator bridging the two contacts. The filament was believed to be made of nickel atoms collected at a structural defect in the oxide during the application of the on-signal. The transition to the 'off'-state was accomplished by applying a signal that ruptures the metallic filament.

Park and Basavaiah[98] reported bistable switching in Zr-ZrO_2-Au sandwich structures. The conductivity of fresh sample was first developed in the atmosphere by the application of a direct voltage across the specimen, while in series with a large resistance in the circuit. The formed samples then could switch between the high-resistance state (hundreds of kΩ) and the low-resistance state with a resistance of a few hundred ohms and occasionally less than 100Ω. Switching from the high to the low resistance state was attributed to the formation

of a single conducting filament across the oxide with the structure characteristic of neither a metal nor a dielectric. Observation of the surface of the samples during the switching operation by means of the scanning electron microscope revealed that in each transition from 'off' to 'on' state a few more filaments build up, but however, only one carries the main current in the 'on' state.

Investigation of the memory switching effects in evaporated SiO layers sandwiched between silver and cobalt electrodes led Manhart[109] to propose a filamentary model. In this model diffusion of metal ions from electrodes into the insulator were believed to be responsible for the formation of the filaments. Memory switching could be observed after a forming process in devices with one or both electrodes made of silver and not with aluminium electrodes. Forming was carried out by applying a single rectified sine-wave pulse of V=12-15V and a duration of about 0.5 sec across the sample. The I-V characteristic of the high-resistance state was non-linear and showed a field dependence of the form $\sigma \propto \exp E^{\frac{1}{2}}$, similar to the Poole-Frenkel effect or Schottky emission mechanism. Contrary to the high-resistance state, the resistance of the 'on' state was found to be independent of the sample area, showing a linear I-V characteristic with a positive temperature coefficient of resistivity. The transition from 'off' to 'on' state (set operation) could be accomplished by applying a voltage pulse of V = 6-8V with smooth edges and relatively long duration

greater than 0.1m sec. The inverse transition (reset operation) was achieved by a very short pulse of V = 10V with steep edges and duration of 10-1000n sec. Two explanations have been given for the observed memory switching effect:

(i) The short pulse during the reset operation heats only the narrowest part of the filament. The enhanced diffusion from this part breaks up the conducting filament. Only a long pulse (in set operation) is able to heat the boundaries sufficiently to cause new diffusion from the electrodes.

(ii) The short reset pulse with steep edges melts the narrowest part of the conductive filament. The rapid cooling of the metal portion of the filament then causes the mixture of SiO and metal to freeze in. The set pulse heats up a path in the mixed SiO and metal region, remelting it. Because of the smooth edge of the set pulse the hot channel is cooled down slowly and the difference in the freezing points of the metal and the SiO results in a separation of the two constituents, thereby restoring a continuous metal filament.

Recently Rakhshani and Hogarth[80] (1978) studied low-voltage switching effects in M-SiO/BaO-M sandwich structures. Devices were first electroformed in air in the presence of a high series resistance in the circuit. Formed samples then could switch between the 'off' and 'on' states. The authors have proposed a mono-filamentary model to account for the observed switching phenomena. Formation of a conducting filament across the insulator

layer has been described as a result of a sequence of events occurring such as; voltage instability at the threshold voltage, thermal runaway, energy discharge and raising the temperature along a filamentary path, and metal injection into the channel. Transitions from the 'on' to 'off' state were considered to be a result of thermally-assisted rupturing of the filament.

4.5.3. Experimental Details

Thin films of SiO/B_2O_3 complex oxides sandwiched between silver and copper metal electrodes were prepared on Corning glass substrates by the conventional vacuum deposition method, as was described in Chapter 3. In some devices, the counter-electrodes were simply made by applying drops of silver paste, instead of evaporated strips of silver or copper electrodes. Electrical measurements were carried out in air at atmospheric pressure, employing the electrical circuit shown in Fig. 4.28. The current passing through the sample was measured by an electronic avometer EA 113; a valve voltmeter model V-7AU indicated the voltage drop across the device and the power supply used was a Coutant LA 100.2 50V, 1A and/or a LB 500.2 30V, 5A instrument. The resistor R_L was placed in the circuit, in series with the sample, to limit the circulating current in the "on"-state and was in the range of a few tens of ohms to a few

tens of kilohms. Key K provided instantaneous high current flow through the 'on'-state by shorting the load resistance to switch off the device.

4.5.4. Results and Discussion

Devices of M-SiO/B_2O_3-M structures, with silver and copper electrodes, exhibited switching characteristics with memory after an initial electroforming process in air at atmospheric pressure. The forming was carried out by the application of a direct voltage of V=15-25V across the virgin device in series with a large resistor of 10-20kΩ in the circuit. The sample is initially in a high resistance-state; the resistance usually being larger than 10^6Ω. At the forming voltage the device breaks (non-destructive) to a high-conductivity state in the range between a few ohms and a few thousands of ohms depending upon the electrode and the loading resistance R_L.

After the forming process, i.e. the development of a high conductivity-state, the samples could be switched between the two resistance 'off' and 'on' states. Switching to the 'on'-state could be achieved either by increasing the applied voltage above a threshold value V_{TH} with a high load resistance in the circuit, or by decreasing the voltage to a certain value V_{on}, with a small load resistance in the circuit when a fast switching to the 'on'-state takes place. A typical memory-switching

characteristic of a Cu-SiO/B_2O_3(2000Å)-Cu device, in the presence of a load resistance of R_L=20kΩ in the circuit, is given in Fig.4.29. The current-voltage characteristic of the sample in the low conductivity 'off'-state obeys the relationship $I \alpha V^n$, where n usually varies between 1 and 5. In the low voltage region (up to 1 V) the characteristic is ohmic and becomes superlinear at higher values of the voltage. The power laws beyond the ohmic region may be due to the space-charge-limited currents as has been reported by other workers [72-80]. However, at the threshold voltage V_{TH} the element switches to the high conductivity 'on'-state, which is ohmic with memory character. The sample remains in this state even after the voltage removal. The 'off'-state could be recovered by the application of a current pulse to the sample.

Fig.4.30 shows a typical memory switching characteristic of an Ag-SiO/B_2O_3(1000Å)-Ag device when in series with a load resistance of R_L=100Ω. In the high conductivity 'on'-state the current flows through the sample until at a critical value of current the sample switches to a low conductivity 'off'-state along the load line. When the voltage is reduced, at a voltage of V_{on}=4V, the sample switches back to the 'on'-state. Switching times were fast, however, in devices with very low loading resistance in the circuit,only after a few switching cycles, instead of a fast transition from the 'off' to the 'on'state, the current increased slowly displaying VCNR in the I-V characteristic. Heat dissipation from the switching elements has been reported

to have an important role in the switching characteristics [115]. Our devices with silver paste drops as counter-electrodes were found to break to the 'on'-state at higher voltages; the transitions from 'off' to 'on'-state also occurred at much higher values of V_{on}, compared to the values obtained in devices with ordinary evaporated top electrodes. Blowing air onto the surface of the samples, i.e. increasing the rate of heat transfer, also increased the value of V_{on}. It was further observed that V_{on} decreases with increasing the device temperature and increases by placing higher values of R_L in the circuit. Referring to the previous works on switching behaviour in MIM structures, the memory switching observed in our devices can be explained by a model based on the formation of a single conducting filament across the insulating layer during the forming process as follows;

When a direct voltage is applied to a virgin device the current passing through the sample increases due to different electronic processes. The presence of non-uniformities in the geometrical, structural and chemical nature of the device results in the inhomogeneities in the field which in turn may encourage the formation of a conducting channel. The constriction of the current through such a channel raises the temperature of the device by Joule heating until at a threshold voltage a thermal runaway occurs and the voltage across the sample collapses to a small value. The discharge of the stored charge, due to the voltage collapse, increases the temperature of the channel probably up to some

hundred of degrees, leading to the diffusion of metal atoms into the hot channel, forming a metallic filamentary path.

Formation of a filamentary path across the thin layers of dielectrics and semiconducting glasses and also the injection of metal ions into insulators have been observed, both theoretically and experimentally, by a number of investigators (83-80-84-111-43-109-112). Although Gibbons and Beadle (73) suggested that the switching process in metal oxides is due to the oxide itself and not electrodes, it has been shown that in some insulators such as SiO/BaO and SiO the formation of a metallic filament across the insulator is largely due to the injection of metal ions from the electrodes into the insulator (80-109). The evidence for the diffusion of electrode metal atoms (Au) during memory switching in thin selenium films (4500Å thick) has been given by Collins and Jones (113), presumably to form some sort of conducting filament.

However, once the filament is formed the sample switches to a high-conductivity 'on'-state. Returning the sample to its original low-conductivity 'off' state can be achieved by increasing the 'on'-state current, e.g. by means of shorting the load resistance in the circuit, inducing thermal rupturing of the metallic filament at a weak point along its length, similar to the model of Dearnaley et al. In devices with silver paste drops as top electrodes, thermal energy can more readily be dissipated, hence higher voltages are required to develop

the instability if an electrothermal mechanism rather than a purely electronic mechanism is to be involved in the instability[114-115]. The larger V_{on} observed in these samples may also be related to the effect of using good heat sinks compared to those having ordinary thin evaporated top electrodes. The appearance of VCNR in the current-voltage characteristics of the samples with very low-value series resistance in the circuit, after a few switching cycles, can be attributed to the formation of further filaments during the switching operations.

CHAPTER FIVE

SUMMARY AND CONCLUSIONS

The d.c. electrical properties of thin films of the evaporated dielectric system SiO/B_2O_3 with different electrode materials have been studied. Under vacuum conditions, devices with different electrodes of copper, silver and aluminium could undergo an electroforming process when a voltage greater or equal to the forming voltage V_F, was applied across the sample. The forming voltage was found to depend on the dielectric thickness, temperature and the electrode material. Copper and silver electrode devices were readily electroformed, but higher voltages and longer times were needed for the forming process in devices with aluminium electrodes. A linear correlation between $\ln I_c$ and $V_b^{\frac{1}{2}}$ was observed in un-formed samples having Al electrodes and the conduction mechanism was found to be consistent with Schottky emission. Vacuum-electroformed samples exhibited voltage-controlled negative resistance characteristics and electron emission into a vacuum. The peak current in the I_c-V_b characteristic of all the samples with different electrode materials occurred at voltages between 3 and 5V and the onset of the emission current coincided approximately with the voltage corresponding to the peak current. Devices having copper electrodes had relatively stable current-voltage characteristics with a higher degree of reproducibility than devices carrying silver and aluminium electrodes which showed

current fluctuations in their I-V curves.

Electroforming was possible with a reversed polarity in devices with Cu and Ag electrodes. The level of current in negatively electroformed samples, however, was much lower than in those electroformed with the top electrode positively biased.

Contrary to previous observations, our devices with Cu and Ag electrodes could be electroformed in air, showing VCNR characteristics. However, the negative resistance region in the I-V characteristic of air-electroformed samples disappeared after a few voltage cycles.

The behaviour of the vacuum-electroformed samples was found to depend on the pressure of ambient air. On increasing the pressure in the chamber, a decrease in the current was observed until at a pressure of 1 torr the negative resistance region completely disappeared. The vacuum-electroformed samples also showed a pressure-voltage memory effect when operated in air at atmospheric pressure. The high-impedance state induced in this way could be erased by reducing the air pressure and applying a threshold voltage of about 3.5V across the sample.

On decreasing the temperature the level of the circulating current decreased in a similar manner to its decrease with increasing air pressure. At temperatures below a critical value the VCNR was only observed for the first voltage increase and a high-impedance state was established on reducing the applied voltage to zero. Time-dependent transitions of the high-impedance state

lower-impedance states at low temperatu...
...red in our devices carrying Cu electrodes. Such ...sitions could occur by loading the sample by a ...age at low temperature for a relatively long time. ... transition times were found to depend on the ...mperature of the device, the maximum voltage by which ...he memory state is induced and the loading voltage. Fast transitions to the normal low-impedance state at low temperature were also possible by temperature cycling of the device and then applying a threshold voltage of $V_T \approx 2.5-3.5V$. This threshold voltage is temperature-independent in the range between +23°C and down to at least -160°C.

Referring to the various models which have been proposed to explain the electroforming process and the observed related phenomena in MIM structures (discussed in Chapter 2), the above results can be best explained by the polyfilamentary model of Dearnaley et al which is further supported by the surface topographical observations of the samples. The sensitivity of our devices to the ambient pressure of air and the establishment of the high-impedance state in air may be explained by considering the physical structure of the assumed conducting filaments in the model of Dearnaley et al. The ambient atmosphere probably reacts with the filaments and prevents conduction by oxidation or neutralization of the traps by oxygen. The observed thermal-voltage memory and the relaxation of the high-impedance memory states have also been successfully described by the

filamentary model, using the polarization and de-polarization mechanisms of local regions of the insulator.

The defect regions over the surface of samples produced during the electroforming process and electrical operation, both in vacuum and atmospheric pressure of air, were investigated by means of a scanning electron microscope. The formation of these defects on the sample electrodes is believed to be due to the growth of conducting filaments across the insulator and the consequence of Joule heating as a result of the current carried by the filaments. Accumulation of gas, most likely oxygen, under the anode layer during the electroforming of the device in vacuum supports the idea of an electrolytic process occurring along the filaments. Electron emission into a vacuum takes place from the positive ends of the filaments. Partial evaporation of the top electrode is a result of the pressure of gas under the electrode as well as the considerable heating due to the current passing through the filaments.

Defects observed at the cathode are quite different from those at the anode. These defects seem to take the form of congested materials (cations) around the negative ends of the filament, as a result of the electrolytic process. The observed defects at the anode of air-electroformed samples are porous in structure. These defects never peel off, probably because of the pressure of air which prevents peeling of the electrode. Moreover, a change in the electrode composition is expected to occur (probably local oxidation of the electrode) due to

the reactions occuring at the gas-metal boundaries at the high temperatures produced at the positive ends of the filaments. This is possibly the reason that air-electroformed samples show VCNR only for a few voltage cycles.

Devices of M-SiO/B_2O_3-M structures with silver and copper electrodes, exhibited switching characteristics with memory after an initial electroforming process in air. This has been described by a mono-filamentary model, based on the formation of a metallic filament across the insulator, during the forming process. This filament can be thermally ruptured and regrown in the presence of an electric field and favourable conditions.

Finally, it can be concluded that the filamentary model of Dearnaley et al, together with the idea of a solid-state electrolytic process which occurs along the filaments as well as the metal injection into the filamentary paths, is capable of explaining most of the observed effects in our samples.

From the technical point of view it is doubtful whether the switching and electron emitting devices studied in this thesis are yet ready for industrial development. More attention will need to be paid to the reproducibility of properties and to the achievement of highly stable characteristics before this next stage is reached.

REFERENCES

1. COUTTS. T.J.; "Active and Passive Thin Film Devices" (Academic Press, London, New York San Francisco, 1978).
2. KREYNINA. G.S., SELIVANOV, L.N. and SHUMSKAIA, T.I.; Radio Eng. Elect. Phys. 5, 219 (1960).
3. OVSHINSKY, S.R.; Phys. Rev. Lett, 21, 1450 (1968).
4. CHOPRA, K.L.; "Thin Film Phenomena", (McGraw-Hill, New York, 1969).
5. GLANG, R; "Handbook of Thin Film Technology", Ed. Maissel. L.I. and Glang, R. Chapter 1 (McGraw-Hill, New York, 1970).
6. LAMB, D.R.; "Electrical Conduction Mechanisms in Thin Insulating Films" (Methuen and Co. Ltd., London, 1967).
7. MOTT, N.F.; Phil.Mag, 19, 835 (1969).
8. COHEN, M.H., FRITZSCHE, H., and OVSHINSKY, S.R.; Phys. Rev. Lett, 22, 1065 (1969).
9. DAVIS, E.A. and SHAW, R.F.; J. Non-Crystalline Solids, 2, 406 (1970).
10. DAVIS, E.A. and MOTT, N.F.; Phil.Mag. 22, 903, (1970).
11. CAMPBELL. D.S. and MORLEY, A.R.; Rep. Prog. Phys. 34, 283 (1971).
12. Simmons, J.G., "DC Conduction in Thin Films" (Mills and Boon Ltd., London, 1971).
13. SIMMONS, J.G.; J. Phys (D):Appl.Phys. 4, 613 (1971).
14. MEAD, C.A.; Phys.Rev. 128, 2088 (1962).
15. HILL, R.M.; Thin Solid Films. 1, 39, (1967).
16. JONSCHER, A.K.; Thin Solid Films. 1, 213 (1967).

17. JONSCHER, A.K. and HILL, R.M.; "Physics of Thin Films", Ed. Hass, G., Francombe, M.H. and Hoffman, R.W., Vol 8, p. 169 (Acadmenic Press, London and New York 1975).

18. FRENKEL, J.; Phys.Rev. 54, 647 (1938).

19. JOHANSEN, I.T.; J. Appl. Phys. 37,499 (1966).

20. SIMMONS, J.G.; Phys. Rev. 155, 657 (1967).

21. SIMMONS. J.G.; Transactions of the Metallurgical Society of AIME, 233, 485 (1965).

22. HUNG, C.S. and GLIESSMAN, J.R.; Phys. Rev, 79, 729 (1950).

23. MOTT, N.F. and DAVIS, E.A., "Electronic Processes in Non-Crystalline Materials" (Clarendon Press. Oxford, 1971).

24. MOTT, N.F. and GURNEY, R.N.; "Electronic Processes in Ionic Crystals", (Oxford University Press, 1940).

25. ROSE, A.; Phys. Rev. 97, 1538 (1955).

26. LAMPERT, M.A. and MARK, P.; "Current Injection in Solids", (Academic Press, New York, 1970).

27. KREYNINA, G.S.; Radio Eng. Elect. Phys., 7, 166 (1962).

28. KREYNINA, G.S.; Radio Eng. Elect. Phys, 7, 1949 (1962).

29. HICKMOTT, T.W.; J. Appl. Phys, 33, 2669 (1962).

30. SIMMONS, J.G. and VERDERBER, R.R.; Proc. Roy. Soc., A301, 77 (1967).

31. RAKHSHANI, A.E. and HOGARTH, C.A.; Int.J. Electronics, 42, 465 (1977).

32. MOHSENIAN, A.; Ph.D. Thesis, Brunel University (1977).

33. GREEN, P.D., BUSH, E.L., and RAWLINGS, I.R.; Proc. Symp. On Deposited Thin Film Dielectric Materials, Ed. F. Vratny (The Electrochemical Society: New York, 1968).

34. SUTHERLAND, R.R.; J. Phys. D: Appl. Phys, 4, 468, (1971).

35. MANN, H.T.; J. Appl. Phys., 35, 2173, (1964).

36. ZOR, M; Ph.D. Thesis, Brunel University (1977).

37. HOGARTH, C.A. and ZOR, M.; Thin Solid Films, 27, L5 (1975).

38. GUNDLACH, K.H. and KADLEC, J.; Phys. Stat. Sol. A10, 371, (1972).

39. COLLINS, R.A., BOWMAN, G. and SUTHERLAND, R.R.; J. Phys. D: Appl. Phys, 4, L49 (1971).

40. HIRANO, M, KURIKI, S. and MATSUMOTO. G; Appl. Phys. Lett. 26, 80 (1975).

41. RAKHSHANI, A.E., HOGARTH, C.A. and ABIDI, A.A.; J. Non-Crystalline Solids, 20, 25 (1976).

42. VERDERBER, R.R., SIMMONS, J.G., and EALES, B.; Phil. Mag, 16, 1049 (1967).

43. PIVOT, J, BOUDELLE, M., CACHARD, A. and DUPUY, C.H.S.; Phys. Stat. Sol. (a) 2, 319 (1970).

44. HICKMOTT, T.W.; Thin Solid Films, 9, 431, (1972).

45. DEARNALEY, G., STONEHAM, A.M. and MORGAN, D.V.; Rep. Prog. Phys, 33, 1129 (1970).

46. BERNARD, J., DELACOTE, G. and MENTALECHETA, Y.; Phys. Stat. Sol. 31, 315 (1969).

47. HOGARTH, C.A. and TAHERI, E.H.Z.; Int. J. Electronics 37, 145 (1974).

48. ABIDI, A.A. and HOGARTH, C.A.; Thin Solid Films, 22, 203 (1974).

49. HICKMOTT, T.W.; J. Appl. Phys, 36, 1885 (1965).

50. AHMED, H.; J. Appl. Phys. 43, 242 (1971).

51. TAHERI, E.H.Z. and HOGARTH, C.A.; J. Non-Crystalline Solids. 15, 386 (1974).

52. SIMMONS, J.G., VERDERBER, R.R., LYTOLLIS, J. and LOMAX. R.; Phys. Rev. Lett, 17, 675 (1966).

53. GOULD, R.D. and COLLINS, R.A.; Appl. Phys. Lett, 16, 393 (1970).

54. GOULD, R.D., HOGARTH, C.A. and COLLINS, R.A.; J. Non-Crystalline Solids, 12, 131 (1973).

55. HRACH. R. and MAY, J.; Phys. Stat. Sol (a), 4, 637 (1971).

56. GOULD, R.D. and HOGARTH, C.A.; Phys. Stat. Sol.(a) 41, 439 (1977).

57. EMMER, I.; Phys. Stat. Sol. (a) 3, K-191 (1970).

58. EMMER, I.; Thin Solid Films, 20, 43 (1974).

59. TANAKA, K., UEMURA, Y. and IWATA, M.; Thin Solid Films, 50, L25 (1978).

60. BIDADI, H. and HOGARTH, C.A.; Int. J. Electronics, 36, 287 (1974).

61. HICKMOTT, T.W.; J. Appl. Phys, 35, 2679 (1964).

62. VERDERBER, R.R. and SIMMONS, J.G.; Radio Elect. Eng., 33, 347 (1967).

63. BARRIAC, C, PINARD, P. and DAVOINE, F.; Phys. Stat. Sol. 34, 621, (1969).

64. DEARNALEY, G.; Phys. Lett. 25A, 760 (1967).

65. DEARNALEY, G., MORGAN, D.V. and STONEHAM, A.M.; J. Non-Crystalline Solids, 4, 593 (1970).

66. REVESZ, A.G.; Phys. Stat. Sol. 24, 115 (1967).

67. RALPH, J.E. and WOODCOCK, J.M.; J. Non-Crystalline Solids, 7, 236 (1972).

68. COHEN, M.H.; J. Non-Crystalline Solids, 2, 432 (1970).

69. GEPPERT, D.V.; Proc. IEEE, 51, 223 (1963).

70. CHOPRA, K.L.; J. Appl. Phys., 36, 184 (1965).

71. HIATT, W.R. and HICKMOTT, T.W.; Appl. Phys. Lett, 6, 106 (1965).

72. ARGALL, F.; Solid-State-Electronics, 11, 535 (1968).

73. GIBBONS, J.F. and BEADLE, W.E.; Solid-State-Electronics, 7, 785 (1964).

74. PEARSON, A.D., DEWALD, J.F., NORTHOVER, W.R. and PECK, W.F.; Advanced in Glass Technology, Part 1, P. 357, (Plenum Press, New York, 1962).

75. DRAKE, C.F., SCANLAN, I.F. and ENGEL, A.; Phys. Stat. Sol. 32, 193 (1969).

76. REGAN. M., and DRAKE, C.F.; Mat. Res. Bull, 6, 487 (1971).

77. MORIDI, G.R. and HOGARTH, C.A.; Int. J. Electronics, 44, 297 (1978).

78. SUTHERLAND, R.R., LEGG, K.O. and COLLINS, R.A.,; Thin Solid Films, 6, R39 (1970).

79. MORGAN, D.V. and HOWES, M.J.; Phys. Stat. Sol. (a), 21, 191 (1974).

80. RAKHSHANI, A.E. and HOGARTH, C.A.; Int. J. Electronics 44, 593 (1978).

81. FRITZSCHE, H.; I.B.M. J. Res. Develop., 13, 515 (1969).

82. HENISCH, H.K., FAGEN, E.A. and OVSHINSKY, S.R.; J. Non-Crystalline Solids, 4, 538 (1970).

83. RIDELY, B.K.; Proc. Phys. Soc, (London) 82, 945 (1963).

84. UTTECHT. R.,STEVENSON, H, SIE, C.H., GRIENER, J.D., and RAGHAVAN, K.S.; J. Non-Crystalline Solids, 2, 358 (1970).

85. KURIKI, S., NOYA, A. and MATSUMOTO, G; Thin Solid Films, 48, 27 (1978).

86. OVSHINSKY, S.R. and FRITZSCHE, H.; IEEE Trans. Electron Devices, ED-20, 91 (1973).

87. ALDER, D.; Critical Reviews in Solid State Science, 2, 317 (1971).

88. HOGARTH, C.A. and WRIGHT, L.A.; Proceeding of International Conference on Physical Semi-conductors, 1274 (Moscow 1968).

89. HOGARTH, C.A. and IQBAL, T.; Int. J. Electronics, 47, 349 (1979).

90. SUTHERLAND, R.R., WILLIAMSON, J.P.A., and COLLINS, R.A.; J. Phys. D: Appl. Phys, 5, 1686 (1972).

91. OHTA, K., NISHIDA, J. and HAYASHI, T.; Japan. J. Appl. Phys, 7, 784 (1968).

92. BIDADI, H. and HOGARTH, C.A.; Thin Solid Films, 2, 319 (1975).

93. TIMSON. P.A. and HOGARTH, C.A.; Thin Solid Films, 10, 321 (1972).

94. HOGARTH, C.A. and TAHERI, E.H.Z.; Thin Solid Films, 10, 455 (1972).

95. TAHERI, E.H.Z., HOGARTH, C.A., and GOULD, R.D.; Phys. Stat. Sol. (a) 12, 563 (1972).

96. BIDADI, H.; Ph.D. Thesis, Brunel University (1974).

97. HOGARTH, C.A. and BIDADI, H.; Thin Solid Films, 13, S27 (1972).

98. PARK, K.C. and BASAVAIAH, S.; J. Non-Crystalline Solids, 2, 284 (1970).

99. RAKHSHANI, A.E. and HOGARTH, C.A.; J. Non-Crystalline Solids, 21, 147, (1976).

100. BUDENSTEIN, P.P. and HAYES, P.J.; J. Appl. Phys. 38, 2837, (1967).

101. GRUNDY, P.J. and JONES, G.A.; "Electron Microscopy in the Study of Materials" (Edward Arnold, London, 1976).

102. KAMMLOTT, G.W.; Surface Science, 25, 120 (1971).

103. BIEDERMAN, H.; Thin Solid Films, 18, 39 (1973).

104. BEAM, W.R. and ARMSTRONG, A.L.; Proc. IEEE, 52, 300 (1964).

105. HICKMOTT, T.W. and HIATT, W.R.; Solid State Electronics, 13, 1033 (1970).

106. BASAVAIAH, S. and PARK, K.C.; IEEE Trans. Electron Devices ED-20, 149 (1973).

107. ARGALL, F; Electronics Lett. 2, 282 (1966).

108. KHAN, M.I., HOGARTH, C.A. and KHAN, M.N.; Int. J. Electronics, 46, 215 (1979).

109. MANHART, S.; J. Phys.D: Appl. Phys, 6, 82 (1973).

110. FUSCHILLO, N., LALEVIC, B, ANNAMALAI, N.K, and SLUSARK, W.,Jr.; J. Non-Crystalline Solids, 22, 159 (1976).

111. SIE, S.H., DUGAN, M.P. and MOSS, S.C.; J. Non-Crystalline Solids, 8-10, 877 (1972).

112. TANAKA, K, OKADA, Y., SUGI, M., IIZIMA, S. and KIKUCHI, M.; J. Non-Crystalline Solids, 12, 100 (1972).

113. COLLINS, R.A. and JONES, G.; J. Phys. D: Appl. Phys., 11, L13 (1978).

114. WARREN, A.C.; IEEE Trans. Electron Devices ED-20, 123 (1973).

115. BARANCOK, D., DIESKA. P., and KREMPASKY, J.; Phys. Stat. Sol. (a) 16, 253 (1973).

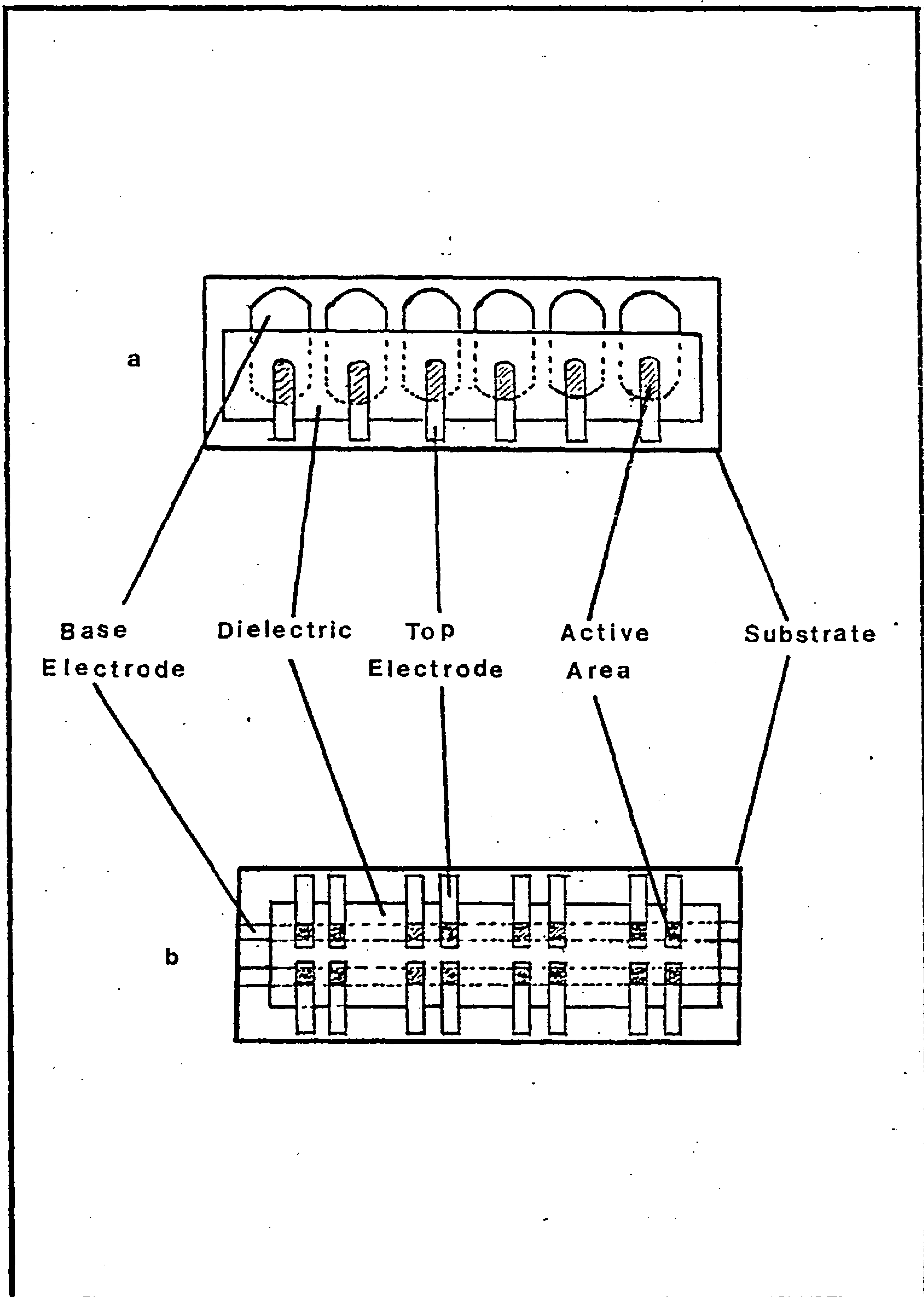

Fig. 3.1. Device arrangements, (a) Configuration 1
(b) Configuration 2.

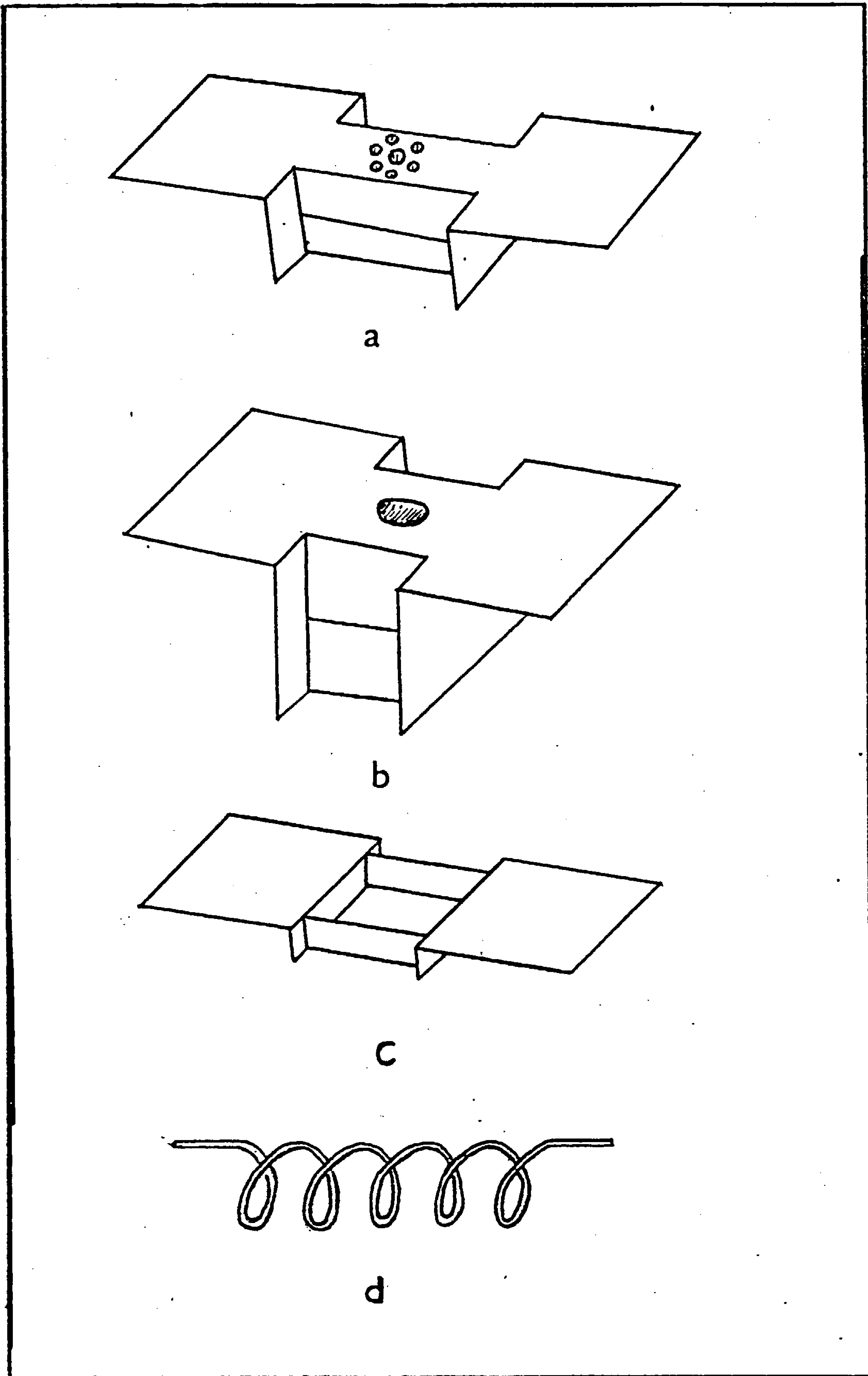

Fig. 3.2. Schematic illustration of various evaporation Sources used to evaporate; (a) SiO (b) B_2O_3 (c) Ag or Cu and (d) Tungsten filament for evaporation Al.

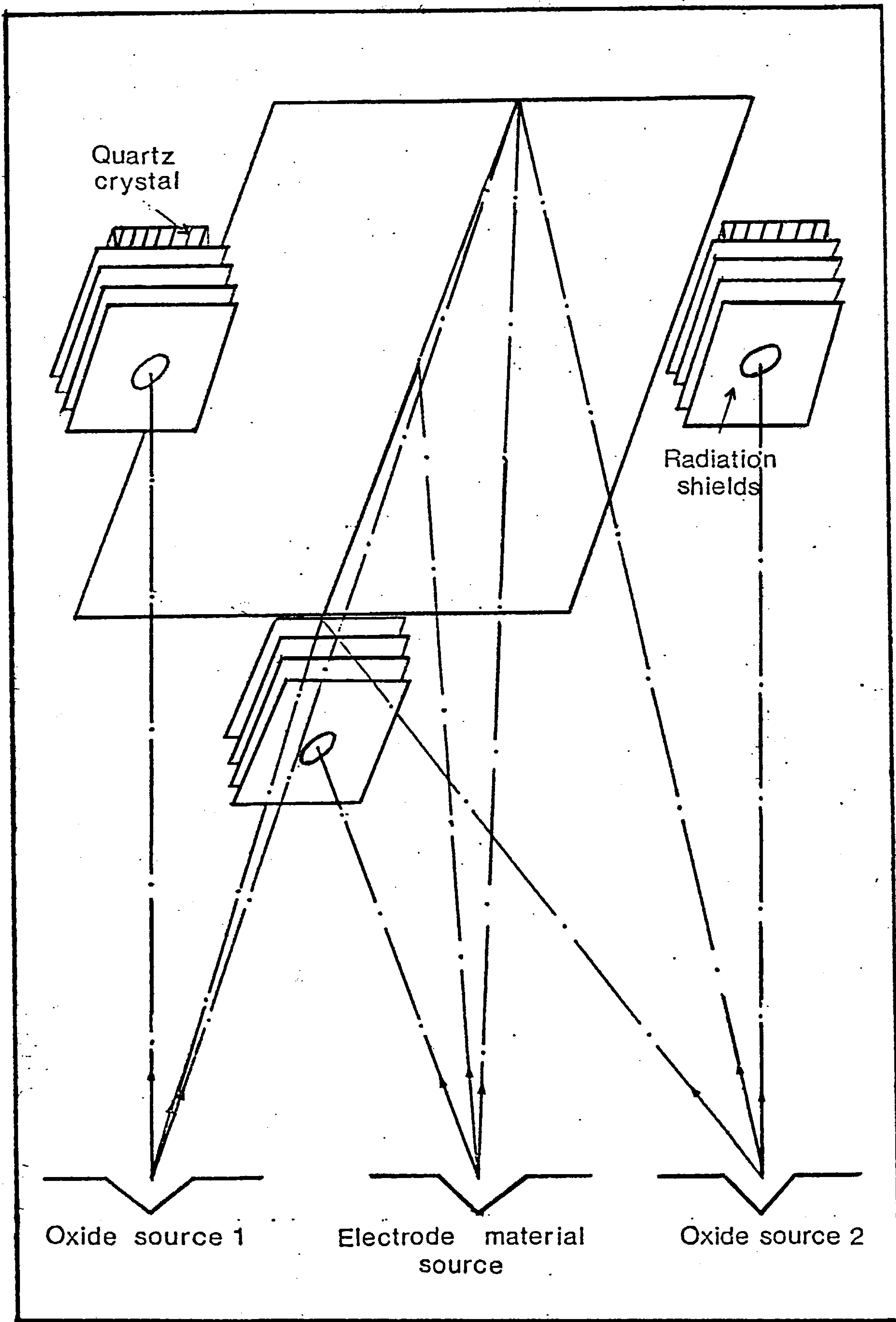

Fig. 3.3. Illustration of the source - substrate - crystal monitor arrangement.

Fig·3·4· Photograph of the vacuum test system with the equipments used for the measurements

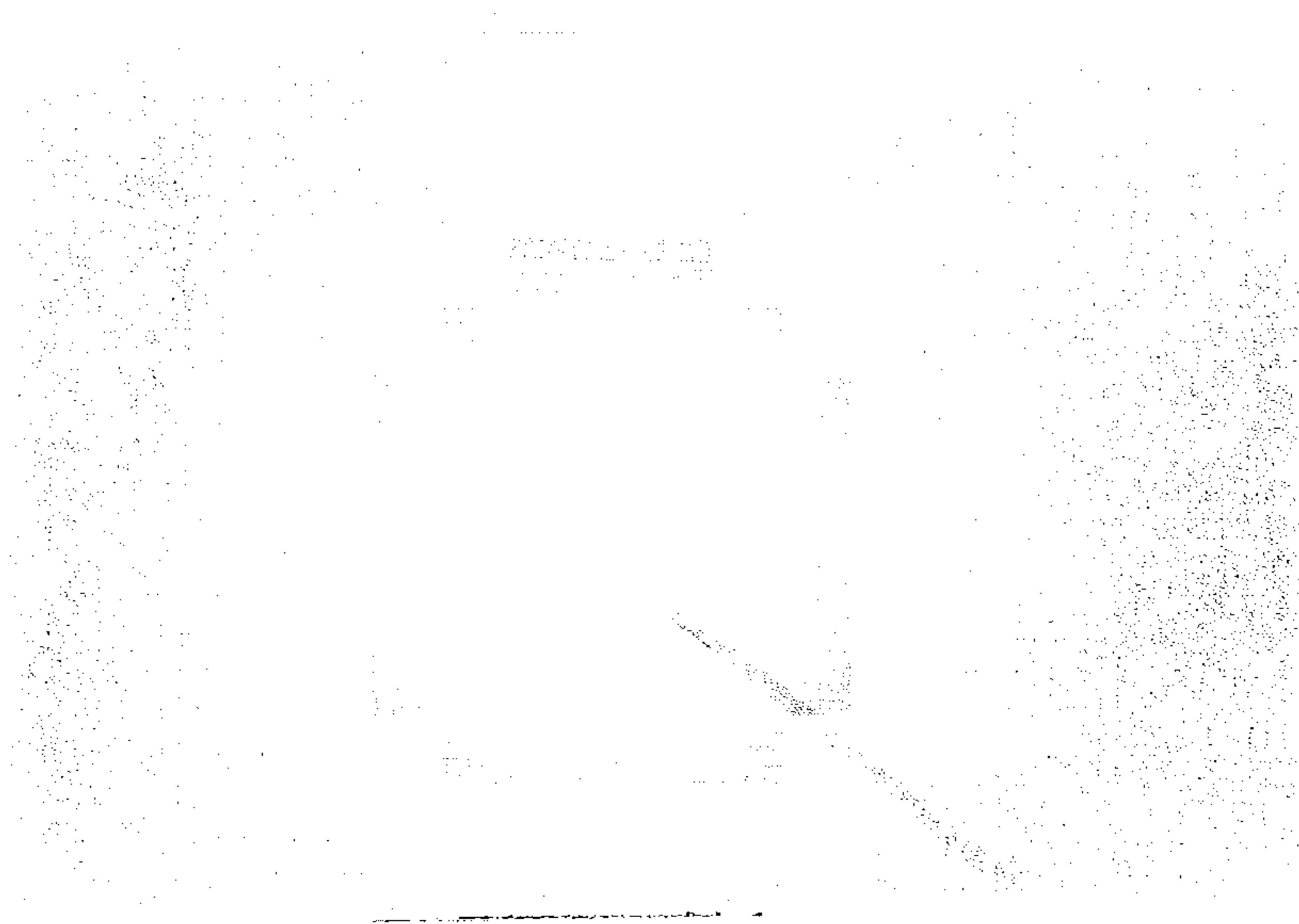

Fig. 4.1. Transmission electron diffraction photograph of a SiO (70%) / B_2O_3 (30%) film.

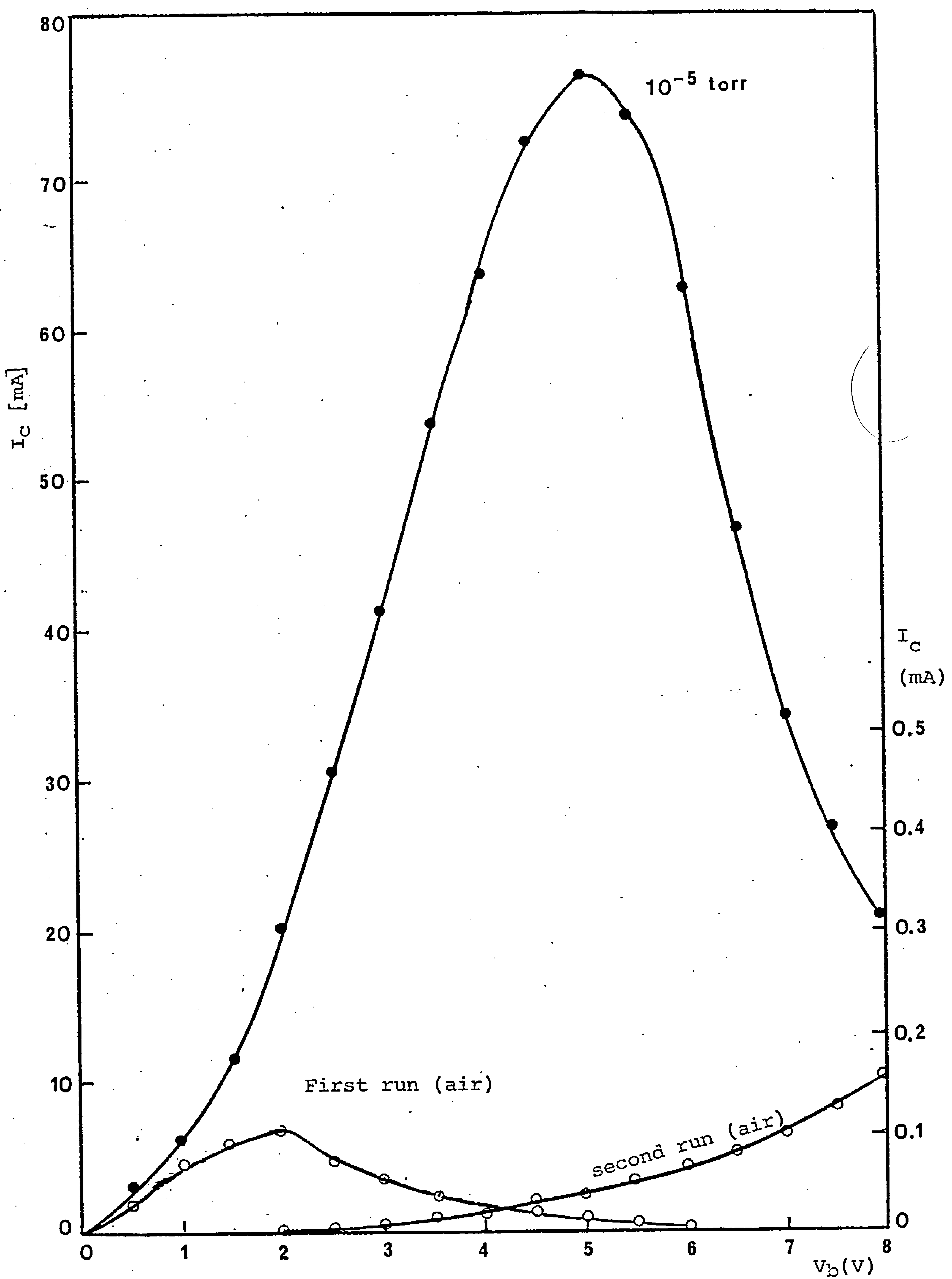

Fig. 4.12. Pressure-Voltage memory in a Cu-SiO/B_2O_3-Cu structure with insulator thickness 1500Å. The scale on the right hand side relates only to the second run.

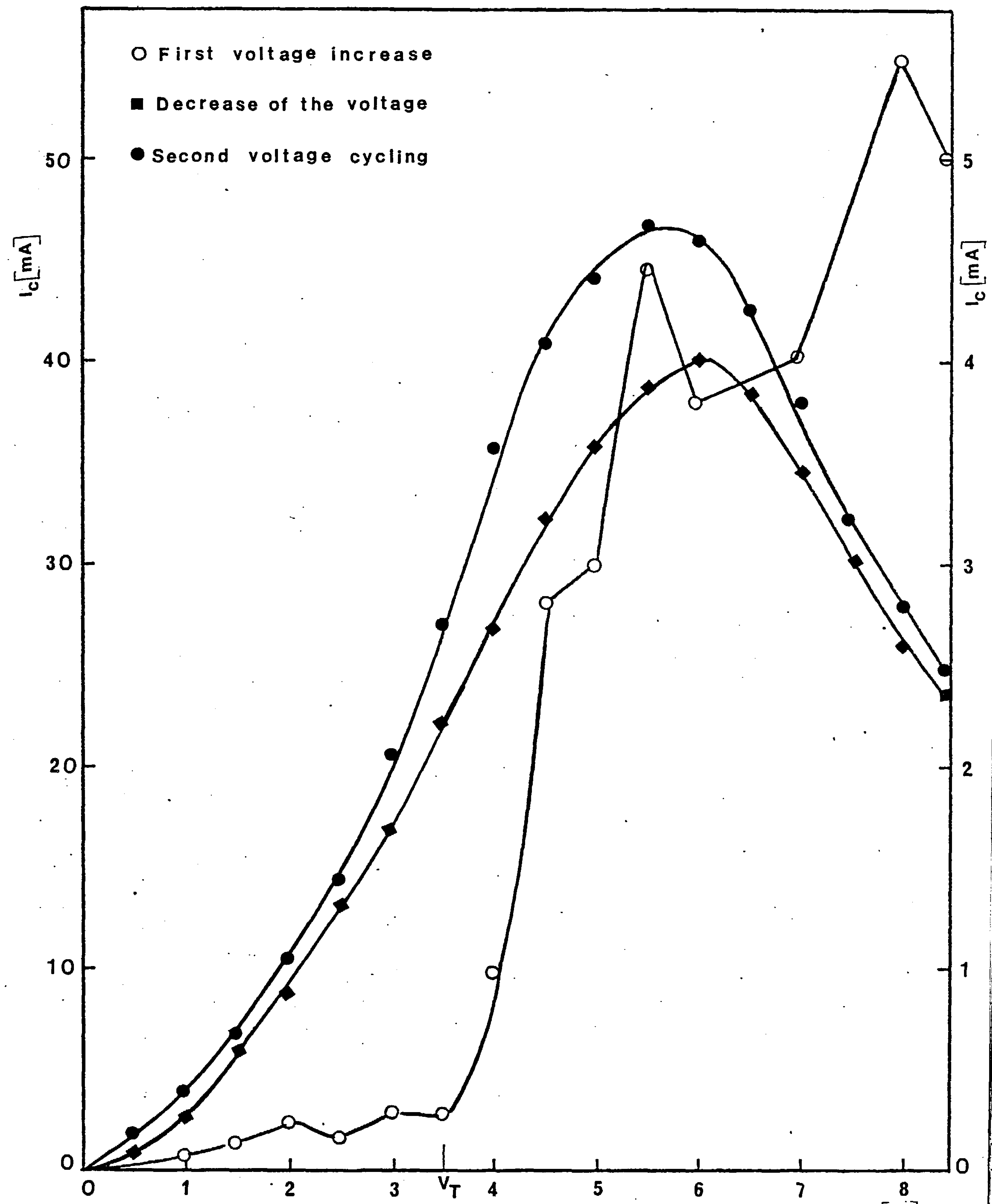

Fig. 4.13. Erasure of the high-impedance state (produced by operating the sample in air) in vacuum of 10^{-5} torr. The right-hand side scale relates only to the points shown by o.

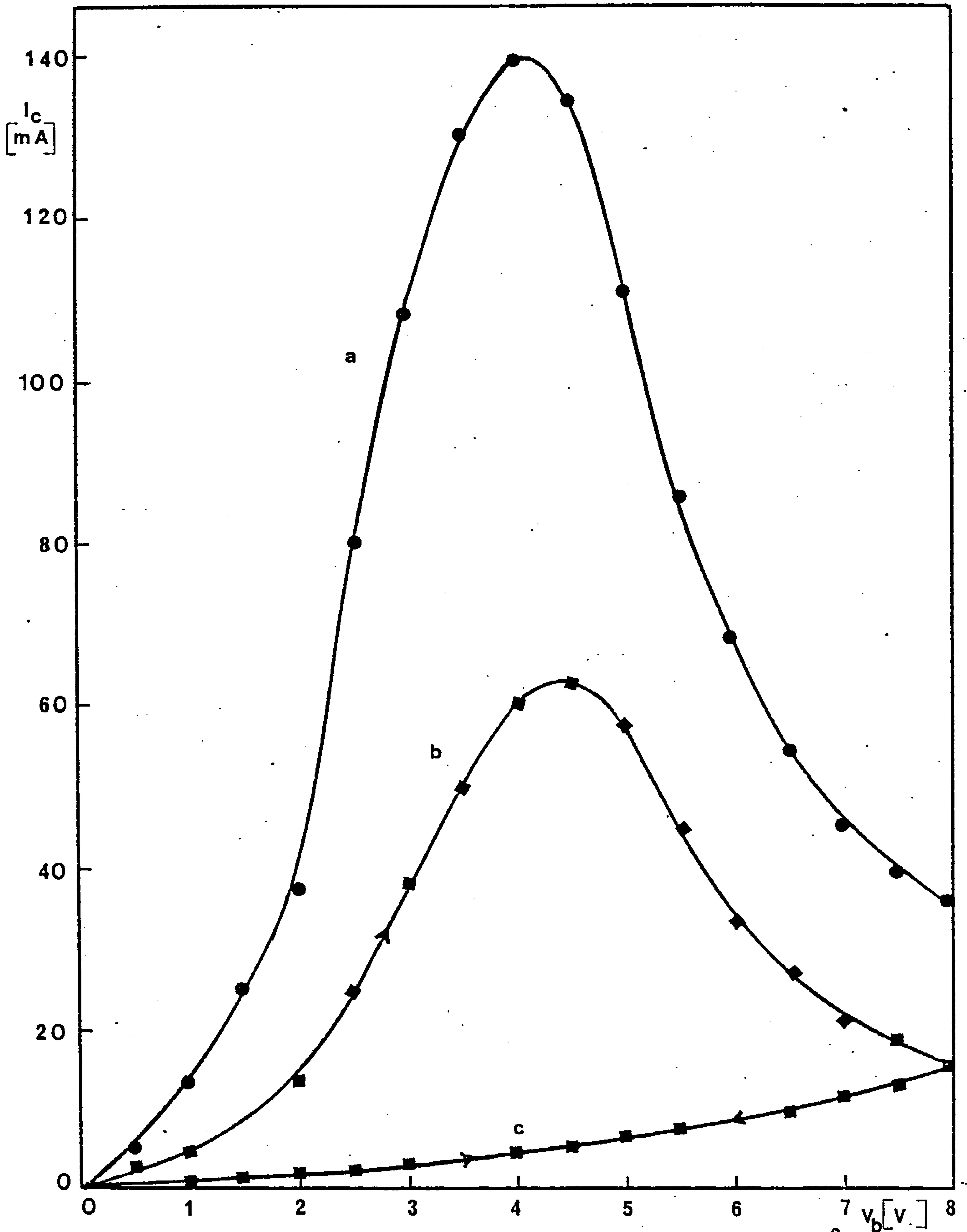

Fig. 4.14. Current-voltage characteristics of a Cu (380Å)-SiO/ B_2O_3(600Å)-Cu(450Å); (a) at room-temperature, (b) first voltage increase at -65 °C, (c) further runs at -65 °C.

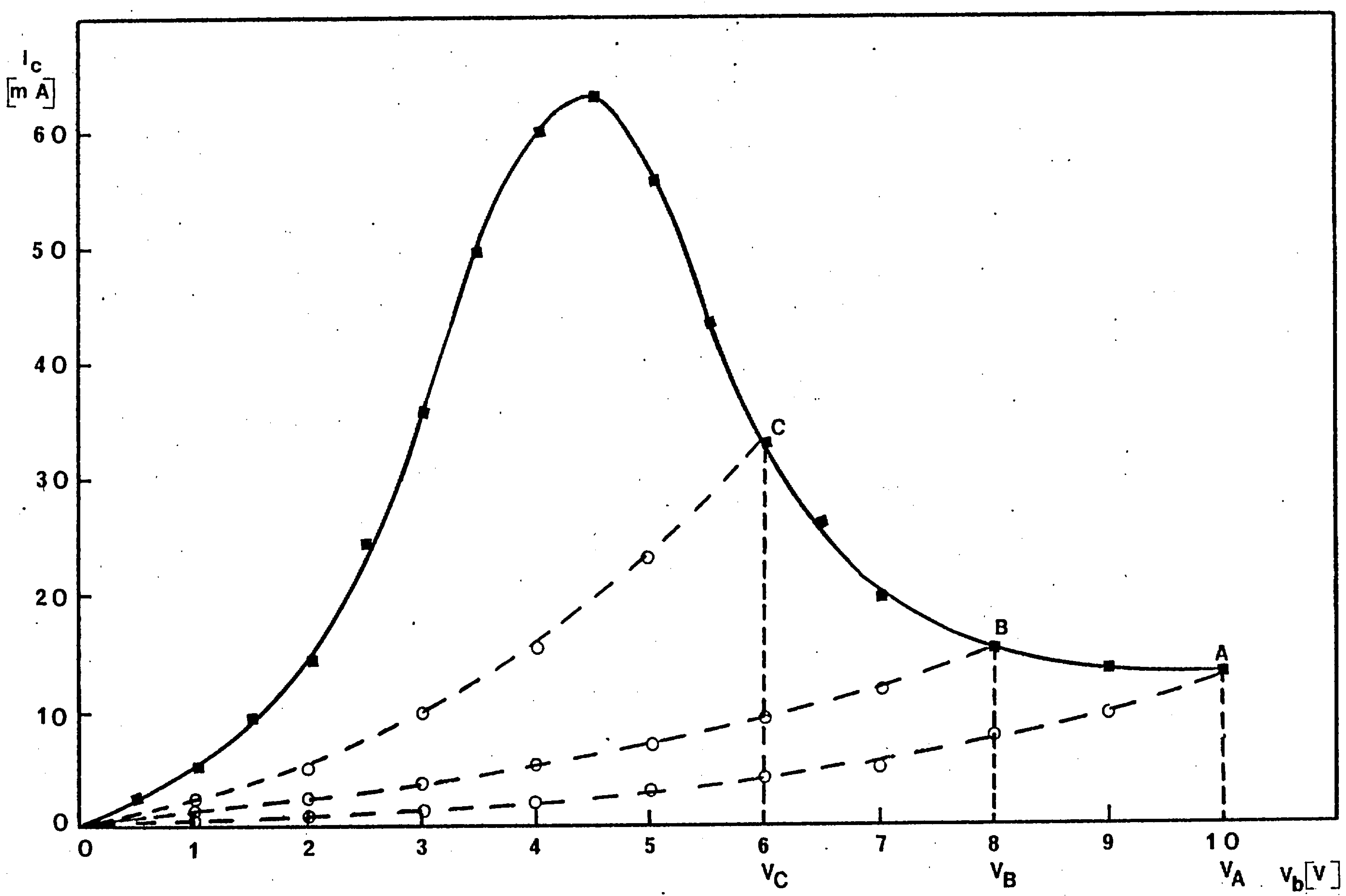

Fig. 4.15. I_c-V_b characteristics of three high-impedance memory states induced in the same device as in Fig. 4.14. at $-65^{\circ}C$.

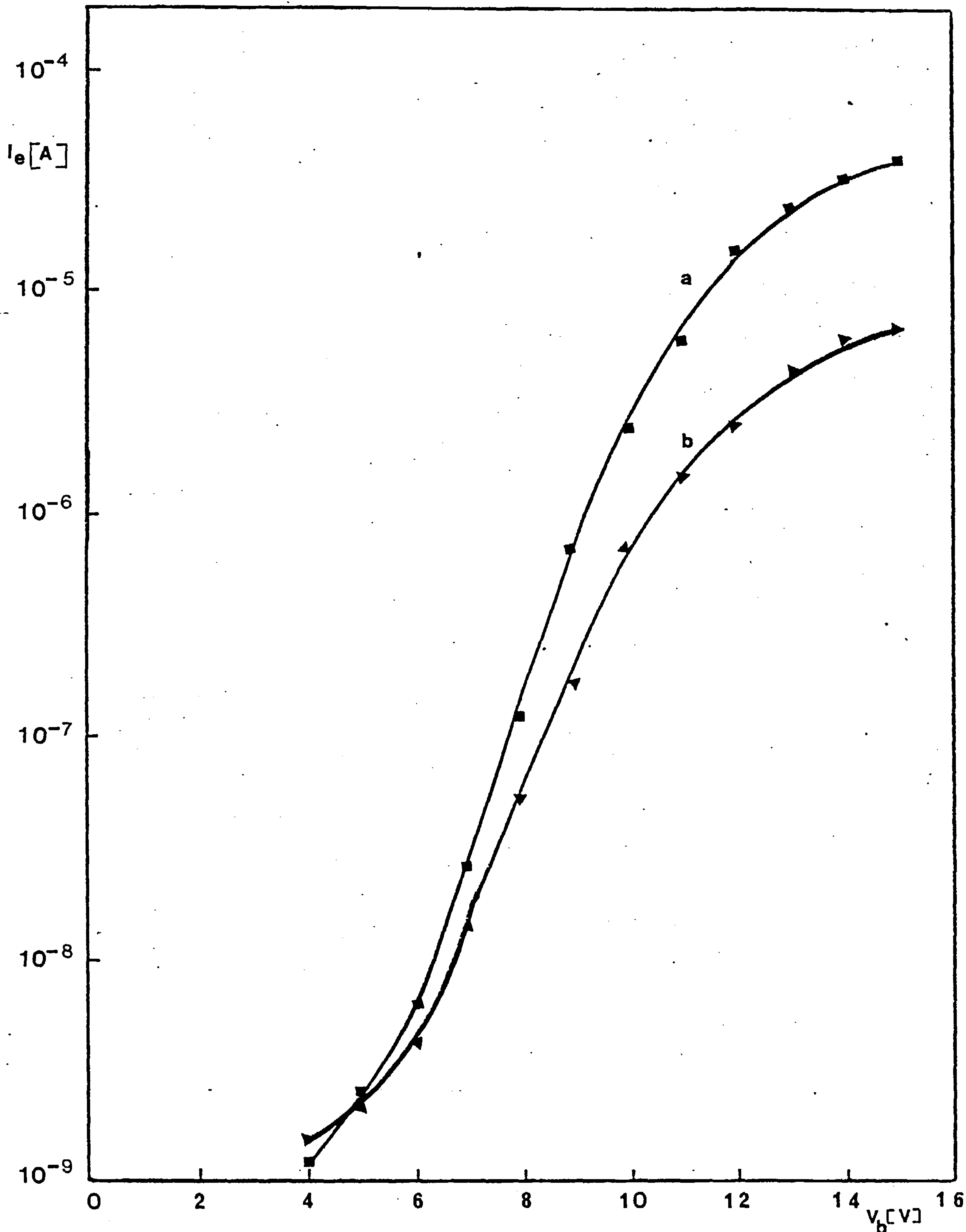

Fig. 4.16. The variation of emission current as a function of applied bias voltage at: (a) room-temperature, (b) -65 °C.

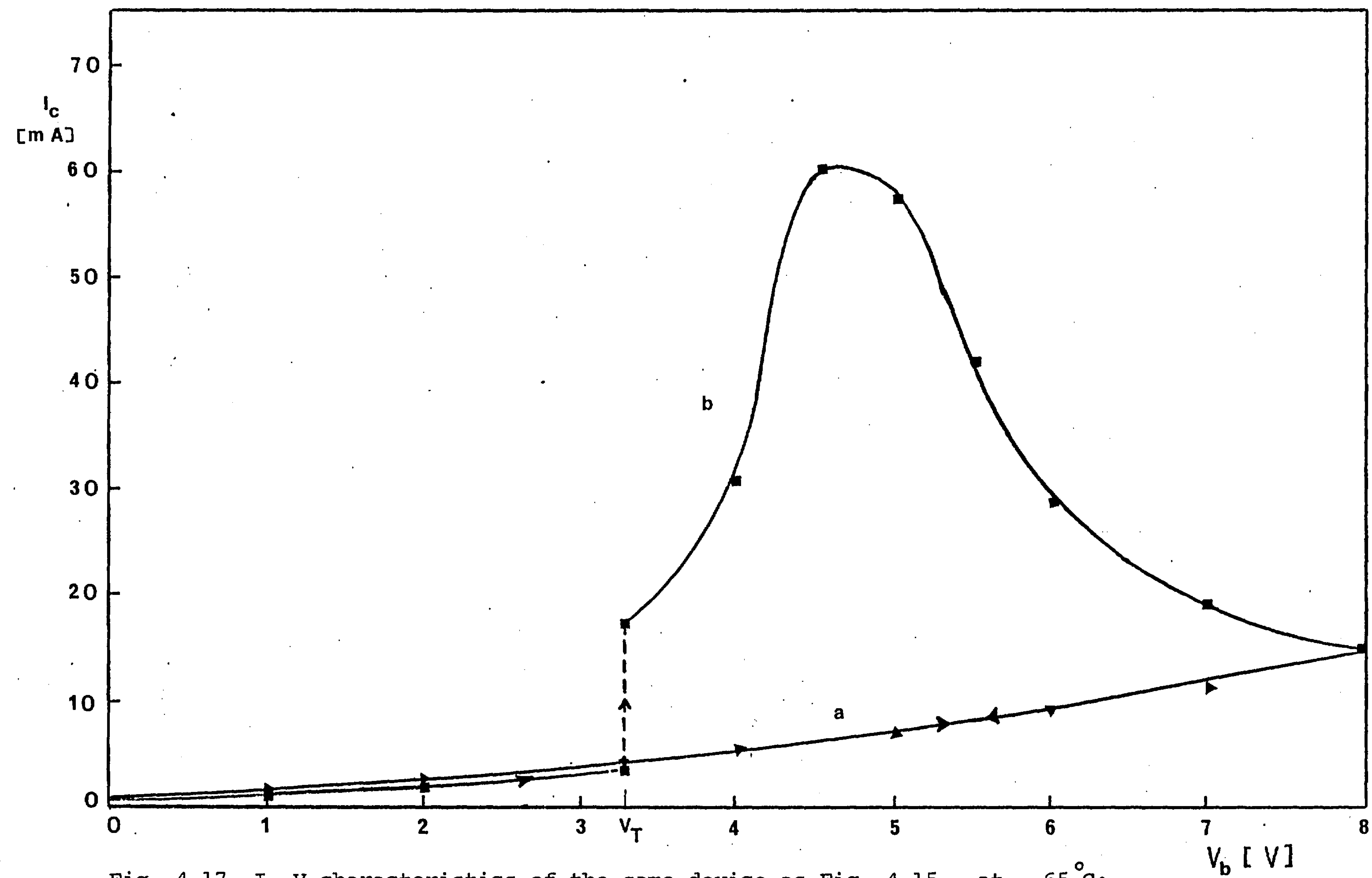

Fig. 4.17. I_C-V characteristics of the same device as Fig. 4.15. at $-65^{\circ}C$;

(a) a high-impedance memory state before temperature cycling, (b) the normal low-impedance state after temperature cycling.

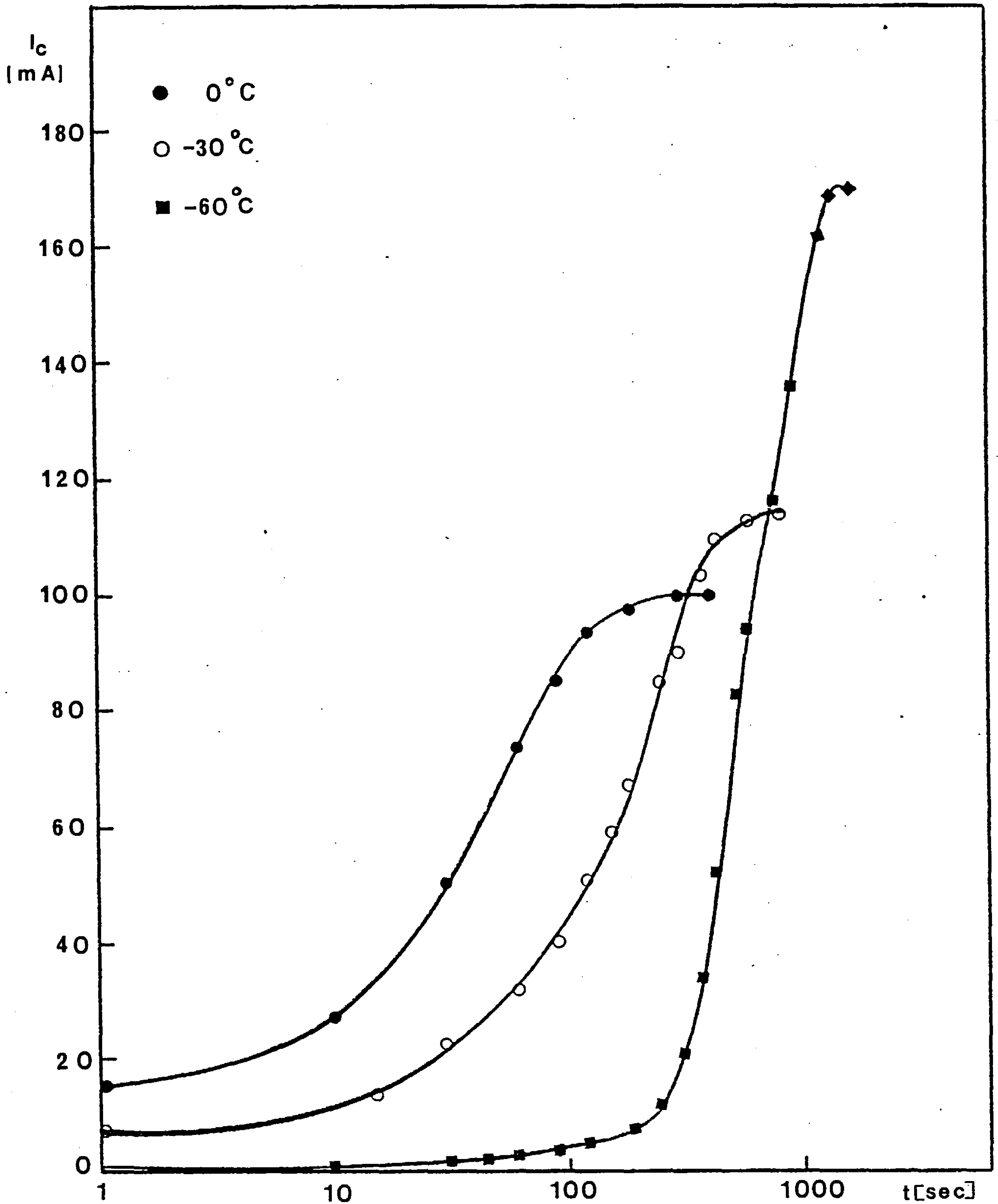

Fig. 4.18. Increasing of relaxation time with decreasing of the temperature for a Cu(760Å)-SiO/ B_2O_3(1680Å)-Cu(1100Å) device; V_A=10V and V_1=5V for all the three different temperatures.

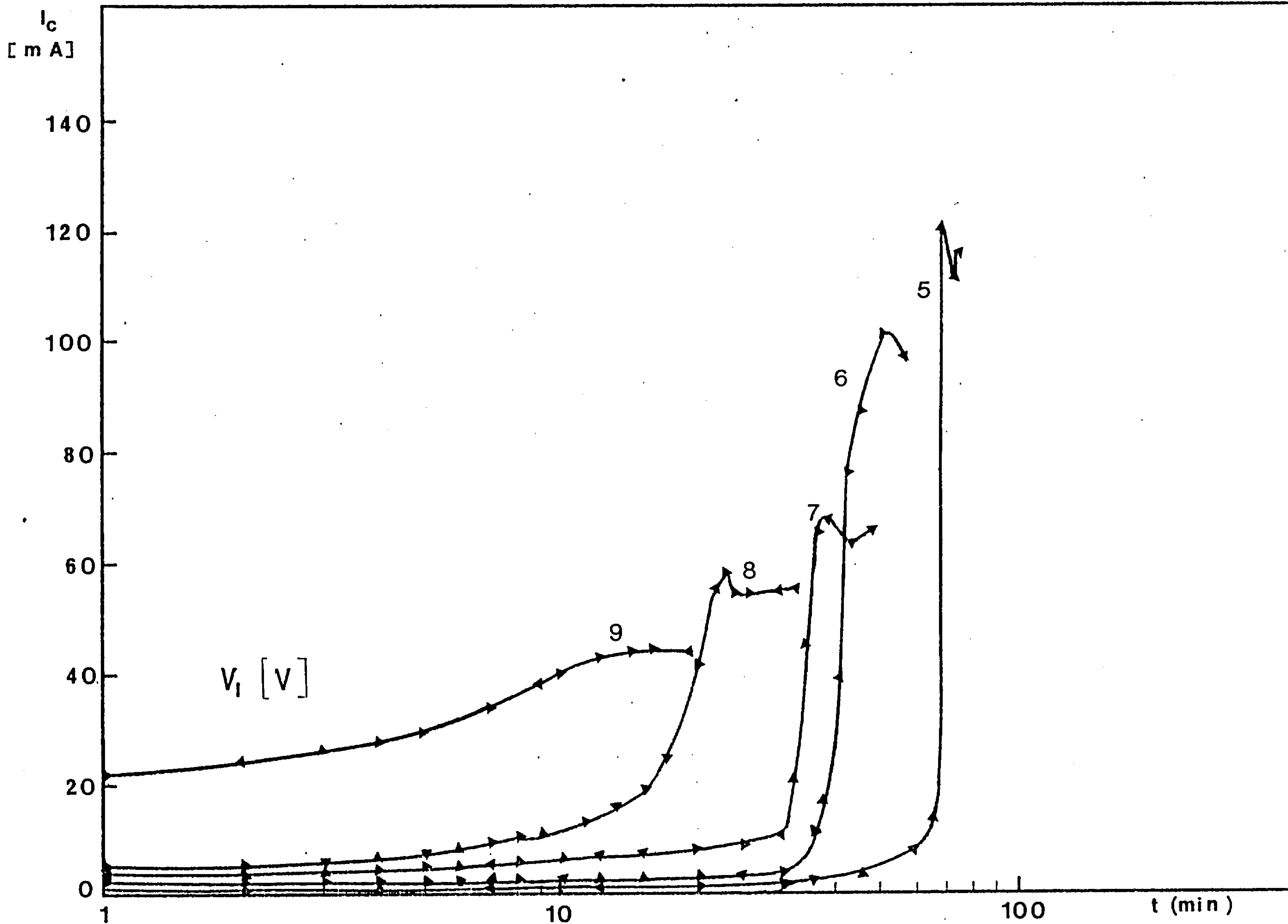

Fig. 4.19. Increase of the transition time with decreasing of the loading voltage V_1 for the same device as Fig. 4.18. All the memory states were induced at $T=-60\,^{\circ}C$ and $V_A=10V$.

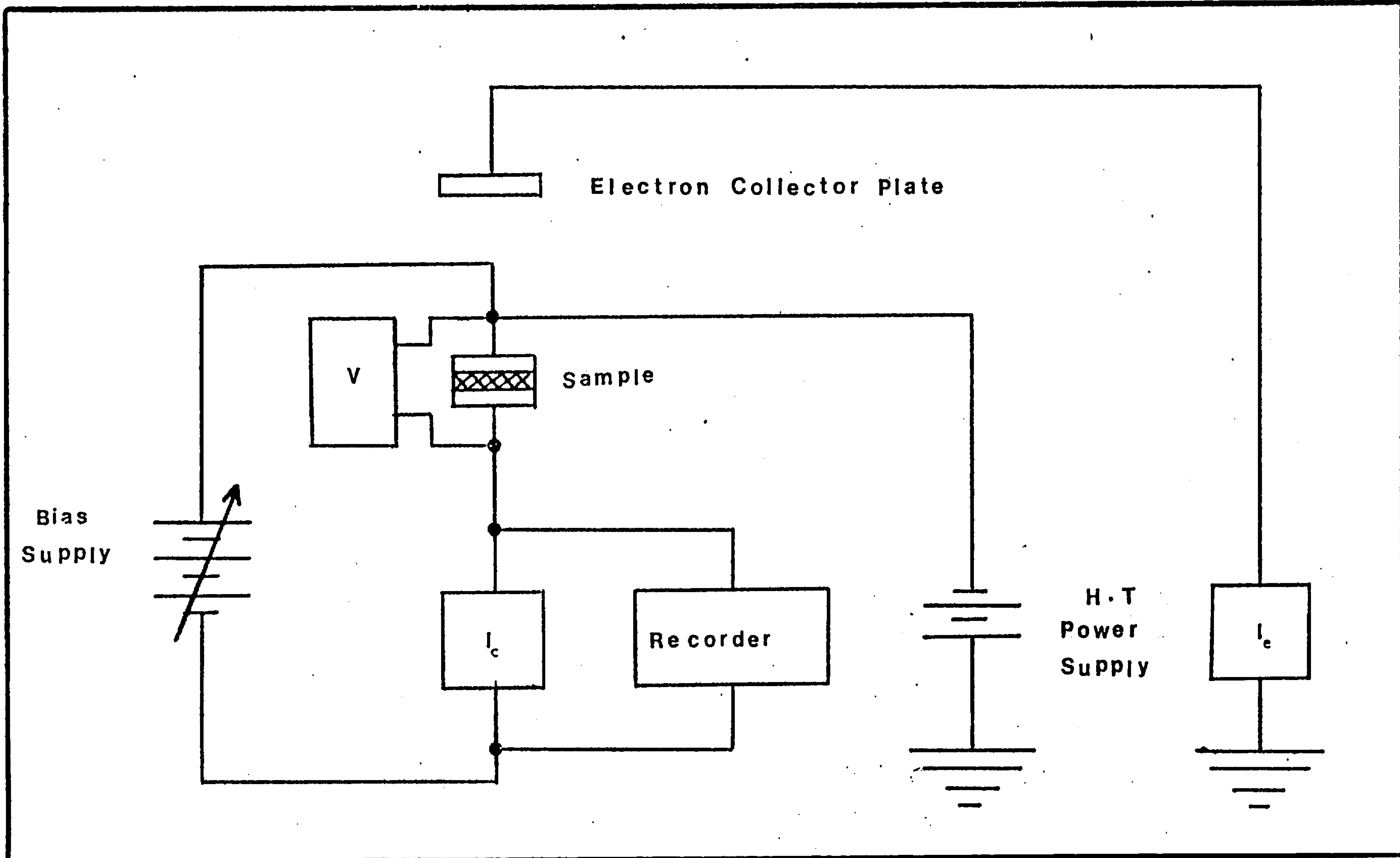

Fig. 4.2. Circuit used for electrical measurements.

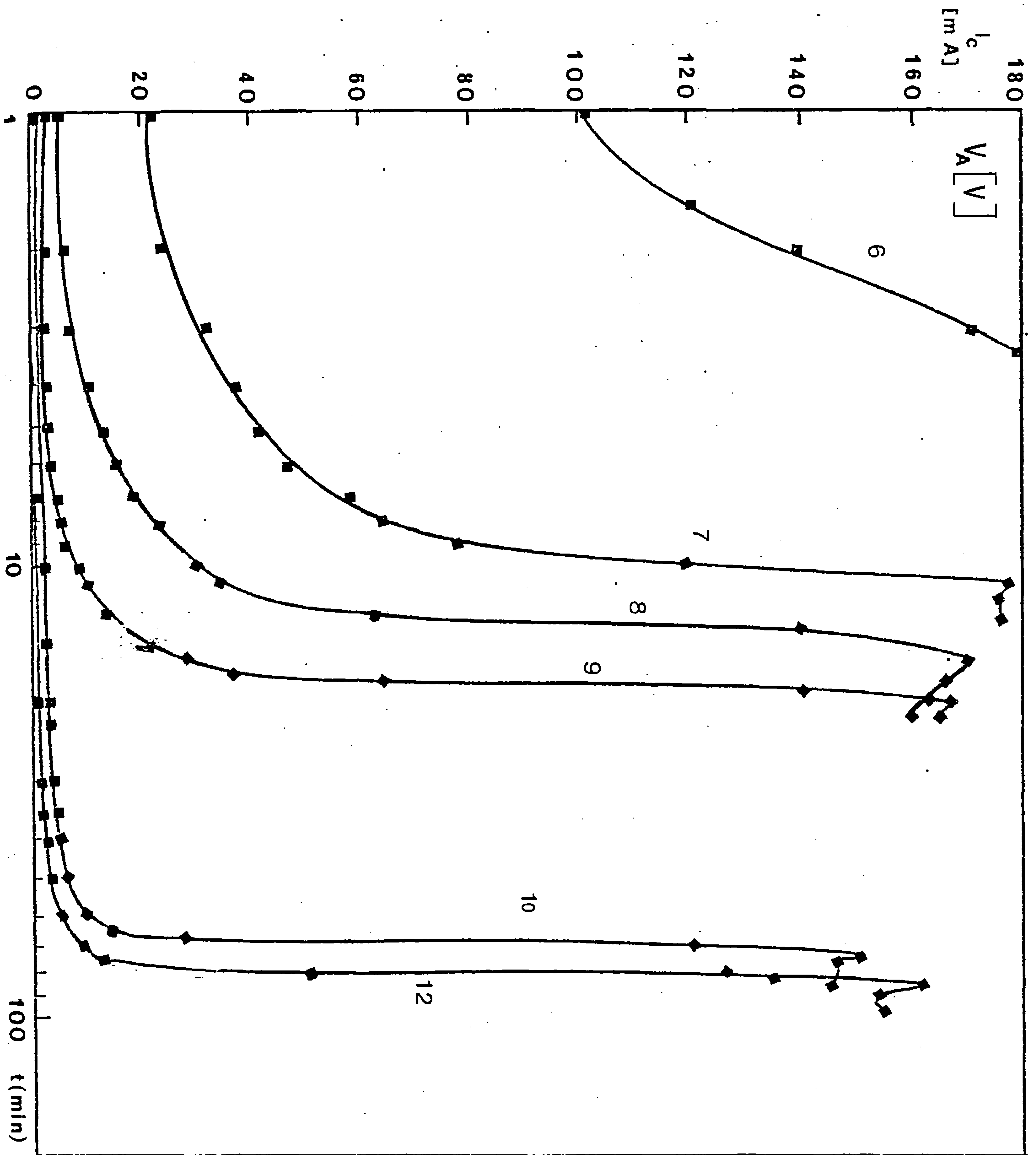

Fig. 4.20. Time-dependence of the relaxation of a set of memory states (induced at different values of V_A) at the same loading voltage of V_1=5V; T=-60°C.

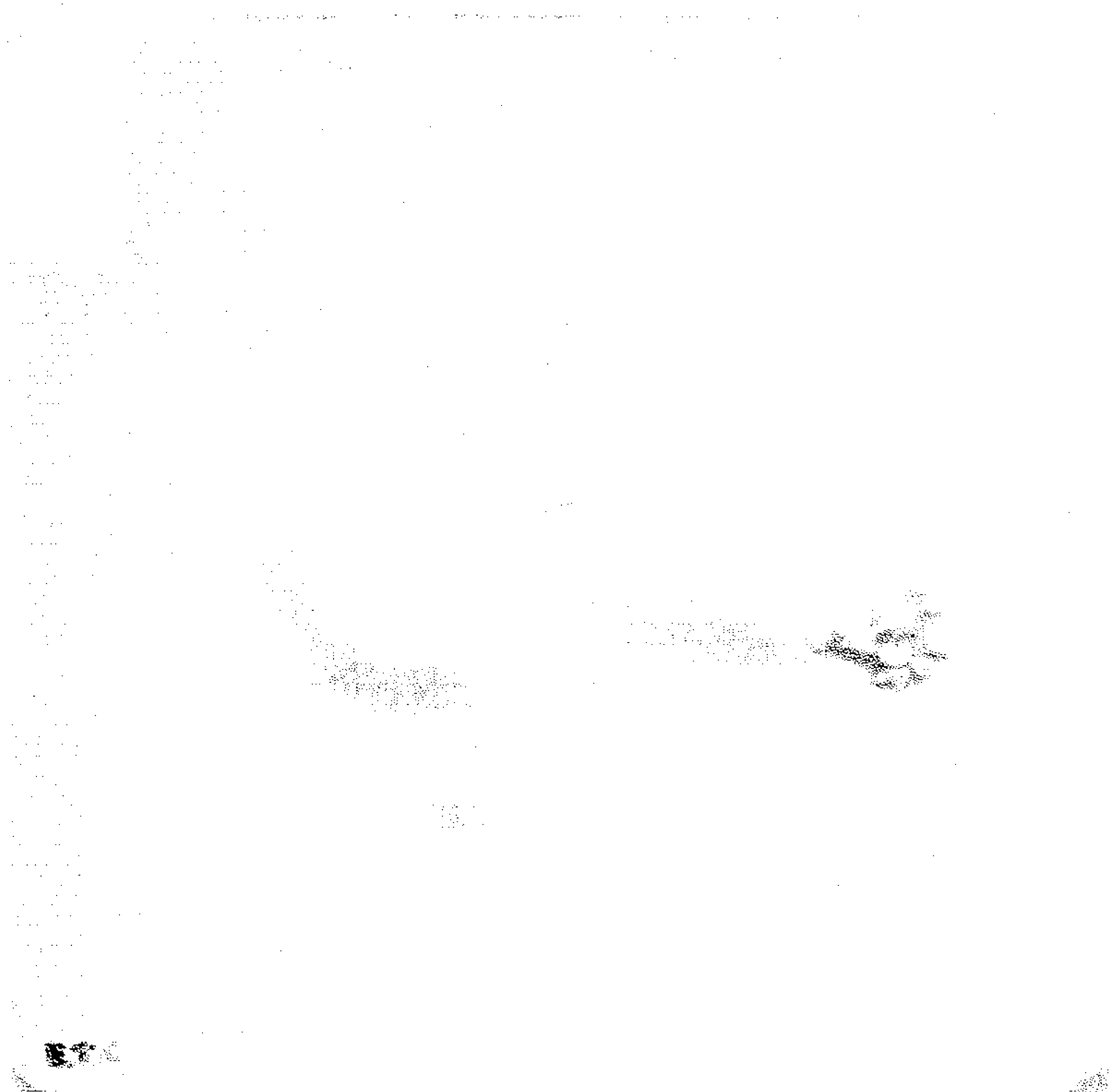

Fig. 4.21. SEM micrograph from the top electrode surface of an Ag - SiO (65%) / B_2O_3 (35%) device with the positively biased top electrode operated in vacuum.
Maximum applied voltage V_b=4.8V. The thickness of dielectric was 1700Å and the top electrode thickness 600Å. Magnification 450X.

Fig. 4.22. Electron micrograph from a defect observed on the top electrode of a device with the same structure as for Fig. 4.21. This device had been electroformed in vacuum. Maximum voltage applied V_b=15V. Magnification 1800X.

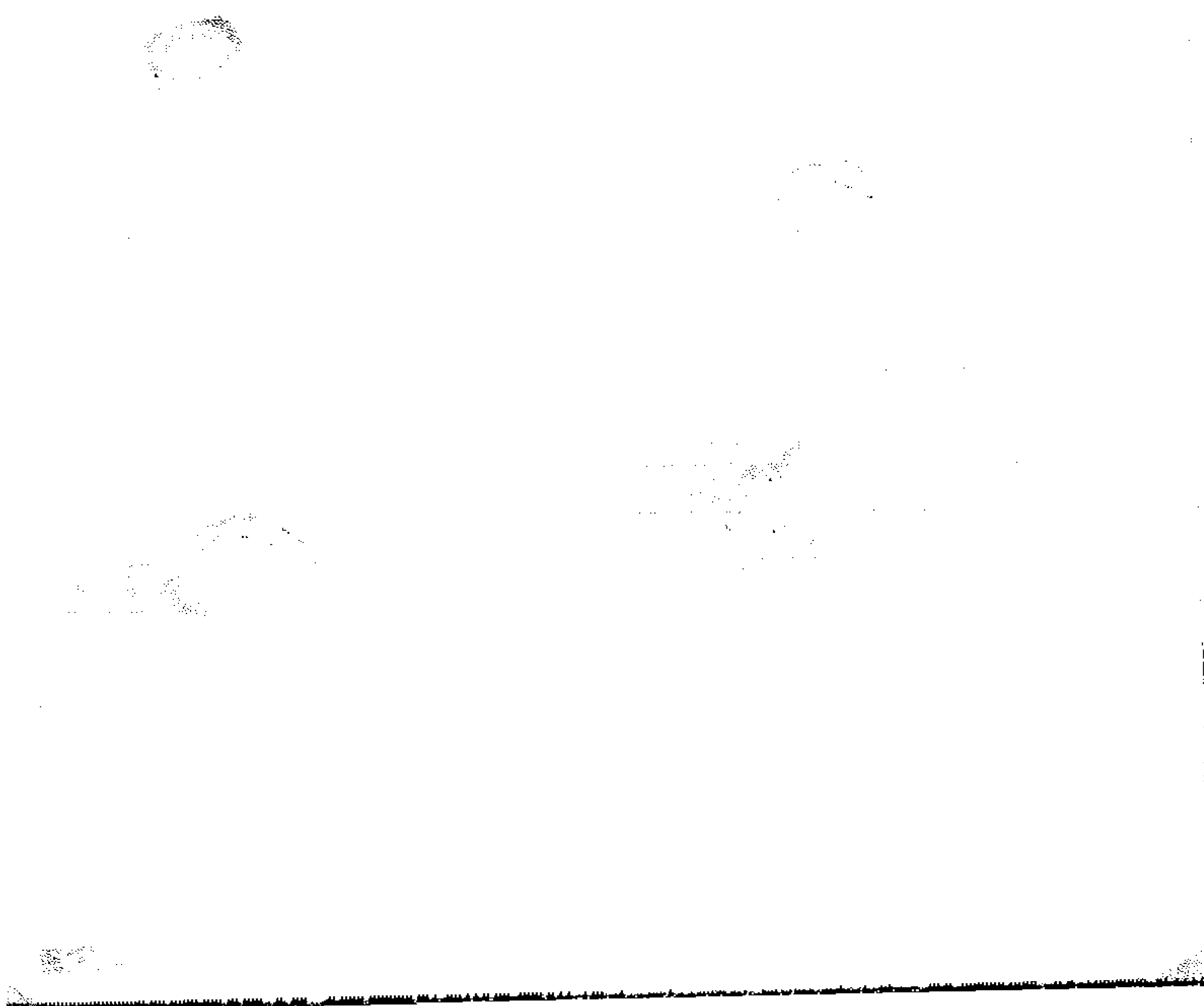

Fig. 4.23 An electron micrograph from defects on the positively biased top electrode of a vacuum-electroformed Cu - SiO (65%) / B_2O_3 (35%) - Cu device. The dielectric and top electrode thicknesses were 1700 and 1000Å, respectively. Magnification 1800X.

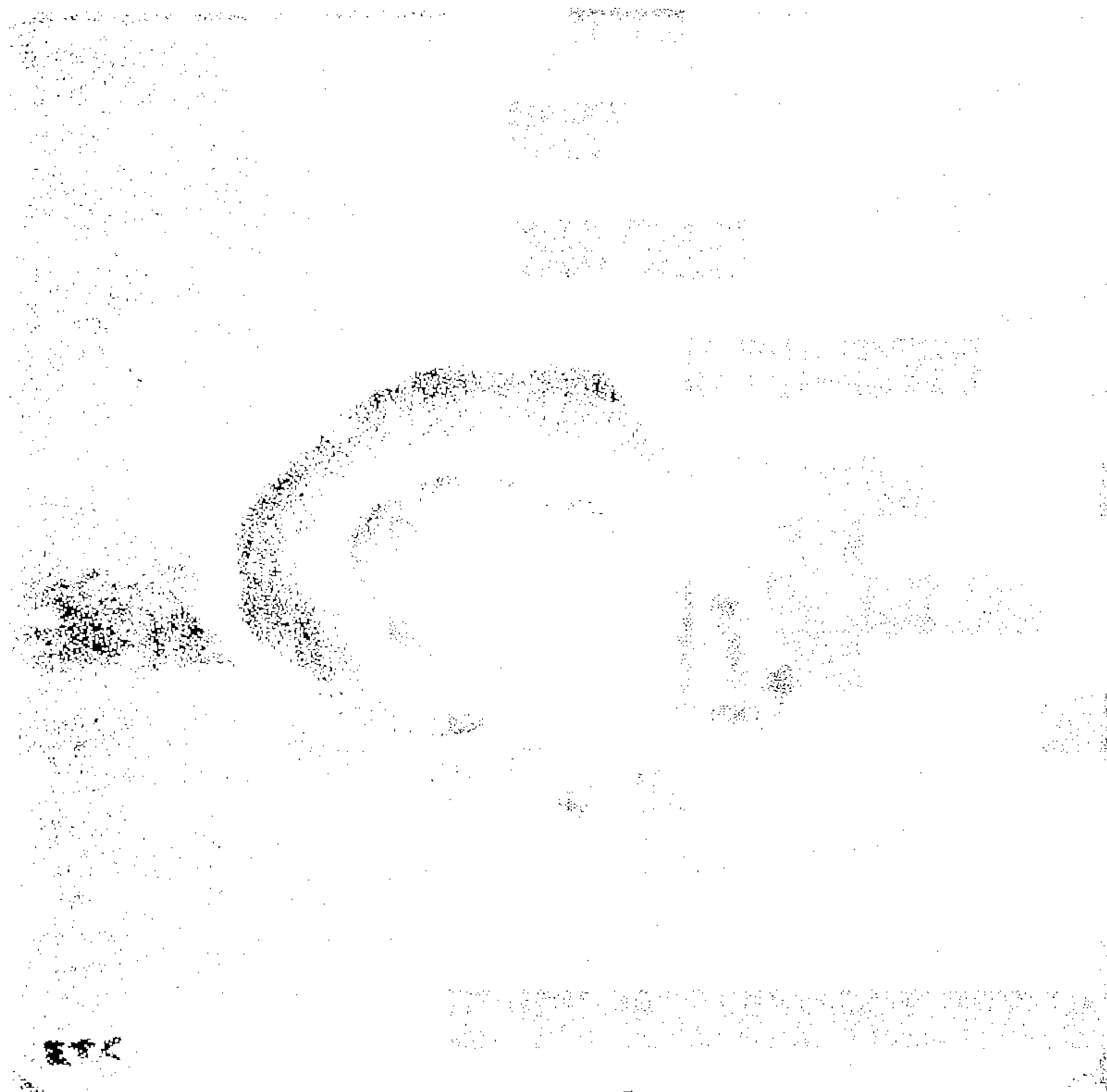

Fig. 4.24 Electron micrograph from one of the defects, with higher magnification of 9000X, on the surface of the same device as in Fig. 4.23.

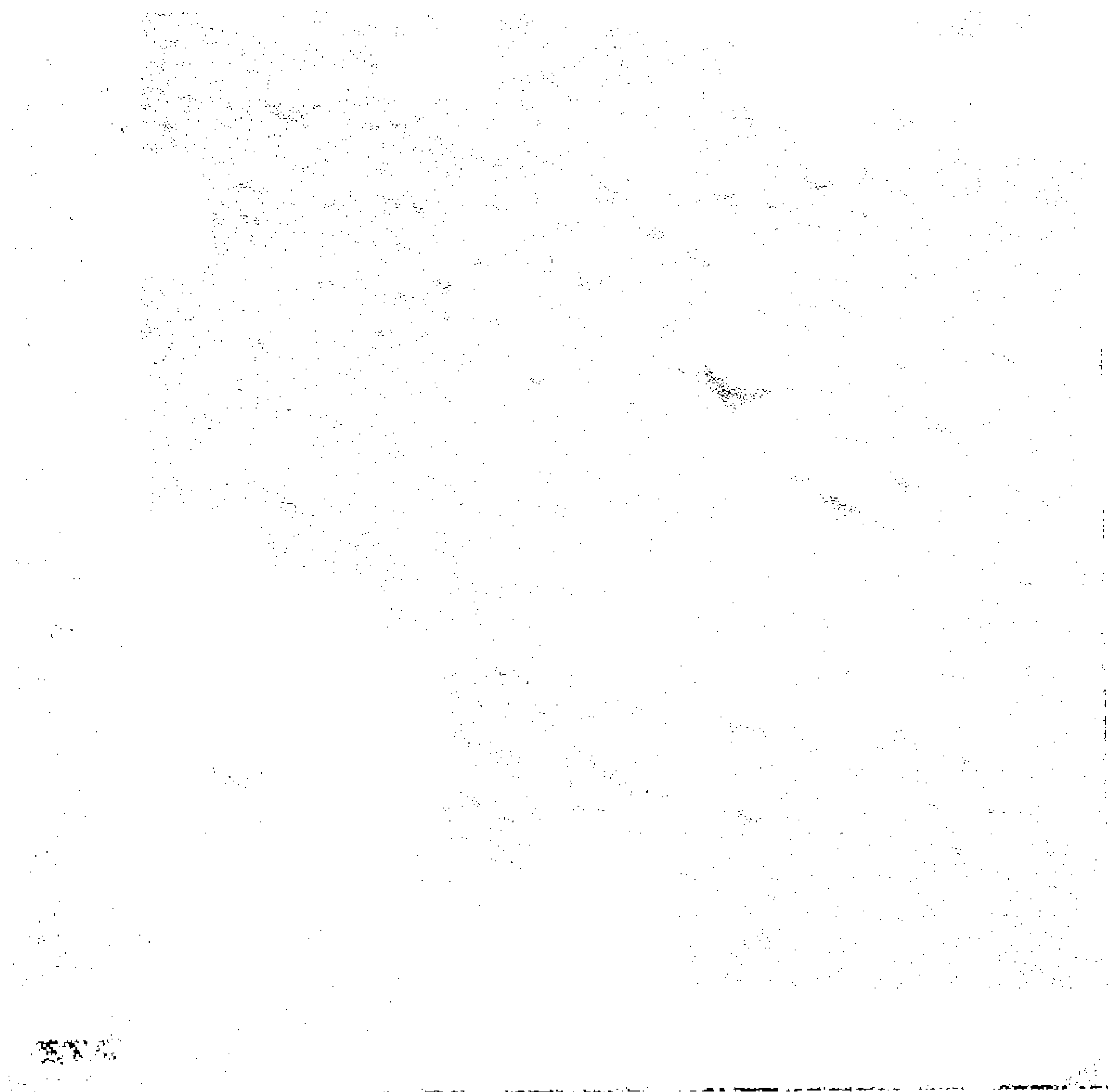

Fig. 4.25. Electron micrograph from the top electrode surface of an Ag - SiO (75%) / B_2O_3 (25%) - Ag device, which had been electroformed in vacuum with negatively biased top electrode. The thickness of dielectric 1700Å and top electrode 600Å. Maximum applied vol V_b=15V. Magnification 4500X.

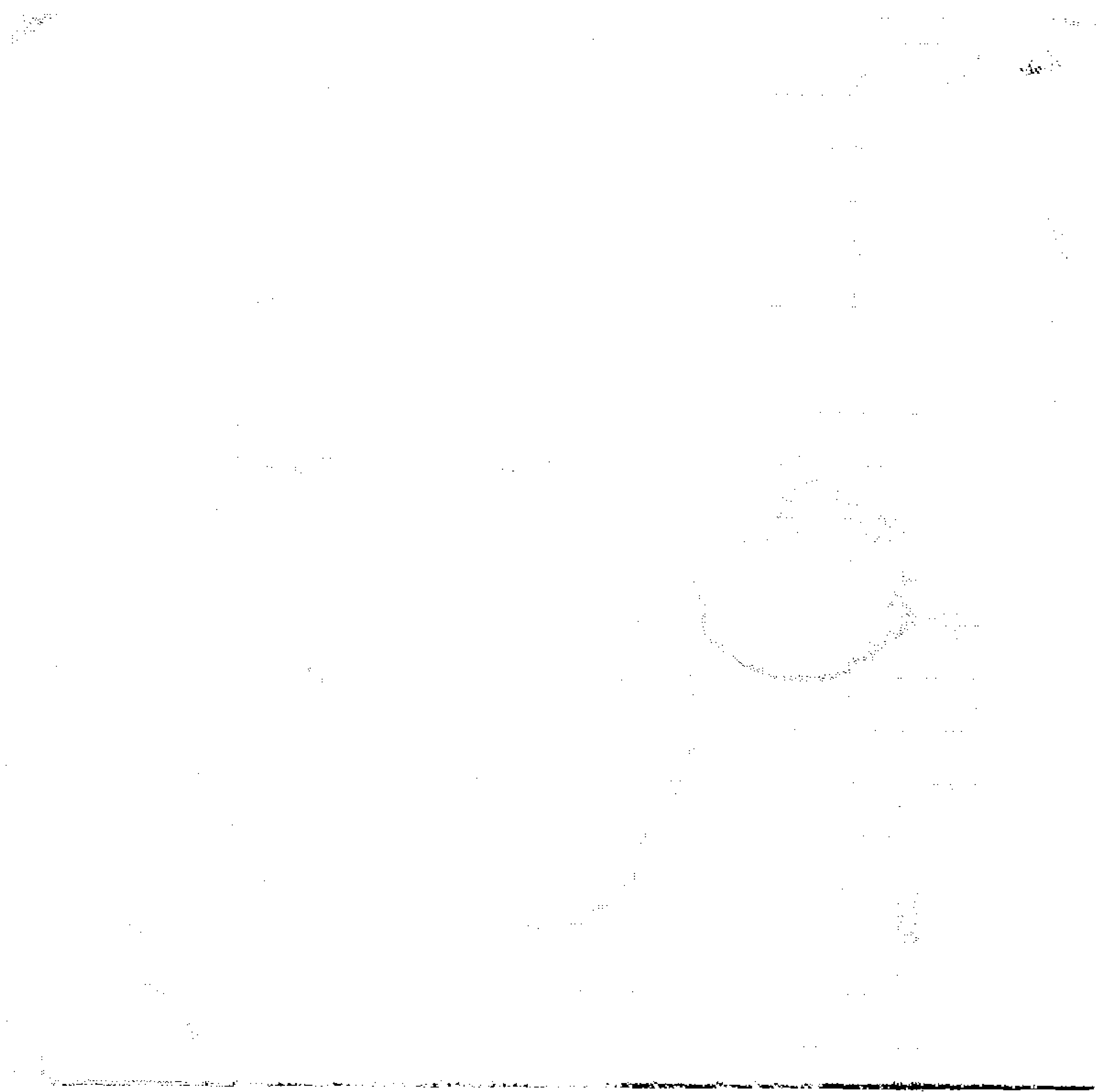

Fig. 4.26. SEM picture from the top electrode of an air-electro-formed device (with the same structure as for Fig.4.25). Magnification 900X.

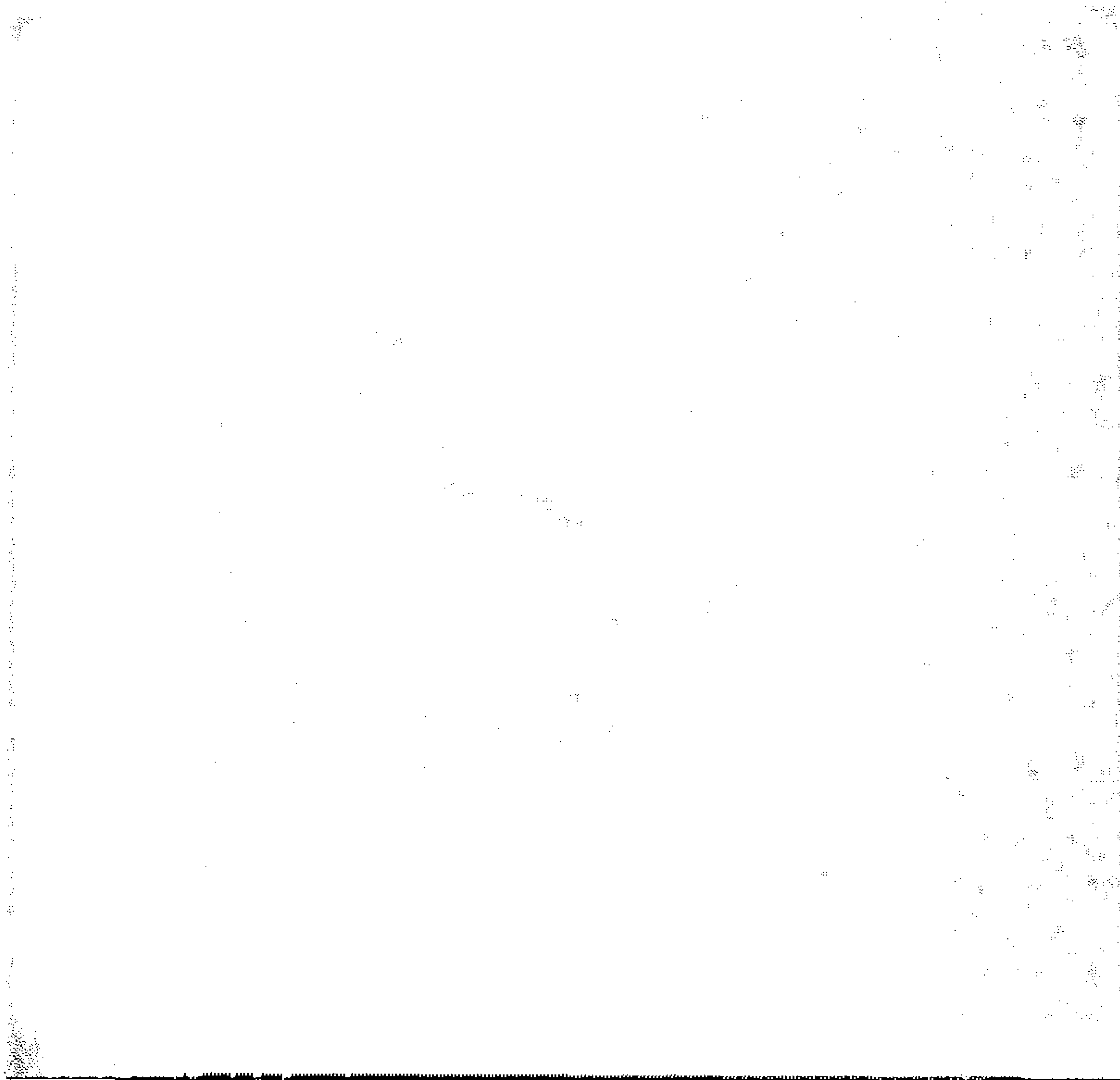

Fig. 4.27. Electron micrograph from the centre of one of the damaged regions shown in Fig. 4.26. Magnification 9000X.

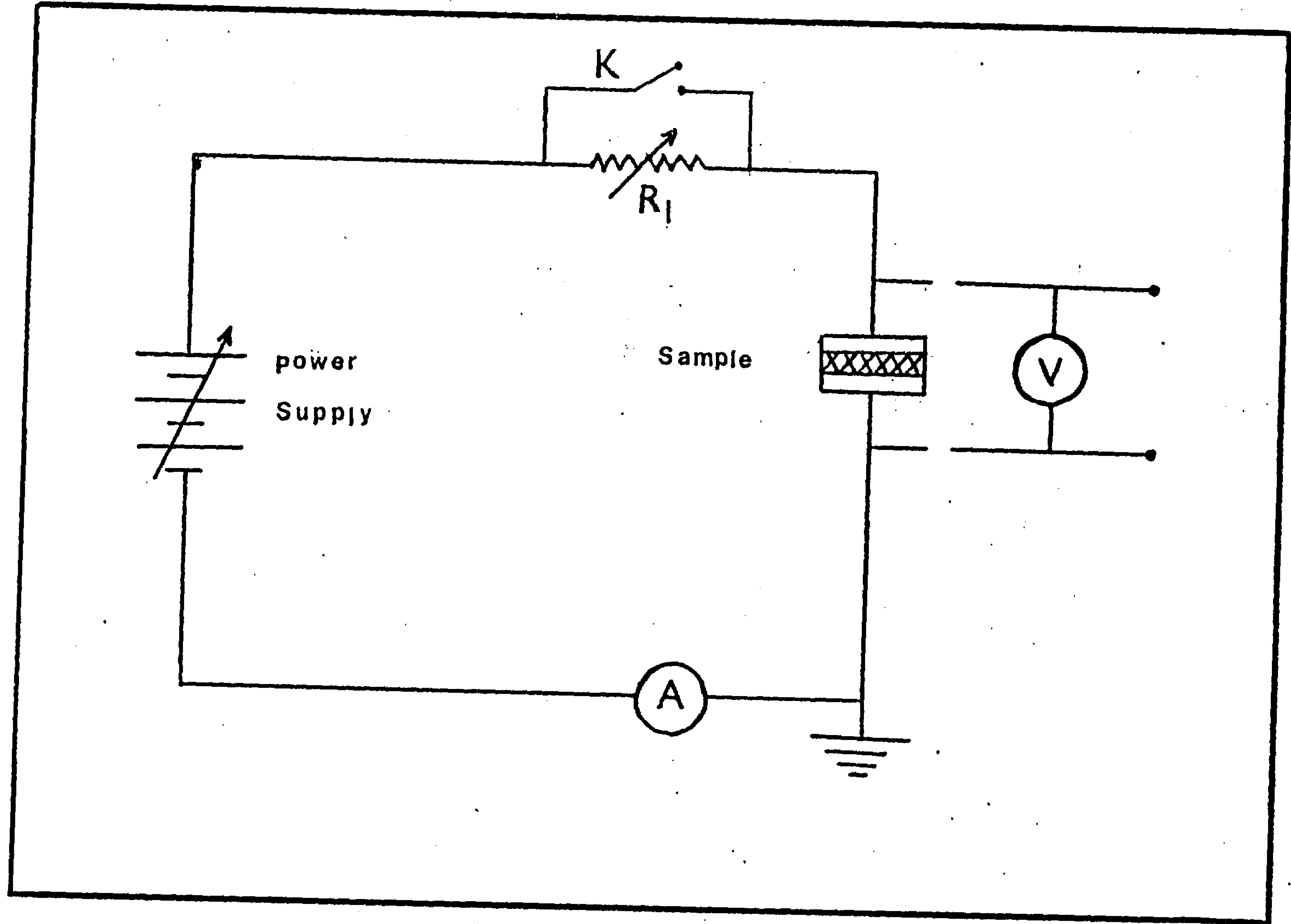

Fig. 4.28. Circuit used for switching studies.

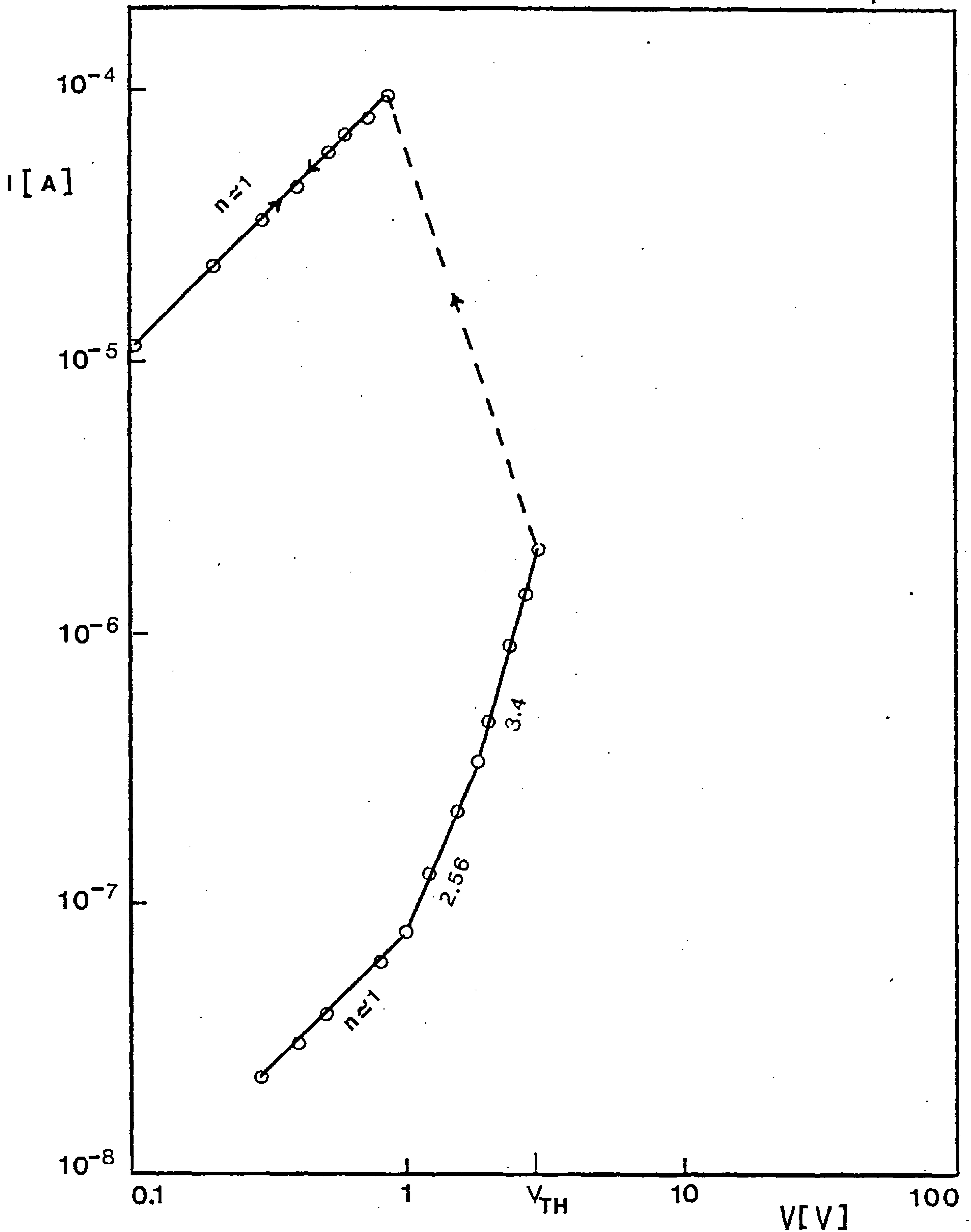

Fig.4.29. Current-voltage characteristics of a typical memory switching of a Cu(380Å)-SiO / B_2O_3 (2000Å)-Cu(450Å) device at room-temperature; R_L=20 kΩ

Fig. 4.3. The development of circulating current during the forming process of a sample with copper electrodes; T = 300K, d = 600Å.

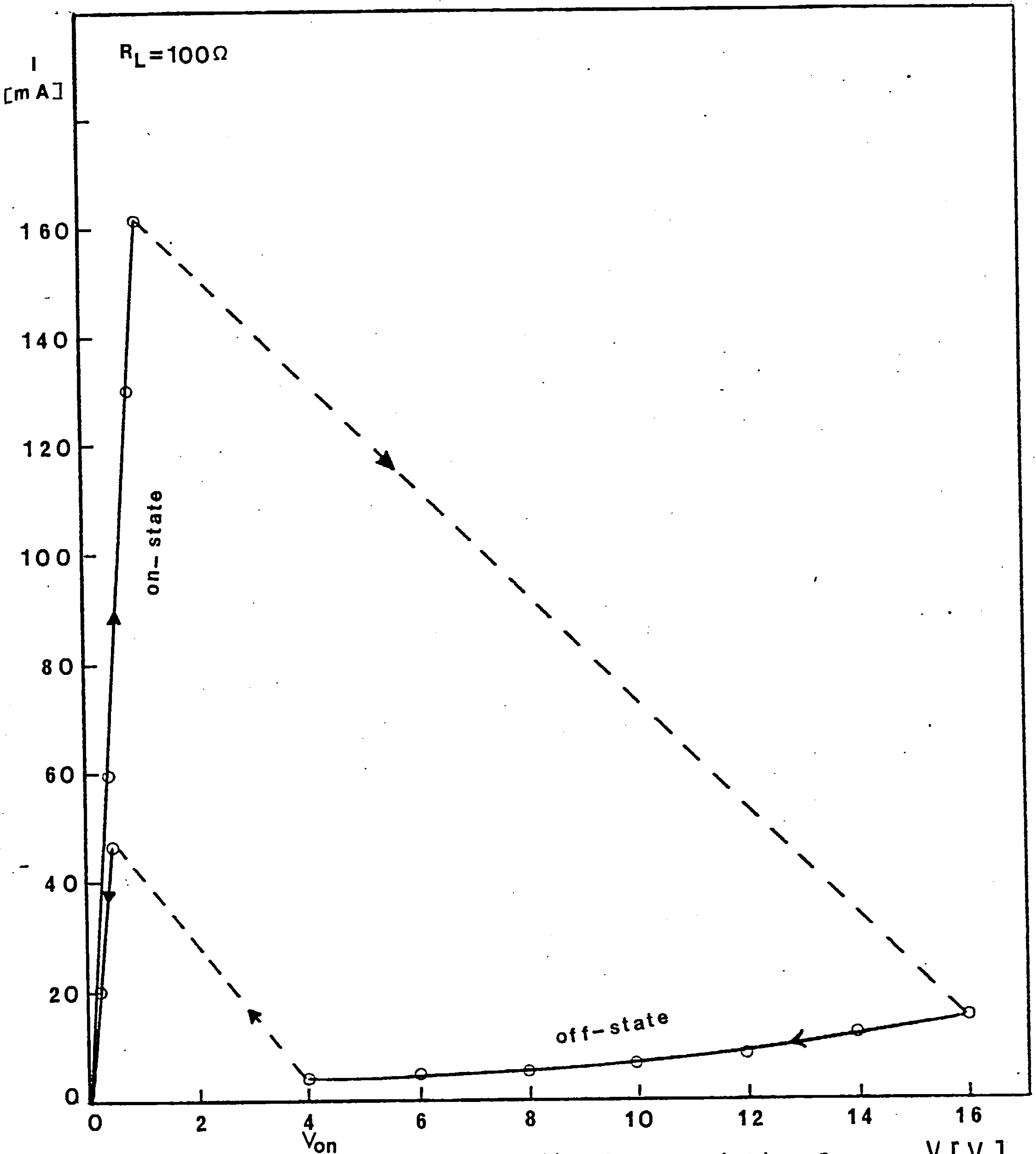

Fig.4.30. A typical memory switching characteristic of an $Ag(700\AA)-SiO/B_2O_3(1000\AA)-Ag(1000\AA)$ sample at room-temperature; $R_L=100\Omega$.

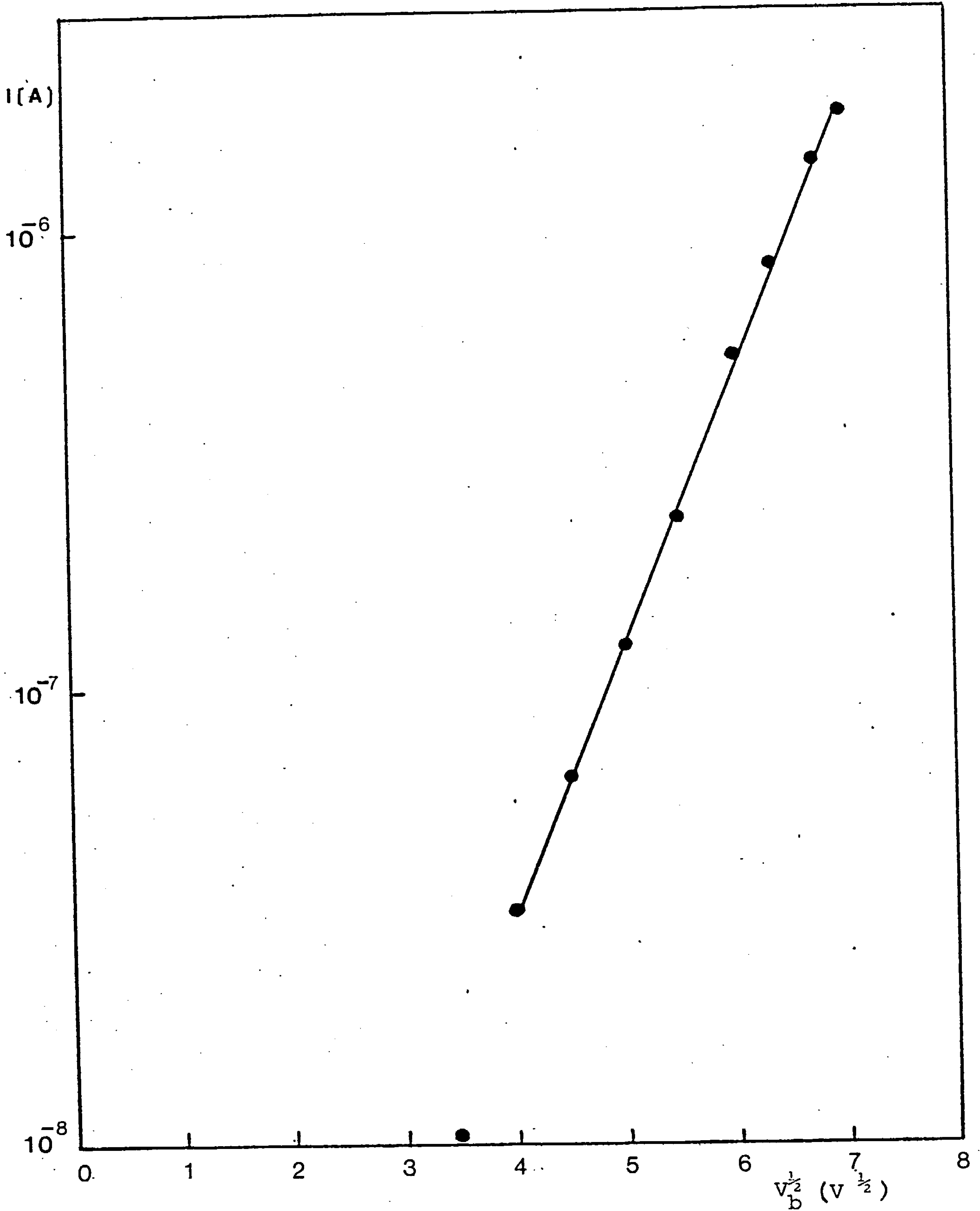

Fig. 4.4. I_c-$V_b^{\frac{1}{2}}$ characteristic of an unformed Al-SiO (80%) / B_2O_3(20%) - Al sample at T = 300°K, dielectric thickness, d = 3500Å.

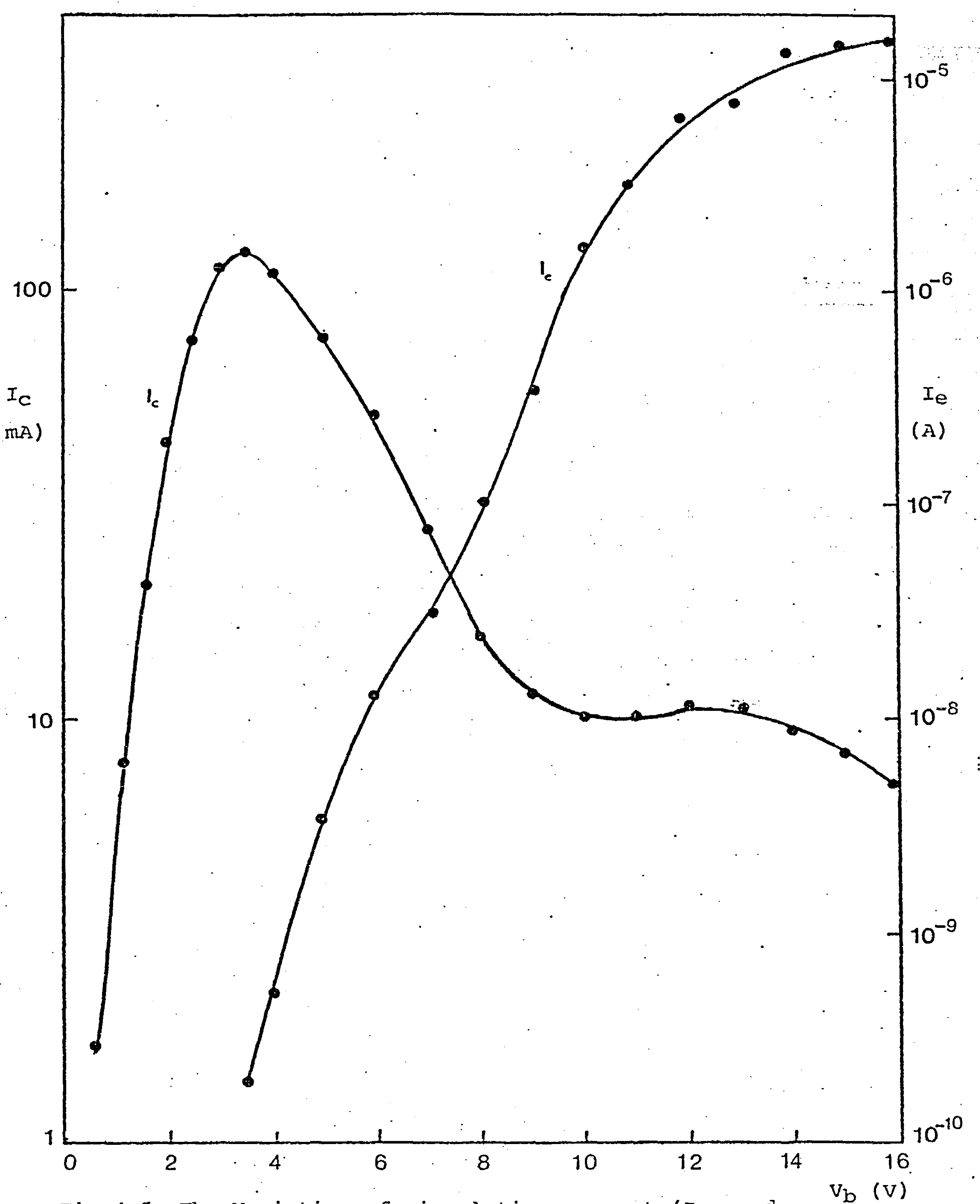

Fig.4.5. The Variation of circulating current (I_C) and emission current (I_e) with applied Voltage V_b for a vacuum-electroformed Cu-SiO/B_2O_3-Cu structure; d = 1700 Å , T = 300 °K.

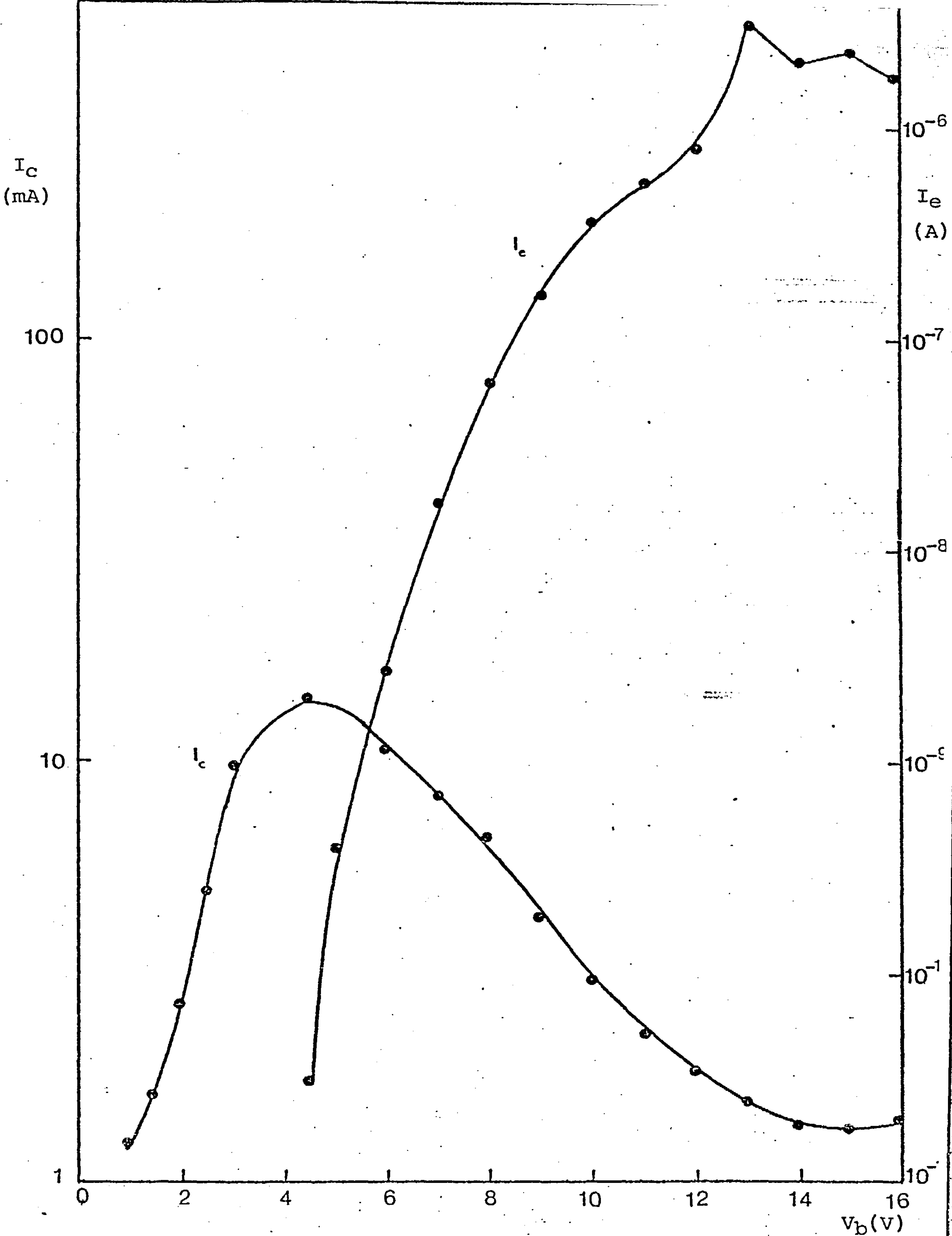

Fig. 4.6. The I_c-V_b and I_e-V_b characteristics for a vacuum - electroformed Ag-SiO/B_2O_3-Ag device; d = 1700Å T = 300°K.

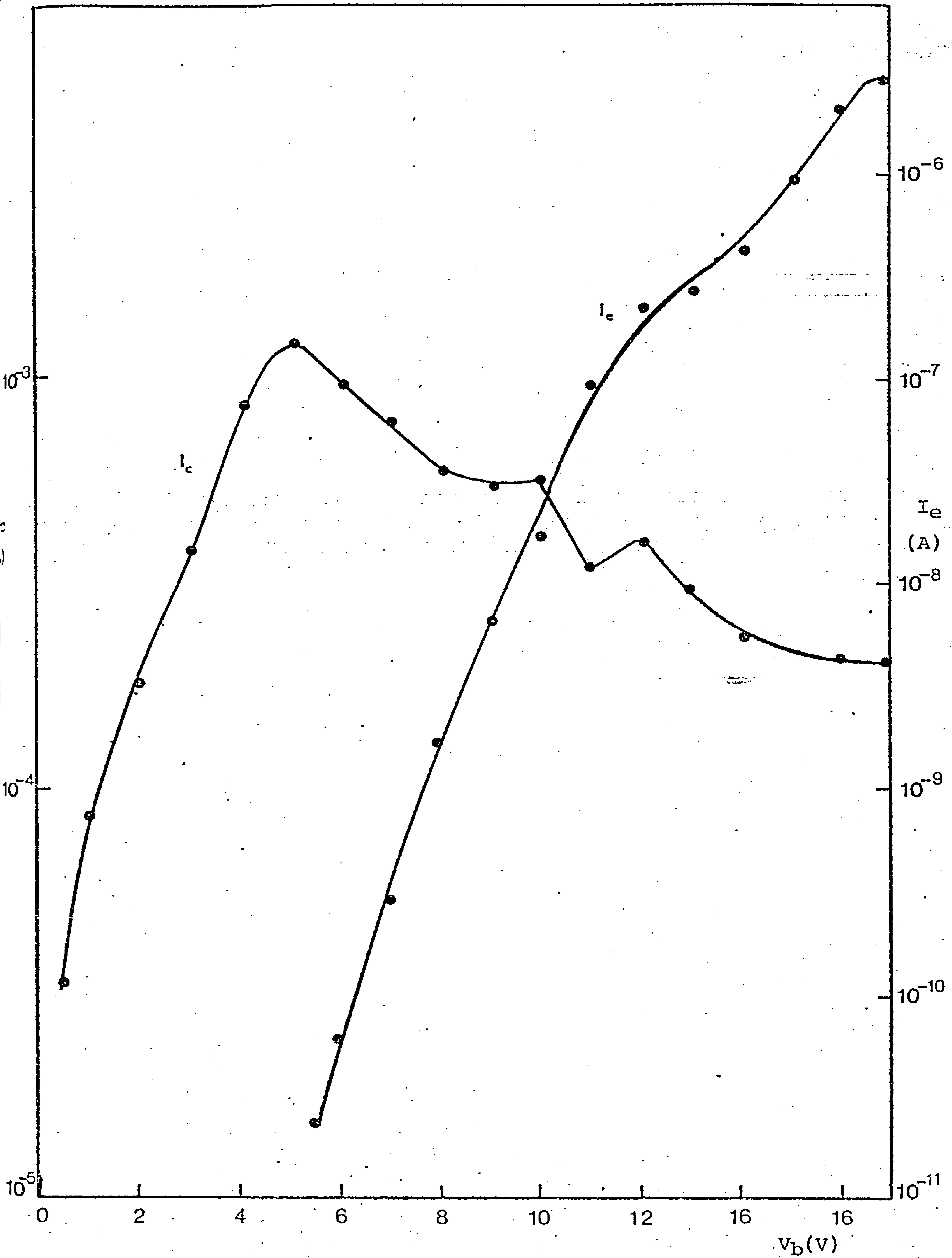

Fig. 4.7. The Variation of I_c and I_e with applied bias voltage V_b, for a sample carrying Al electrodes; d = 1700Å, T = 300K.

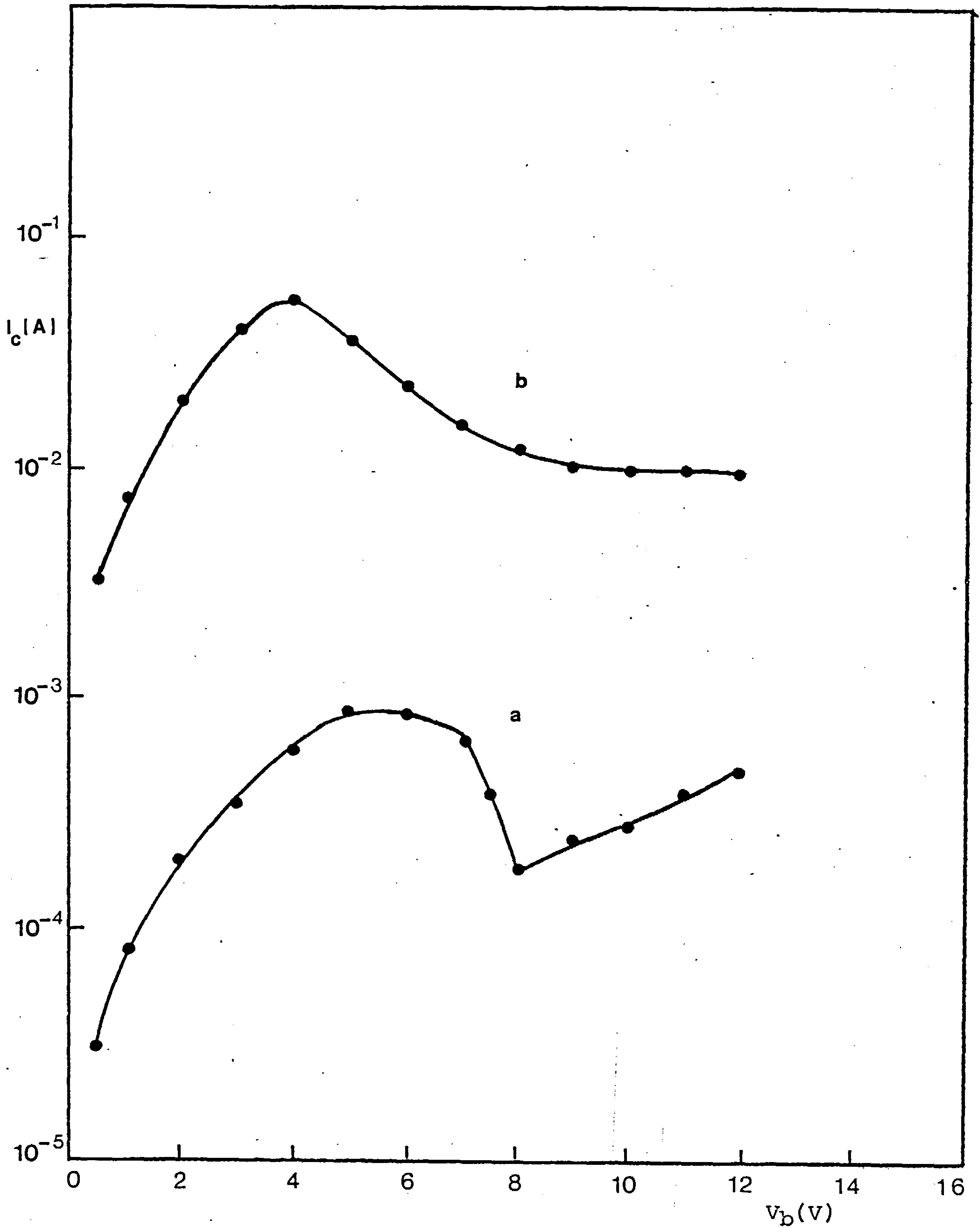

Fig. 4.8. I_c-V_b characteristic of a Cu-SiO/B_2O_3-Cu device;
(a) electroformed with negatively biased top-electrode;
(b) after complete electroforming with top-electrode positive. d = 1250Å.

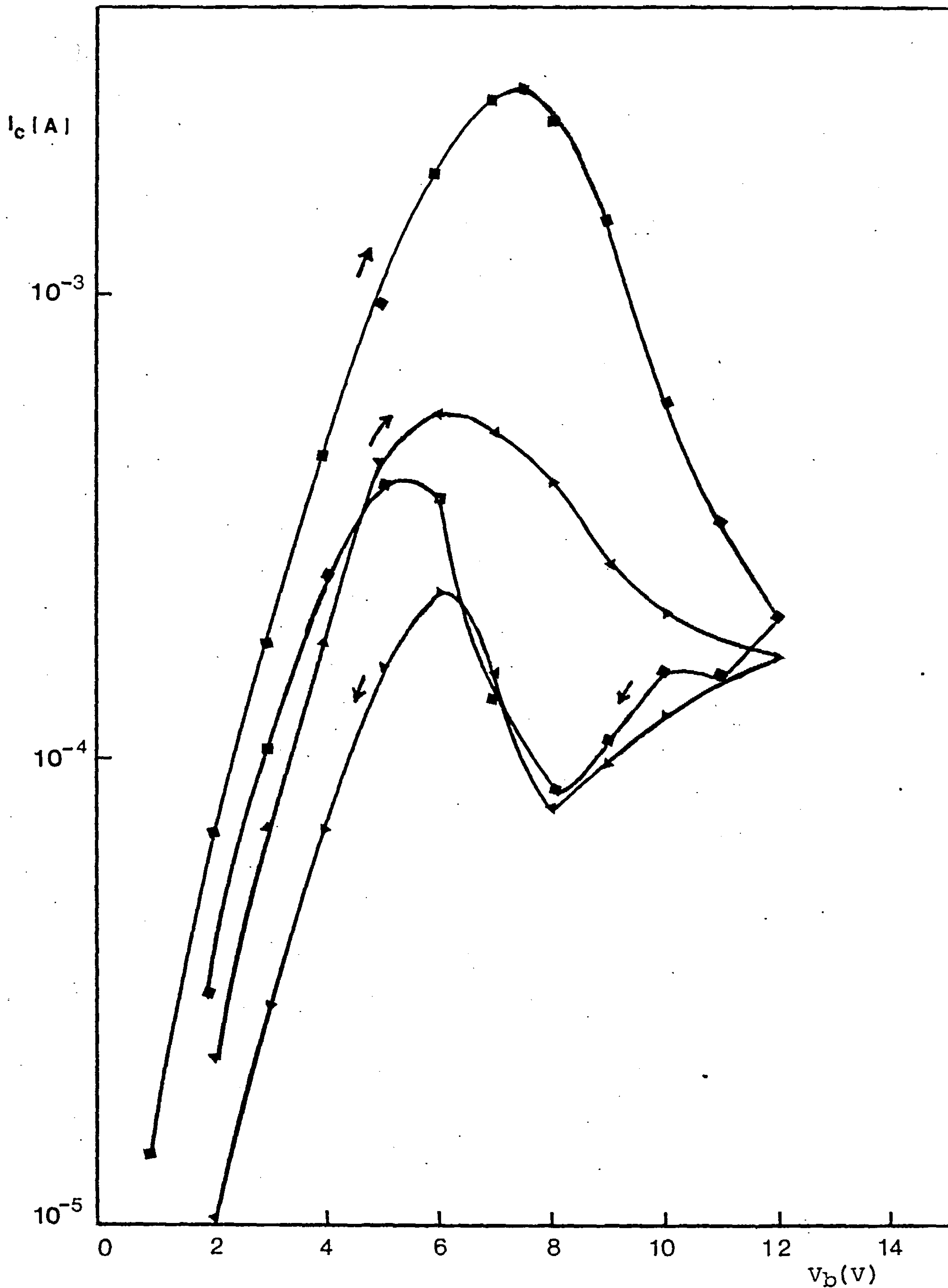

Fig. 4.9. I_c-V_b characteristics of a Cu-SiO/B_2O_3-Cu air-electroformed device; (■) first voltage cycling, (▲) second voltage cycling, d = 1250Å.

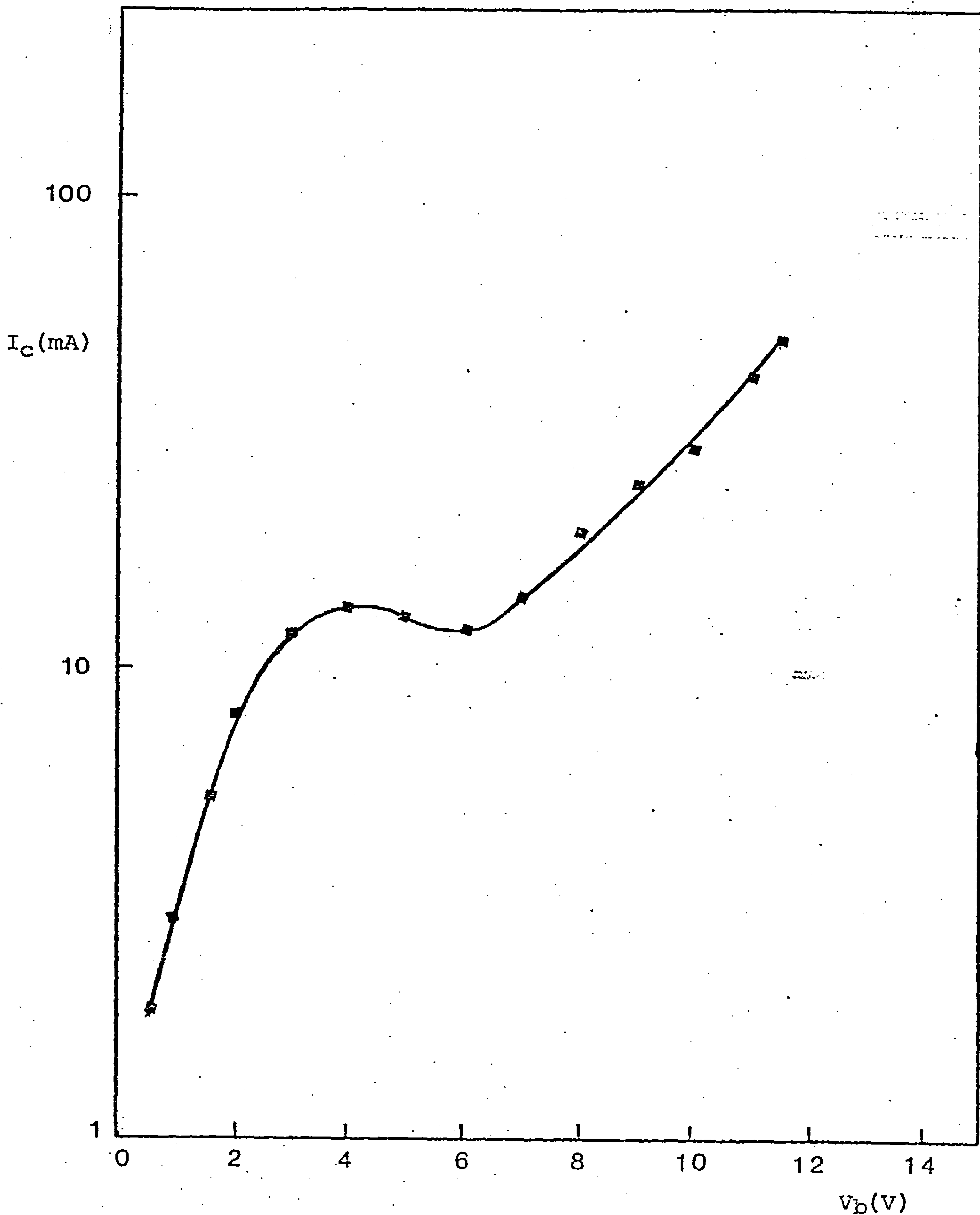

Fig. 4.10. I_c-V characteristic of an Ag-SiO/B_2O_3 (1720Å)-Ag electroformed in air at atmospheric pressure.

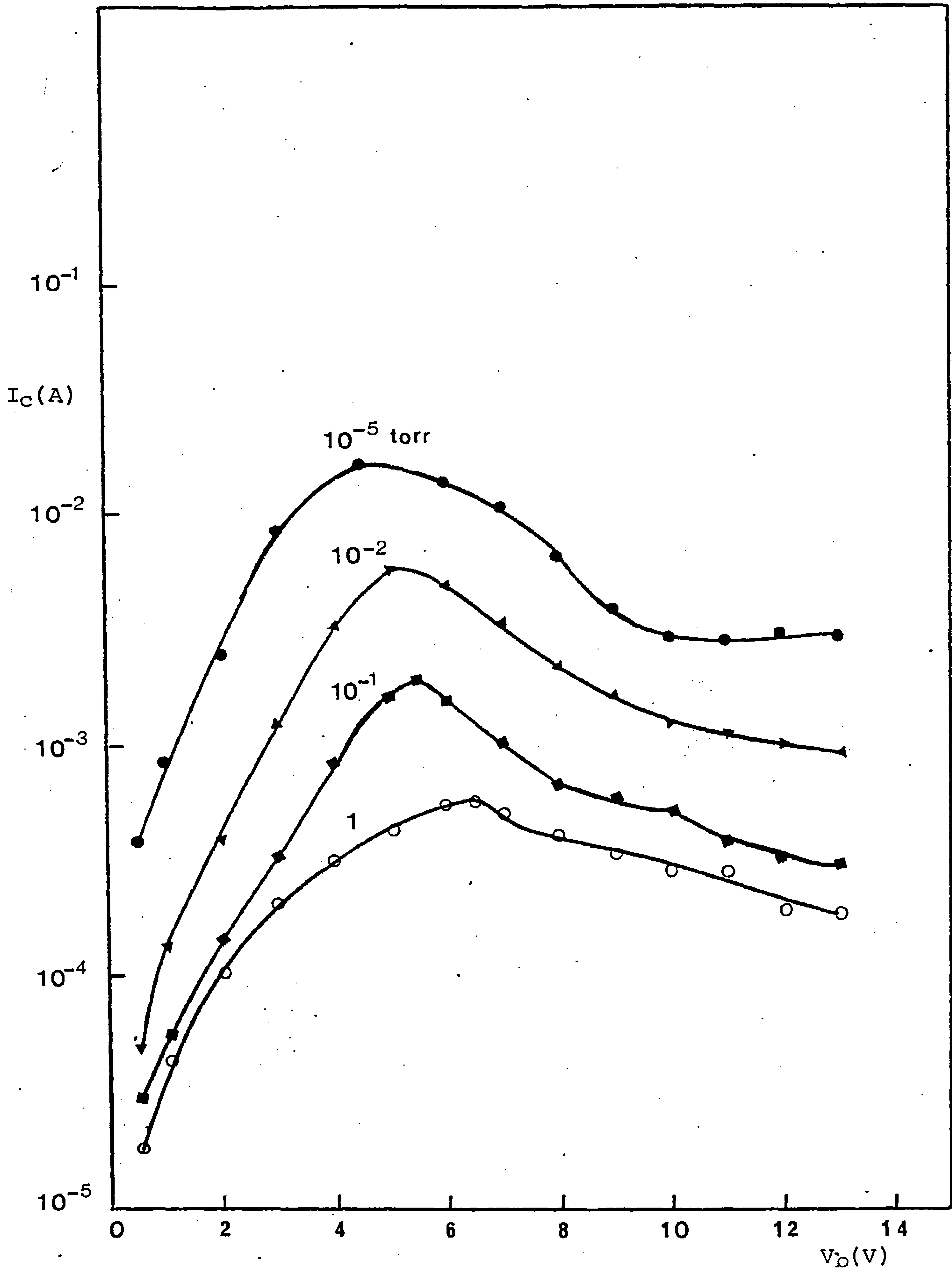

Fig. 4.11. I_c-V characteristics of a vacuum-electroformed Ag-SiO (70%)/B_2O_3 (30%) - Ag device at various pressures of air; d = 3170Å.